APPLICATION OF MASSIVE INTEGRABLE QUANTUM FIELD THEORIES TO PROBLEMS IN CONDENSED MATTER PHYSICS

FABIAN H.L. ESSLER

The Rudolf Peierls Centre for Theoretical Physics,
University of Oxford, 1 Keble Road,
Oxford OX1 3NP, United Kingdom

ROBERT M. KONIK

Department of Physics, Brookhaven National Laboratory,
Upton, NY 11973-5000, USA

We review applications of the sine-Gordon model, the O(3) non-linear sigma model, the U(1) Thirring model, and the O(N) Gross–Neveu model to quasi one-dimensional quantum magnets, Mott insulators, and carbon nanotubes. We focus upon the determination of dynamical response functions for these problems. These quantities are computed by means of form factor expansions of quantum correlation functions in integrable quantum field theories. This approach is reviewed here in some detail.

Table of Contents

In memory of Ian Kogan.

1. Introduction

The study of strongly correlated electrons in low dimensional systems lies at the heart of much of modern condensed matter physics. Interest in these systems arises as the behavior of strongly correlated systems is not in general adequately captured in approximations based upon 'free-particle' non-interacting models. In the presence of generically strong interactions, the physics is typically much richer, exhibiting qualitatively new features.

Accessing this physics presents an imposing challenge. In one route to understanding this physics, quantum field theories can be employed. Field theories are typically able to describe the low energy behavior of strongly correlated systems and so are able to extract universal characteristics. It is these characteristics that are of greatest interest precisely because they provide the most robust experimental signatures and do not, in general, depend upon particular experimental details.

In low dimensions, the study of numerous quantum field theories is aided by their integrability. Integrable theories are characterized by an infinite number of non-trivial conserved charges. The existence of these charges allows for an exact characterization of many features of these models. Both the spectrum and the scattering matrices of an integrable quantum field theory can be explicitly written down. On the other hand, correlation functions in an integrable quantum field theory cannot, in general, be exactly computed. However there exist approaches, based on exploiting the integrability of the model, that can be used to obtain some information on correlation functions. And while incomplete, this information does reflect the non-perturbative structure of the theory.

Of these approaches, we describe in this review one based upon form-factors. Form factors are matrix elements of fields in the theory with exact eigenstates. Under a spectral decomposition, all correlation functions can be written in terms of form factors. While this decomposition is exact, its practical manipulation requires truncation of the spectral sum. In this review we will explore how this truncation may be done and under what conditions exact information on the theory remains available. As the reader will see, the behavior of correlation functions at low energy scales fortuitously remains exactly computable.

The review is organized as follows. In the first substantive section, Section 2, we give in detail the form factor programme to computing correlation functions in integrable quantum field theories. Our purpose here is to be pedagogical. We begin by giving an overview of how form factors are used to calculate zero temperature correlators. In Section 2.2 we then turn to describing the key features of an integrable model for the programme, the spectrum and its associated scattering. Form factors are computable in an integrable model because they must satisfy a series of constraints arising from both consistency with the underlying scattering and various assumed analyticities in the energy-momentum. We list these constraints in Section 2.3. In Section 2.4 we give examples of the application of these constraints to an archetypal integrable theory, the sine-Gordon model. While form factors do not generically give the behavior of correlation functions at all energy scales, they do provide *exact* information at low energies. And at higher energy scales, corrective terms, as a rule, are extremely small. We illustrate this principle in Section 2.6 with the specific example of the Ising model. In the final two subsections we turn to form-factors in more involved settings: form-factors in models with bound states and the use of form-factors to compute correlation functions at finite temperature.

Having given an overview of the form-factor programme, we turn to specific applications. As our first example, we consider applications of the sine-Gordon model to half-integer spin chains. An anisotropic Heisenberg spin-1/2 chain has gapless excitations. In this section we first detail the bosonization of the spin chain and so exhibit the chain's Luttinger liquid phase. We then consider a number of physical perturbations under which the chain becomes gapped and is described by the massive sine-Gordon model. Correlation functions in such perturbed half-integer chains then can be studied using sine-Gordon form factors.

In Section 4, we study integer spin chains using the same techniques. Unlike their half-integer counter parts, an integer spin Heisenberg chain is completely gapped and its low energy behavior is believed to be described by the O(3) non-linear sigma model. For pedagogical reasons we begin the section by giving the map between the two, pointing out what approximations are used. We then turn to a basic description of the O(3) non-linear sigma model including its spectrum, scattering matrices, and form factors of various physical fields. With these form factors in hand, we next consider the computation of various zero temperature spin-spin correlation functions that would be measured in neutron scattering experiments. Having considered the correlation functions at $T = 0$, we turn to their finite temperature counterparts. This will be our primary example demonstrating the possibility of a form-factor computation at $T \neq 0$ and it is done in some detail. Using these techniques we will address the issue of whether transport is ballistic or diffusive at finite temperatures in integer spin chains.

In the next section, Section 5, we turn to applications of the U(1) Thirring model to quasi-one-dimensional Mott insulating chains. Such insulators are modeled by various extended Hubbard models which in turn are related to the U(1) Thirring model. The latter can be bosonized in terms of a free boson and a sine-Gordon model. Using the form factors of various operators in the sine-Gordon model we compute both the optical response as well as the single-particle spectral function of half-filled and quarter filled Mott insulating chains. While this treatment is appropriate to one-dimensional materials, we also show how the case of weakly coupled chains can be treated.

In the final section, Section 6, we consider our last application of form factors, that to Hubbard ladders and armchair carbon nanotubes. In the weak interaction limit, both materials can be described in an RG sense by the SO(8) Gross–Neveu model, an integrable theory of four interacting Dirac fermions. We outline this mapping in some detail and point out its limitations. We then use the form factors of SO(8) Gross–Neveu to compute a number of physical quantities including the optical response and single particle spectral function. We end by pointing out how the results are changed if small, integrable-breaking perturbations are introduced.

2. Correlation Functions in Integrable, Massive Quantum Field Theories

In this section we outline the form-factor programme by which correlation functions in massive integrable field theories can be computed.

2.1. *Computing Correlation Functions with Form Factors: Exact Results at Zero Temperature*

In general computing correlation functions in integrable field theories is an open problem. There exists no general technique that is able to access a generic correlation function at all energy scales. Now progress can be made in certain instances. For certain integrable models, such as Ising model variants, the sine-Gordon model at is free fermion point, and the Bose gas with delta-function interactions, some correlations can be determined with the aid of Fredholm determinants [35, 168, 176]. This method, however, is technically involved, and only works in a handful of cases. More promising is the form-factor programme for the calculation of correlation functions [156, 264]. Form factors do not allow in practice the complete determination of a correlation function. However in a gapped (massive) field theory, they do permit the exact determination of the low energy properties of the corresponding spectral function.

This arises as the form-factor representation of any zero temperature correlation function is obtained by inserting a resolution of the identity corresponding to the basis of eigenstates. (We will consider finite temperature correlation functions later in this section.) Thus, for an operator, $\mathcal{O}(x,\tau)$, we write the spectral decomposition schematically (τ denotes imaginary time, and T time ordering) [a]

$$\begin{aligned} G_T^{\mathcal{O}}(x,\tau) &= -\langle 0|T\big(\mathcal{O}(x,\tau)\mathcal{O}^\dagger(0,0)\big)|0\rangle \\ &= -\sum_{n=0}^{\infty}\sum_{s_n} e^{-\tau E_{s_n}}\langle 0|\mathcal{O}(x,0)|n;s_n\rangle\langle n;s_n|\mathcal{O}^\dagger(0,0)|0\rangle, \quad (\tau>0), \end{aligned} \tag{2.1}$$

where E_{s_n} is the energy of an eigenstate, $|n;s_n\rangle$, with n particles described by quantum numbers, $\{s_n\}$. By inserting a resolution of the identity, we have reduced the problem to one of computing individual matrix elements. In an integrable model the matrix elements of a physical operator between the vacuum and the exact eigenstates can in principle be computed exactly from the two-body S-matrix. However the calculation of these matrix elements, as well as the evaluation of the sums/integrals, $\sum_{s_n}$, becomes increasingly cumbersome as the particle number n becomes large, so that the full expression for the correlation function cannot be evaluated in closed form. Often, however, a truncation of the sum at the level of two or three particle states already provides a good approximation to the full correlation function [53, 69, 70, 181, 185]. On the other hand, this truncation is no longer necessary in a massive theory, if one considers the corresponding spectral function. Only eigenstates with a fixed energy, ω, contribute to the spectral function

$$\begin{aligned} &-\frac{1}{\pi}\,\mathrm{Im}G_T^{\mathcal{O}}(x,-i\omega+\delta) \\ &\qquad=\sum_{n=0}^{\infty}\sum_{s_n}\Big\{\langle 0|\mathcal{O}(x,0)|n;s_n\rangle\langle n;s_n|\mathcal{O}^\dagger(0,0)|0\rangle\delta(\omega-E_{s_n}) \\ &\qquad\quad-\epsilon\langle 0|\mathcal{O}^\dagger(0,0)|n;s_n\rangle\langle n;s_n|\mathcal{O}(x,0)|0\rangle\delta(\omega+E_{s_n})\Big\}, \end{aligned} \tag{2.2}$$

where $\epsilon=\pm$ for fields, $\mathcal{O}$, that are bosonic/fermionic.

[a] The sum over s_n is meant to include integrals over the momenta of all particles and sums over particle/excitation types.

In a massive theory the creation of an extra particle in the intermediate exact eigenstate costs a finite amount of energy, and so the sum in Eq. (2.2) is finite. For example, when ω is smaller than the energy of all three-particle states (i.e. when ω is below the three-particle threshold), then only the form factors with one and two particles ($n = 1, 2$) have to be determined in order to obtain an exact result. All of the spectral functions we have computed in this review are exact at sufficient low energies for this reason.

As knowledge of the exact eigenfunctions in an integrable model is central to computing correlations functions, we consider this in more detail in the next section.

2.2. *The Spectrum and its Scattering in an Integrable Model*

The key feature of an integrable system is the exact knowledge of a basis of eigenstates of the fully interacting Hamiltonian. At the root of integrability is a well defined notion of "particles", or "elementary excitations" in the fully interacting system. These particles scatter off each other according to two-body S-matrices, that is, all particle production processes are absent and particle number is conserved. This is due to special conservation laws which exist in an integrable model, preventing the decay of these particles. In this sense, an integrable system is similar to a Fermi liquid. An additional feature is that new particles can arise as bound states of already existing ones. However the total number of different types of particles is finite which makes the system analytically tractable.

Formally the elementary excitations are created and destroyed through the Faddeev–Zamolodchikov operators, denoted by $A_a(\theta)$. θ is termed the rapidity and it encodes the energy-momentum carried by the excitation via

$$p = \Delta \sinh(\theta), \qquad E = \Delta \cosh(\theta). \tag{2.3}$$

Two excitations will in general scatter according to a non-trivial two-body S-matrix, S. S gives the amplitude of the process by which two particles $\{a, b\}$ scatter into two potentially different particles, $\{a', b'\}$. In terms of the Faddeev–Zamolodchikov operators, this scattering determines the commutation relationship between operators

$$\begin{aligned}
A_a(\theta_1)A_b(\theta_2) &= S_{ab}^{a'b'}(\theta_1-\theta_2)A_{b'}(\theta_2)A_{a'}(\theta_1),\\
A_a^\dagger(\theta_1)A_b^\dagger(\theta_2) &= S_{ab}^{a'b'}(\theta_1-\theta_2)A_{b'}^\dagger(\theta_2)A_{a'}^\dagger(\theta_1),\\
A_a(\theta_1)A_b^\dagger(\theta_2) &= 2\pi\delta_{ab}\delta(\theta_1-\theta_2) + S_{ba'}^{b'a}(\theta_1-\theta_2)A_{b'}^\dagger(\theta_1)A_{a'}(\theta_1).
\end{aligned} \tag{2.4}$$

It is solely a function of $\theta_1 - \theta_2 \equiv \theta_{12}$ by Lorentz invariance.

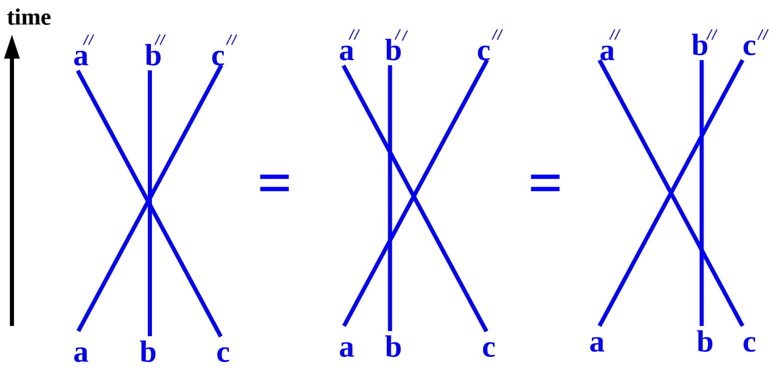

Figure 1. A graphical representation of the Yang–Baxter equation. The left-hand figure represents a three body process by which three particles a, b, and c scatter into a'', b'', and c''. Via integrability, this three-body process can be factorized into two different sets of three two-body processes pictured in the central and leftmost figures. Under the Yang-Baxter relation, these different sets of two-body scattering processes are equivalent.

These two-body S-matrices encode all scattering information in the theory. Scattering processes involving higher number of particles can always be expressed in terms of two-body scattering matrices. Suppose we consider a three particle scattering process, scattering particles $\{a, b, c\}$ into $\{a', b', c'\}$ given by the S-matrix $S_{abc}^{a'b'c'}$. This three-body S-matrix factorizes into a set of two-body S-matrices

$$
\begin{aligned}
S_{abc}^{a'b'c'}(\theta_1, \theta_2, \theta_3) &= S_{ab}^{a'b'}(\theta_1, \theta_2) S_{a'c}^{a''b'}(\theta_1, \theta_3) S_{b'c'}^{b''c''}(\theta_2, \theta_3) \\
&= S_{bc}^{b'c'}(\theta_2, \theta_3) S_{ac'}^{a'c''}(\theta_1, \theta_3) S_{a'b'}^{a''b''}(\theta_1, \theta_2). \qquad (2.5)
\end{aligned}
$$

From the above equation we see that we can factorize the three-body S-matrix in two different ways. This is illustrated graphically in Fig. 1. Because the theory is integrable, the different ways of factorizing are equivalent. This equivalence is known as the Yang-Baxter equation. The ability to factorize the higher-body S-matrices results from the existence in the integrable theory of conserved charges with are non-trivial powers of energy and momentum [178, 282, 312–314].

As two-body scattering provides complete information on an integrable theory, the form factors (even those involving large number of particles) are determined by this S-matrix alone. We will see this in operation in the next section.

2.3. *Computation of Form Factors: Form Factor Axioms*

The form factors of a field $\mathcal{O}$ are defined as the matrix elements of the field with some number of particles, $A_a(\theta)$:

$$f^{\mathcal{O}}_{a_1\cdots a_n}(\theta_1,\cdots,\theta_n) = \langle \mathcal{O}(0,0)A_{a_n}(\theta_n)\cdots A_{a_1}(\theta_1)\rangle. \tag{2.6}$$

These matrix elements are constrained by a variety of requirements arising from the scattering relations just discussed, Lorentz invariance, hermiticity, analyticity, and the locality of the fields. We consider each in turn.

2.3.1. *Scattering Axiom*

For the form factor to be consistent with two body scattering we must have

$$f^{\mathcal{O}}_{a_1,\cdots,a_{i+1},a_i,\cdots,a_n}(\theta_1,\cdots,\theta_{i+1},\theta_i,\cdots,\theta_n) = \\ S^{a'_i,a'_{i+1}}_{a_i a_{i+1}}(\theta_i-\theta_{i+1}) f^{\mathcal{O}}_{a_1,\cdots,a'_i,a'_{i+1},\cdots,a_n}(\theta_1,\cdots,\theta_i,\theta_{i+1},\cdots,\theta_n). \tag{2.7}$$

This relation is arrived at by commuting the i-th and $i+1$-th particle and using the Faddeev–Zamolodchikov algebra in Eq. (2.4).

2.3.2. *Periodicity Axiom*

A second constraint upon the form factor can be thought of as a periodicity axiom. In continuing the rapidity, θ, of a particle to $\theta - 2\pi i$, the particle's energy-momentum is unchanged. However the form-factor is not so invariant. We instead have

$$f^{\mathcal{O}}_{a_1,\cdots,a_n}(\theta_1,\cdots,\theta_n) = f^{\mathcal{O}}_{a_n,a_1,\cdots,a_{n-1}}(\theta_n - 2\pi i,\theta_1,\cdots,\theta_{n-1}). \tag{2.8}$$

This constraint is derived from crossing symmetry [35]. It implicitly assumes that the field $\mathcal{O}$ is local: if $\mathcal{O}$ is non-local additional braiding phases appear in the above relation [36, 170, 263].

These braiding phases arise when two fields are interchanged,

$$\psi(x,t)\mathcal{O}(y,t) = R_{\psi\mathcal{O}}\mathcal{O}(y,t)\psi(x,t)\,, \qquad x<y. \tag{2.9}$$

(On occasion, we must deal with braiding matrices, not merely phases. But we will not consider such a situation in this work.) If $R_{\psi\mathcal{O}}$ is non-trivial we must alter the above periodicity axiom to read

$$f^{\mathcal{O}}_{a_1,\cdots,a_n}(\theta_1,\cdots,\theta_n) = R_{\psi_n\mathcal{O}} f^{\mathcal{O}}_{a_n,a_1,\cdots,a_{n-1}}(\theta_n - 2\pi i,\theta_1,\cdots,\theta_{n-1}). \tag{2.10}$$

Here ψ_n can be thought of as the field which creates the excitation A_n.

In order to employ the periodicity axiom (Eq. (2.10)), we then need to know how to specify the braiding of the fields. In one approach, we identify both fields with their corresponding excitations, $A_{\mathcal{O}}$ and A_n. If both fields are rightmoving, the braiding of the fields is then encoded in the asymptotic limits of the corresponding S-matrix, (see [263]),

$$R_{\mathcal{O}n} = (S^{\mathcal{O}n}_{\mathcal{O}n}(+\infty)). \tag{2.11}$$

If on the other hand the fields are left moving, we find instead $R_{\mathcal{O}n} = (S^{\mathcal{O}n}_{\mathcal{O}n}(-\infty))$.

2.3.3. *Annihilation Pole Axiom*

Another condition related to analyticity that a form factor must satisfy is the annihilation pole axiom. This condition arises in form factors involving a particle and its anti-particle. Under the appropriate analytical continuation, such a combination of particles are able to annihilate one another. As such this condition relates form factors with n particles to those with $n-2$ particles,

$$\begin{aligned} i\ \mathrm{res}_{\theta_n=\theta_{n-1}+\pi i} f(\theta_1,\cdots,\theta_n)_{a_1,\cdots,a_n} &= f(\theta_1,\cdots,\theta_{n-2})_{a'_1,\cdots,a'_{n-2}}\delta_{a_n a'_{n-1}} \\ \times\Bigg(\delta^{a'_1}_{a_1}\delta^{a'_2}_{a_2}\cdots\delta^{a'_{n-2}}_{a_{n-2}}\delta^{a'_{n-1}}_{a_{n-1}} &- R_{\mathcal{O}n} S^{a'_{n-1}a'_1}_{\tau_1 a_1}(\theta_{n-11}) S^{\tau_1 a'_2}_{\tau_2 a_2}(\theta_{n-12})\cdots \\ &\times S^{\tau_{n-4}a'_{n-3}}_{\tau_{n-3}a_{n-3}}(\theta_{n-1n-3}) S^{\tau_{n-3}a'_{n-2}}_{a_{n-1}a_{n-2}}(\theta_{n-1n-2})\Bigg). \end{aligned} \tag{2.12}$$

This relation as written assumes that we are normalizing our particle states as $\langle\theta|\theta'\rangle = 2\pi\delta(\theta-\theta')$. Note that the braiding phase plays a role in this axiom (see r.h.s. of the above equation).

2.3.4. *Lorentz Invariance*

The form factor must also satisfy constraints coming from Lorentz invariance. In general, the form factor of a field, $\mathcal{O}$, carrying Lorentz spin, s, must transform under a Lorentz boost, $\theta_i \to \theta_i + \alpha$, via

$$f^{\mathcal{O}}_{a_1\cdots a_n}(\theta_1+\alpha,\cdots,\theta_n+\alpha) = e^{s\alpha} f^{\mathcal{O}}_{a_1\cdots a_n}(\theta_1,\cdots,\theta_n). \tag{2.13}$$

We will often in this work consider the correlation functions of (topological) current operators. Let us thus consider $j_0(x,t)$, a charge density, and $j_1(x,t)$, its corresponding conserved current. Together they form a Lorentz two-current. (Here $0, 1$ are Lorentz indices.) The form factors for j_0 and j_1

appear as

$$f^{j_\mu}_{a_1\cdots a_n}(\theta_1,\cdots,\theta_n) = \epsilon_{\mu\nu}P^\nu(\theta_i)f_{a_1\cdots a_n}(\theta_1,\cdots,\theta_n), \tag{2.14}$$

where $P^0 = \sum_i \Delta\cosh(\theta_i)$ and $P^1 = \sum_i \Delta\sinh(\theta_i)$. The function, $f_{a_1\cdots a_n}(\theta_1,\cdots,\theta_n)$, on the r.h.s. of Eq. (2.14) is solely a function of $\theta_i - \theta_j$.

2.3.5. *Form Factor Normalization*

It is sometimes possible to determine the absolute normalization of a set of form-factors. (Of course, normalization of form-factors with different particle numbers but of the same field can be fixed, among other ways, by the use of the annihilation pole axiom.) In the case of current operator we can rely upon the action of the conserved charge

$$Q = \int dx j_0(x,0),$$

upon the single particle states with charge q. We expect (with the normalization of Section 2.3.3)

$$\langle\theta,q|Q|\theta',q\rangle = 2\pi q\delta(\theta-\theta'). \tag{2.15}$$

Using crossing, we can relate this matrix element to a two-particle form factor,

$$\langle\theta,q|Q|\theta',q\rangle = \langle Q|\theta-i\pi,\bar{q};\theta',q\rangle, \tag{2.16}$$

where $\bar{q}$ denotes the charge conjugate of q. Thus we are able to fix the normalization of the two particle form factor in a natural fashion (and so all other higher particle form factors through the annihilation pole axiom).

With operators other than currents, we can always fix the phase of the normalization using hermiticity. For this purpose it is sufficient to consider 2-particle form factors. Hermiticity then gives us

$$\begin{aligned}\langle\mathcal{O}(0,0)A_{a_2}(\theta_2)A_{a_1}(\theta_1)\rangle^* &= \langle A^\dagger_{a_1}(\theta_1)A^\dagger_{a_2}(\theta_2)\mathcal{O}^\dagger(0,0)\rangle\\ &= \langle\mathcal{O}^\dagger(0,0)A_{\bar{a}_1}(\theta_1-i\pi)A_{\bar{a}_2}(\theta_2-i\pi)\rangle\,,\end{aligned} \tag{2.17}$$

where the last line follows from crossing and so

$$f^{\mathcal{O}}_{a_1a_2}(\theta_1,\theta_2)^* = f^{\mathcal{O}^\dagger}_{\bar{a}_2\bar{a}_1}(\theta_2-i\pi,\theta_1-i\pi). \tag{2.18}$$

2.3.6. *Minimality Principle*

These conditions do not uniquely specify the form factors. It is easily seen that if $f(\theta_1, \cdots, \theta_n)_{a_1,\cdots,a_n}$ satisfies these axioms then so does

$$f(\theta_1, \cdots, \theta_n)_{a_1,\cdots,a_n} \frac{P_n(\cosh(\theta_{ij}))}{Q_n(\cosh(\theta_{ij}))}\ , \tag{2.19}$$

where P_n and Q_n are symmetric polynomials in $\cosh(\theta_{ij}), 1 \le i, j \le n$, and are such that

$$P_n|_{\theta_n=\theta_{n-1}+\pi i} = P_{n-2}\,; \quad Q_n|_{\theta_n=\theta_{n-1}+\pi i} = Q_{n-2}\,. \tag{2.20}$$

To deal with this ambiguity, we employ a minimalist axiom. We choose P_n and Q_n such that P_n/Q_n has the minimal number of poles and zeros in the physical strip, $\mathrm{Re}(\theta) = 0$, $0 < \mathrm{Im}\theta < 2\pi$. Additional poles are only added in accordance with the theory's bound state structure. Using this minimalist ansatz, one can determine P_n/Q_n up to a constant.

2.4. *Simple Example: Form Factors for the Sine-Gordon Model in the Repulsive Regime*

In this section we consider form factors of fields in the sine-Gordon model in its repulsive regime. The sine-Gordon model is described by the following action

$$S = \frac{1}{16\pi}\int dxd\tau\,[\partial_\mu\Phi\partial^\mu\Phi - \mu\cos(\beta\Phi)]\,. \tag{2.21}$$

For $\beta > 1/\sqrt{2}$ this theory describes repulsively interacting solitons alone, i.e. there are no bound states. Classically these solitons arise as interpolations of the field $\Phi(x, t)$ between minima of the cosine potential. The two solitons are characterized by a topological $U(1)$ charge, +/-.

As it is integrable, the model is characterized solely by a two particle S-matrix. Its nonzero, $U(1)$-conserving elements are given by

$$\begin{aligned}
S^{++}_{++}(\theta) = S^{--}_{--}(\theta) \equiv S_0(\theta) &= -\exp\left[\int_0^\infty \frac{dx}{x}\,\sinh\left(\frac{x\theta}{i\pi}\right)\frac{\sinh((\frac{1}{2}-\frac{\xi}{2})x)}{\cosh(\frac{x}{2})\sinh(\frac{x\xi}{2})}\right],\\
S^{+-}_{+-}(\theta) = S^{-+}_{-+}(\theta) &= -\frac{\sinh(\frac{\theta}{\xi})}{\sinh(\frac{\theta-\pi i}{\xi})}\,S_0(\theta),\\
S^{+-}_{-+}(\theta) = S^{-+}_{+-}(\theta) &= -\frac{i\sin(\frac{\pi}{\xi})}{\sinh(\frac{\theta-\pi i}{\xi})}\,S_0(\theta),
\end{aligned} \tag{2.22}$$

where

$$\xi = \frac{\beta^2}{1-\beta^2} \ . \tag{2.23}$$

With this brief description in hand we go on to compute two particle form-factors in this theory.

2.4.1. *Soliton-Antisoliton Form Factor for the Current Operator*

We will first consider the form factor of the current correlator with a two soliton state. The (topological) current operator in sine-Gordon is given by

$$j^\mu = \epsilon^{\mu\nu}\partial_\nu\Phi\,, \tag{2.24}$$

(where $\epsilon^{01}=1$). As the operator itself carries no $U(1)$ charge, it couples to a soliton-anti-soliton pair. The matrix element has the general form

$$f^\mu_{\epsilon_1\epsilon_2}(\theta_1,\theta_2) = \langle 0|j^\mu(0,0)|A^\dagger_{\epsilon_2}(\theta_2)A^\dagger_{\epsilon_1}(\theta_1)\rangle\,. \tag{2.25}$$

To determine $f^\mu_{\epsilon_1\epsilon_2}(\theta_1,\theta_2)$, we note that the current couples anti-symmetrically to the soliton-anti-soliton pair (as is clear if one examines the limit $\beta^2=1/2$ where the model reduces to free massive fermions). Thus $f^\mu_{\epsilon_1\epsilon_2}(\theta_1,\theta_2)$ takes the form,

$$f^\mu_{\epsilon_1\epsilon_2}(\theta_1,\theta_2) = \epsilon_{\epsilon_1\epsilon_2}f^\mu(\theta_1,\theta_2)\,, \tag{2.26}$$

where ϵ is the anti-symmetric tensor. We can scalarize the above by explicitly exhibiting the piece of the form factor satisfying Lorentz invariance,

$$f_\mu(\theta_1,\theta_2) = \left(e^{(\theta_1+\theta_2)/2} - (-1)^\mu e^{-(\theta_1+\theta_2)/2}\right)f(\theta_{12})\,. \tag{2.27}$$

Having so constrained the form of $f^\mu_{\epsilon_1\epsilon_2}(\theta_1,\theta_2)$, we now apply the scattering axiom. Using the anti-symmetry of $f^\mu_{\epsilon_1\epsilon_2}(\theta_1,\theta_2)$ in the indices ϵ_1,ϵ_2, we find

$$f^\mu_{\epsilon_2\epsilon_1}(\theta_2,\theta_1) = S(\theta_{12})f^\mu_{\epsilon_2\epsilon_1}(\theta_1,\theta_2)\,, \tag{2.28}$$

where

$$S(\theta) = \frac{\sinh(\frac{\theta}{\xi}) - i\sin(\frac{\pi}{\xi})}{\sinh(\frac{\theta-\pi i}{\xi})}\,S_0(\theta) = -\exp\left(\int_0^\infty \frac{dx}{x}\sinh\left(\frac{x\theta}{i\pi}\right)G_c(x)\right), \tag{2.29}$$

$$G_c(x) \equiv G_{c1}(x) + G_{c2}(x)\,,$$

$$G_{c1}(x) = \frac{\sinh((\frac{\xi}{2}-1)x)}{\sinh(\frac{x\xi}{2})} - \frac{\cosh((\frac{\xi}{2}-1)x)}{\cosh(\frac{\xi x}{2})}\,;\quad G_{c2}(x) = \frac{\sinh((\frac{1}{2}-\frac{\xi}{2})x)}{\cosh(\frac{x}{2})\sinh(\frac{x\xi}{2})}\,. \tag{2.30}$$

We note that $S(\theta)$ tends to -1 as θ goes to zero. This implies the form factor will vanish in the same limit. As the current operator is local and bosonic, the braiding here is trivial. The periodicity axiom reading

$$f^{\mu}_{\epsilon_2\epsilon_1}(\theta_2,\theta_1) = f^{\mu}_{\epsilon_1\epsilon_2}(\theta_1 - 2\pi i,\theta_1) \tag{2.31}$$

thus reduces to

$$f(-\theta) = f(\theta - 2\pi i). \tag{2.32}$$

A minimal solution of these constraints on the form factor is

$$\begin{aligned} f^{\mu}_{\epsilon_1\epsilon_2}(\theta_1,\theta_2) &= iA\epsilon_{\epsilon_1,\epsilon_2}(e^{(\theta_1+\theta_2)/2} - (-1)^{\mu}e^{-(\theta_1+\theta_2)/2})s(\theta_{12}/2) \\ &\times \exp\left[\int_0^\infty \frac{dx}{x}\frac{G_c(x)}{\sinh(x)}\sin^2(\frac{x}{2\pi}(i\pi+\theta_{12}))\right], \end{aligned} \tag{2.33}$$

where iA is some normalization with mass dimension $[m]$. The phase of A is determined through the hermiticity condition

$$f^{\mu}_{\epsilon_1\epsilon_2}(\theta_1,\theta_2)^* = f^{\mu}_{\epsilon_2\epsilon_1}(\theta_2 - i\pi,\theta_1 - i\pi). \tag{2.34}$$

This implies that A is real.

We note that

$$\exp\left[\int_0^\infty \frac{dx}{x}\frac{G_{c1}(x)}{\sinh(x)}\sin^2(\frac{x}{2\pi}(i\pi+\theta_{12}))\right] = \frac{1}{\cosh(\frac{\theta+i\pi}{2\xi})}. \tag{2.35}$$

The form factor can then be written in the same form appearing in Ref. [264],

$$\begin{aligned} f^{\mu}_{\epsilon_1\epsilon_2}(\theta_1,\theta_2) &= iA\epsilon_{\epsilon_1,\epsilon_2}(e^{(\theta_1+\theta_2)/2} - (-1)^{\mu}e^{-(\theta_1+\theta_2)/2})\frac{s(\theta_{12}/2)}{\cosh(\frac{\theta+i\pi}{2\xi})} \\ &\times \exp\left[\int_0^\infty \frac{dx}{x}\frac{G_{c2}(x)}{\sinh(x)}\sin^2(\frac{x}{2\pi}(i\pi+\theta_{12}))\right]. \end{aligned} \tag{2.36}$$

2.4.2. *Soliton-Antisoliton Form Factor for Non-Local Operators*

We now consider the two soliton form factor of the non-local operator, $e^{\pm i\frac{\beta}{2}\Phi}$. This operator's non-locality can be seen if we relate the field Φ to the current operator

$$e^{\pm i\frac{\beta}{2}\Phi} = e^{\pm i\frac{\beta}{2}\int_{-\infty}^{x}dx' j^0(x,t)}. \tag{2.37}$$

This non-locality will lead to a non-trivial braiding relation for the field.

Again these operators carry no $U(1)$ charge and so will couple to a soliton-anti-soliton pair. It will prove to be convenient to consider form-factors involving symmetric and anti-symmetric combinations of the solitons,

$$f^{\pm}_S(\theta_1,\theta_2) = \langle 0|e^{\pm i\frac{\beta}{2}\Phi}|A^\dagger_-(\theta_2)A^\dagger_+(\theta_1)\rangle + \langle 0|e^{\pm i\frac{\beta}{2}\Phi}|A^\dagger_+(\theta_2)A^\dagger_-(\theta_1)\rangle\,,$$

$$f^{\pm}_A(\theta_1,\theta_2) = \langle 0|e^{\pm i\frac{\beta}{2}\Phi}|A^\dagger_-(\theta_2)A^\dagger_+(\theta_1)\rangle - \langle 0|e^{\pm i\frac{\beta}{2}\Phi}|A^\dagger_+(\theta_2)A^\dagger_-(\theta_1)\rangle\,. \quad (2.38)$$

As the operators $e^{\pm i\frac{\beta}{2}\Phi}$ are Lorentz scalars, these form factors are solely a function of $\theta_{12} = \theta_1 - \theta_2$. Applying the scattering axiom to the form factors we find

$$\begin{aligned} f^{\pm}_S(-\theta) &= S_S(\theta)f^{\pm}_S(\theta)\,,\\ f^{\pm}_A(-\theta) &= S_A(\theta)f^{\pm}_A(\theta)\,, \end{aligned} \quad (2.39)$$

where

$$\begin{aligned} S_S(\theta) &= \frac{\sinh(\frac{\theta+\pi i}{2\xi})}{\sinh(\frac{\theta-\pi i}{2\xi})}\exp\left(\int_0^\infty \frac{dx}{x}\sinh(\frac{x\theta}{i\pi})G_{c2}(x)\right),\\ S_A(\theta) &= -\frac{\cosh(\frac{\theta+\pi i}{2\xi})}{\cosh(\frac{\theta-\pi i}{2\xi})}\exp\left(\int_0^\infty \frac{dx}{x}\sinh(\frac{x\theta}{i\pi})G_{c2}(x)\right), \end{aligned} \quad (2.40)$$

and $G_{c2}(x)$ is as for the current form-factor. The non-locality of the fields, $e^{\pm i\frac{\beta}{2}\Phi}$, relative to the solitons implies that R should be taken to be -1 in the periodicity axiom (see Eq. (2.10)). Thus we have

$$\begin{aligned} f^{\pm}_{+-}(-\theta) &= -f^{\pm}_{-+}(\theta-2\pi i)\,,\\ f^{\pm}_{-+}(-\theta) &= -f^{\pm}_{+-}(\theta-2\pi i)\,. \end{aligned} \quad (2.41)$$

In terms of the symmetric and anti-symmetric combinations we obtain

$$\begin{aligned} f^{\pm}_S(-\theta) &= -f^{\pm}_S(\theta-2\pi i)\,,\\ f^{\pm}_A(-\theta) &= f^{\pm}_A(\theta-2\pi i)\,. \end{aligned} \quad (2.42)$$

Having expressed the constraints on the form factors in this way, we can readily write down a minimal solution

$$\begin{aligned} f^{\pm}_S(\theta_1,\theta_2) &= A^{\pm}_S\frac{\sinh(\theta_{12}/2)}{\sinh(\frac{\theta_{12}+\pi i}{2\xi})}\exp\left[\int_0^\infty \frac{dx}{x}\frac{G_{c2}(x)}{\sinh(x)}\sin^2(\frac{x}{2\pi}(i\pi+\theta_{12}))\right],\\ f^{\pm}_A(\theta_1,\theta_2) &= A^{\pm}_A\frac{\sinh(\theta_{12}/2)}{\cosh(\frac{\theta_{12}+\pi i}{2\xi})}\exp\left[\int_0^\infty \frac{dx}{x}\frac{G_{c2}(x)}{\sinh s(x)}\sin^2(\frac{x}{2\pi}(i\pi+\theta_{12}))\right], \end{aligned} \quad (2.43)$$

where $A^{\pm}_{S/A}$ are normalization constants. We now turn to their determination.

From the hermiticity condition,

$$f^{\pm}_{S/A}(\theta_1,\theta_2)^* = f^{\mp}_{S/A}(\theta_2 - i\pi, \theta_1 - i\pi), \tag{2.44}$$

we see that $A^{\pm *}_{S} = A^{\mp}_{S}$ and $A^{\pm *}_{A} = -A^{\mp}_{A}$. The operators $e^{\pm i\frac{\beta}{2}\Phi}$ have a nonzero vacuum expectation value. Using the annihilation pole axiom it is possible to relate the value of $A^{\pm}_{S}$ to this expectation value. In this case it reads

$$i\mathrm{res}_{\theta_1=\theta_2-\pi i} f^{\pm}_{S}(\theta_1,\theta_2) = \langle e^{\pm i\frac{\beta}{2}\Phi}\rangle. \tag{2.45}$$

We thus obtain $A^{\pm}_{S} = \frac{1}{2\xi}\langle e^{\pm i\frac{\beta}{2}\Phi}\rangle$. Using the transformation properties under charge conjugation we conclude that $A^{+}_{S} = A^{-}_{S}$. To relate $A^{\pm}_{S}$ and $A^{\pm}_{A}$ we appeal to the free fermion limit ($\beta^2 = 1/2$) where it can be seen that $A^{+}_{S} = A^{+}_{A}$ (Ref. [264]). We will assume this holds for all relevant β.

2.5. *Relevance of Higher Particle Form Factors: Ising Model as an Example*

We have argued in Section 2.2 that to obtain exact information on spectral functions at low energies it is enough to include form factors involving only a few particles or excitations. However as a rule of thumb, form factor calculations fare even better. In practice, form factor sums have been found to be strongly convergent for operators in massive theories [53, 69, 70]. To obtain a good approximation to correlators involving such fields *at all energies*, only the first few terms need to be kept. Even in massless theories where there are no explicit thresholds, convergence is good provided the engineering dimension of the operator matches its anomalous dimension [181, 185]. At high energies where higher particle form factors do begin to contribute, their contributions are progressively (often exponentially) smaller. We will illustrate this with a simple example, the spectral function of the spin-spin correlator in the Ising model.

The field theory describing the near-critical Ising model is that of a massive Majorana (real) fermion with action

$$S = \frac{1}{8\pi}\int dx d\tau \left(\psi\partial_{\bar z}\psi + \bar\psi\partial_z\bar\psi + 2im\psi\bar\psi\right), \tag{2.46}$$

where $z/\bar z = (\tau \pm ix)$. ψ and $\bar\psi$ are the left and right moving self-conjugate components of the Majorana spinor. The mass of the fermion corresponds to the distance from criticality $m \sim (T_c - T)$ which we will assume to be positive (the model is in its ordered phase). The fundamental excitation, $A_a(\theta)$, of the model arises from the mode expansions of the Fermi fields,

$$\psi = \sqrt{m}\int_{-\infty}^{\infty}\frac{d\theta}{\sqrt{2\pi i}}e^{-\theta/2}\Big(A(\theta)e^{-m(ze^{-\theta}+\bar{z}e^{\theta})} - A^{\dagger}(\theta)e^{m(ze^{-\theta}+\bar{z}e^{\theta})}\Big),$$
$$\bar{\psi} = -i\sqrt{m}\int_{-\infty}^{\infty}\frac{d\theta}{\sqrt{2\pi i}}e^{\theta/2}\Big(A(\theta)e^{-m(ze^{-\theta}+\bar{z}e^{\theta})} + A^{\dagger}(\theta)e^{m(ze^{-\theta}+\bar{z}e^{\theta})}\Big). \quad (2.47)$$

The defining commutation relations of A and $A^\dagger$ are $\{A(\theta), A^\dagger(\theta')\} = 2\pi\delta(\theta-\theta')$.

While the form factors of the Fermi fields are trivial (only the one particle form factors are non-zero), the form factors of the spin fields, $\sigma(x,t)$, are more complicated (ultimately a result of the spin and Fermi fields being mutually non-local). From Refs. [39, 52, 168, 304], we have

$$\langle 0|\sigma(0,0)|A(\theta_{2n})\cdots A(\theta_1)\rangle \equiv f(\theta_1,\cdots,\theta_{2n})$$
$$= i^n\prod_{i<j}^{2n}\tanh\Big(\frac{\theta_i-\theta_j}{2}\Big). \quad (2.48)$$

Only even numbers of fermions couple to the spin field (in contrast, odd numbers of fermions couple to the disorder field). The fermion S-matrix of this model is $S=-1$. The mutual non-locality of the spin, σ, and Fermi, ψ, fields is encoded in the braiding phase, $R_{\sigma\psi}=-1$. Knowing $S=R_{\sigma\psi}=-1$, it is easy to check that the form factors in Eq. (2.48) satisfy the axioms of Section 2.3.

The spectral function of the spin-spin correlator is defined as

$$S(\omega,k) = -\mathrm{Im}\Big[\frac{1}{\pi}\int_{-\infty}^{\infty}dx\int_{-\infty}^{\infty}d\tau e^{i\omega\tau-ikx}\big(-\langle T(\sigma(x,\tau)\sigma(0,0))\rangle\big)|_{\omega\to -i\omega+\epsilon}\Big]. \quad (2.49)$$

Here $\langle T(\sigma(x,\tau)\sigma(0,0))\rangle$ is the time ordered correlator in imaginary time. If we insert a resolution of the identity in between the two fields, do the Fourier transforms, and take the appropriate analytic continuation, we find at positive frequencies

$$S(\omega>0,k) = 2\pi\sum_{n=1}^{\infty}\frac{1}{2n!}\prod_{i=1}^{2n}\int_{-\infty}^{\infty}d\hat{\theta}_i\ \delta(k-m\sum_{i=1}^{2n}\sinh(\theta_i))$$
$$\times\delta(w-m\sum_{i=1}^{2n}\cosh(\theta_i))\ |f(\theta_1,\cdots,\theta_{2n}|^2, \quad (2.50)$$

where $d\hat{\theta} \equiv d\theta/(2\pi)$. Integrating over θ_1 and θ_2 we obtain

$$S(\omega > 0, k) = \frac{2}{\pi} \sum_{n=1}^{\infty} \frac{1}{2n!} \prod_{i=3}^{2n} \int_{-\infty}^{\infty} d\hat{\theta}_i \frac{1}{\sqrt{\omega'^2 - k'^2 - 4m^2}} \frac{1}{\sqrt{\omega'^2 - k'^2}}$$
$$\times \Theta(\omega' - \sqrt{k'^2 + 4m^2}) |f(\theta_1, \cdots, \theta_{2n}|^2, \tag{2.51}$$

where θ_1 and θ_2 are given by

$$\omega' = w - m \sum_{i=3}^{2n} \cosh(\theta_i);$$
$$k' = k - m \sum_{i=3}^{2n} \sinh(\theta_i);$$
$$\theta_1 = \begin{cases} \cosh^{-1}\left(\frac{1}{2m}(\omega' + |k'|\sqrt{1 - \frac{4m^2}{\omega'^2 - k'^2}})\right) & \text{if } k' > 0; \\ -\cosh^{-1}\left(\frac{1}{2m}(\omega' + |k'|\sqrt{1 - \frac{4m^2}{\omega'^2 - k'^2}})\right) & \text{if } k' < 0; \end{cases}$$
$$\theta_2 = \sinh^{-1}\left(\frac{k'}{m} - \sinh(\theta_1)\right). \tag{2.52}$$

We plot as a function of energy, ω, the first three non-zero contributions (the 2-particle, the 4-particle, and the 6-particle) to the spectral function in Fig. 2. We first note that the 2n-particle form-factor only contributes for energies $\omega > 2nm$. Thus the plot of these contributions is exact for $\omega < 16m$. We also see that for energies beyond $4m$ the higher particle contributions barely register. The 4-particle contribution, at its peak, is still 1/3000 of the 2-particle contribution. And the 6-particle contribution is considerably smaller yet. To be seen, it must be plotted on a scaled magnified by 10^8. We thus learn that to compute the spectral function to energies far above the mass gap, it would seem to be sufficient to consider only the two-particle contribution. While we have only shown this to be the case in the off-critical Ising model, it is a generic feature of all massive integrable models. We will see another example in Section 4 with the spin spectral function of the $O(3)$ non-linear sigma model.

2.6. *Form Factors for Integrable Models with Bound States*

When there are bound states in an integrable model, additional analytical requirements are imposed upon the form factors. Suppose we have an excitation, A_c, which is a bound state of excitations, A_a and A_b. The presence of this bound state is indicated by the analytic structure of the two-body

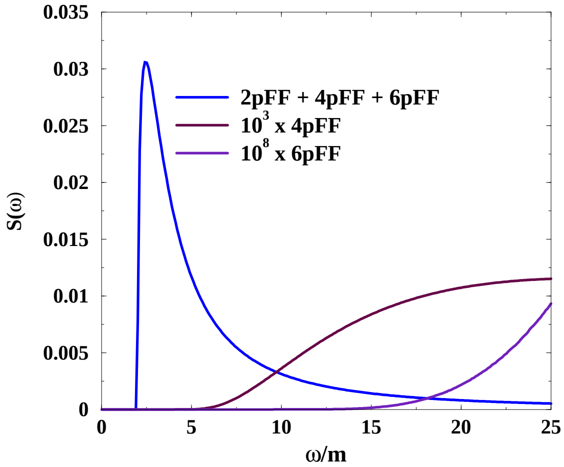

Figure 2. Plots of the response function derived from the spin-spin correlator in the Ising model. In the first plot, the contributions from the two through six particle form factors are included. We in addition plot the individual contributions of the four and six particle form factors. We see that the four and six particle form factors, to be seen, require a magnified scale.

S-matrix between particles A_a and A_b. The S-matrix must have a pole at iu^c_{ab} of the form

$$S^{ab}_{ab}(\theta) \sim i\,\frac{g^c_{ab}g^{ab}_c}{\theta - iu^c_{ab}}\,. \tag{2.53}$$

The coefficients forming the residue of the pole, g^c_{ab}, effectively measure the strength with which the two particles bind.

We can formally indicate that A_a and A_b have a bound state A_c via

$$ig^c_{ab}A_c(\theta) = \mathrm{res}_{\delta=0}\ A_a(\theta+\delta+i\bar{u}^{\bar{b}}_{a\bar{c}})A_b(\theta - i\bar{u}^{\bar{a}}_{b\bar{c}})\,. \tag{2.54}$$

Here $\bar{u}^{\bar{a}}_{b\bar{c}} = \pi - u^{\bar{a}}_{b\bar{c}}$ and $u^{\bar{a}}_{b\bar{c}}$ is the location of the pole in the two-body S-matrix between A_b and $A_{\bar{c}}$ indicative of the formation of the bound state, $A_{\bar{a}}$. The locations, u, of the various poles satisfy a simple relation

$$2\pi = u^c_{ab} + u^{\bar{a}}_{b\bar{c}} + u^{\bar{b}}_{a\bar{c}}\,, \tag{2.55}$$

which can be proven on the basis of kinematical considerations. If m_a and m_b are the masses of the particles A_a and A_b, then the mass of the bound state, m_c, satisfies $m_c^2 = m_a^2 + m_b^2 + 2m_am_b\cos(u^c_{ab})$.

The form of Eq. (2.54) indicates that we are able to relate $n-1$ particle to n-particle form factors in the presence of bound states. In particular we have

$$
\begin{aligned}
& i g^c_{ab} f(\theta_1, \cdots, \theta_{n-2}, \theta_{n-1})_{a_1,\cdots,a_{n-2},c} = \\
& \qquad \mathrm{res}_{\delta=0} f(\theta_1, \cdots, \theta_{n-2}, \theta_{n-1} - i\bar{u}^{\bar{a}}_{b\bar{c}}, \theta_{n-1} + \delta + i\bar{u}^{\bar{b}}_{a\bar{c}})_{a_1,\cdots,a_{n-2},a,b} \,. \quad (2.56)
\end{aligned}
$$

Thus with theories with bound states, consistency demands that form-factors come equipped with poles indicative of the bound states together with constraints upon the corresponding residues.

2.7. *Form Factors in Finite Temperature Correlators*

Up to this point we have only considered correlation functions at zero temperature. However the form factor approach can also be fruitful at finite temperatures. A finite temperature expansion of correlators is given in terms of a trace over the Boltzmann density matrix,

$$
\begin{aligned}
G^{\mathcal{O}}(x,t) &= \frac{1}{\mathcal{Z}} \mathrm{Tr}(e^{-\beta H} \mathcal{O}(x,t)\mathcal{O}(0,0)) \\
&= \frac{\sum_{ns_n} e^{-\beta E_{s_n}} \langle n, s_n | \mathcal{O}(x,t)\mathcal{O}(0,0) | n, s_n\rangle}{\sum_{ns_n} e^{-\beta E_{s_n}} \langle n, s_n | n, s_n\rangle} \,. \qquad (2.57)
\end{aligned}
$$

Here the state, $|n, s_n\rangle$, denotes a set of n-particles carrying quantum numbers, $\{s_n\}$. Inserting a resolution of the identity between the two fields as we did in the zero temperature case then leads us to a double sum,

$$
G^{\mathcal{O}}(x,t) = \frac{\sum_{\substack{ns_n \\ ms_m}} e^{-\beta E_{s_n}} \langle n, s_n | \mathcal{O}(x,t) | m, s_m\rangle \langle m, s_m | \mathcal{O}(0,0) | n, s_n\rangle}{\sum_{ns_n} e^{-\beta E_{s_n}} \langle n, s_n | n, s_n\rangle} \,. \qquad (2.58)
$$

We thus again have reduced the evaluation of the finite temperature correlator to the evaluation of form factors.

To evaluate this expression for the correlator, we again focus on the associated spectral function, $G^{\mathcal{O}}(k,\omega)$. In computing $G^{\mathcal{O}}(k,\omega)$, only terms in the form factor sum with a given energy, ω, and momentum, k, contribute to the sum, i.e.

$$
\begin{aligned}
G^{\mathcal{O}}(k,\omega) = \frac{1}{\mathcal{Z}} \sum_{\substack{ns_n \\ ms_m}} & \delta(\omega - E_{s_n} + E_{s_m}) \delta(k - p_{s_n} + p_{s_m}) \\
& \times e^{-\beta E_{s_n}} \langle n, s_n | \mathcal{O}(0,0) | m, s_m\rangle \langle m, s_m | \mathcal{O}(0,0) | n, s_n\rangle, \quad (2.59)
\end{aligned}
$$

as enforced by the presence of the two delta functions. For any ω, k, this dramatically reduces the number of matrix elements one must compute.[b] This reduction nonetheless usually leaves a difficult computation. However we can exploit the gapped nature of the spin chain to make the problem more tractable. Because the theory is gapped or massive (with gap, Δ), the correlator admits a low temperature expansion of the form,

$$G^{\mathcal{O}}(k,\omega) = \sum_n \alpha_n(k,\omega) e^{-n\beta\Delta}. \tag{2.60}$$

For the particular correlators of concern in this review and for the range of ω and k in which we are interested, each α_n is determined by a single matrix element. Because we can compute these matrix elements, we obtain an *exact* low temperature expansion.

The ability to compute such an expansion should be compared with the approach taken by LeClair and Mussardo [183] (following Ref. [182]). These authors argued that it was possible to use the same form-factors we employ here to compute finite temperature correlators. However rather than directly evaluate individual terms in the sum appearing in Eq. (2.58), they first conjectured an ansatz involving a resummation of terms in the sum. This procedure was criticized in Ref. [249] (see also Ref. [51]). There it was argued that while this worked for the computation of one-point functions, it was problematic for two-point functions.[c] Rather Ref [249] put forth the view that such problems should be attacked through the use of form factors computed against a thermalized vacuum [107, 108, 176]. However the counterexample cited in [249], a computation involving interacting quantum Hall edge states, involved a gapless theory, and so is in a different class than the models considered in this review. (Without a gap, the low temperature expansion we consider above ceases to make sense.) The results of Section 4 show that it is indeed possible, at least in certain cases, to make sense of the form-factor expansion of two point functions at finite temperature. But while one can make sense of this expansion, it will not be possible to directly compare computations in this review to the ansatz posited in [183]. Their ansatz as is applies only to diagonal theories where scattering does not permute internal quantum numbers, contrary, for example, to the case of the O(3) non-linear sigma model considered in Section 4.

[b] Here $G^{\mathcal{O}}$ is simply the Fourier transform of $G^{\mathcal{O}}(x,t)$, but similar considerations also apply to the corresponding retarded correlator.

[c] That such a procedure is valid for one point functions is also supported by the study in Ref. [236] where form-factors are used to compute CFT correlators.

2.7.1. *Regularization of Form Factors*

Unlike in the zero temperature case, at finite temperature we must compute form factors with particles both to the right and to the left of the field, $\mathcal{O}$,

$$\langle A_{b_m}(\tilde{\theta}_m)\cdots A_{b_1}(\tilde{\theta}_1)\mathcal{O}(0,0)A_{a_n}(\theta_n)\cdots A_{a_1}(\theta_1)\rangle.$$

To understand such an object we must contend with the possibility that $\tilde{\theta}_i = \theta_j$, $a_i = b_j$ for some i, j. From the algebra of the Faddeev–Zamolodchikov operators (Eq. (2.4)), we know the commutation relations involve δ-functions, i.e.

$$A_{a_i}(\tilde{\theta}_i)A^{\dagger}_{b_j}(\theta_j) = 2\pi\delta(\tilde{\theta}_i - \theta_j)\delta_{a_i b_j} + \cdots\ . \tag{2.61}$$

It is crucial to include the contributions of the δ-functions to the correlators. To do so, we must understand the above form factor to equal

$$\begin{aligned}\langle A_{b_m}\ &(\tilde{\theta}_m)\cdots A_{b_1}(\tilde{\theta}_1)\mathcal{O}(0,0)A_{a_n}(\theta_n)\cdots A_{a_1}(\theta_1)\rangle \\ &= \sum_{\substack{\{a_i\}=A_1\cup A_2\\ \{b_i\}=B_1\cup B_2}} S_{A,A_1}S_{B,B_1}\langle B_1|A_1\rangle\langle B_2|\mathcal{O}(0,0)|A_2\rangle_{\text{connected}}.\end{aligned} \tag{2.62}$$

The sum in the above is over all possible subsets of $\{a_i\}$ and $\{b_i\}$. The S-matrix S_{A,A_1} arises from the commutations necessary to rewrite $A_{a_n}(\theta_n)\cdots A_{a_1}(\theta_1)|0\rangle$ as $A_2A_1|0\rangle$ and similarly for S_{B,B_1}. The matrix element, $\langle B_1|A_1\rangle$, is evaluated using the Faddeev–Zamolodchikov algebra. In this way (ill-defined) terms proportional to $\delta(0)$ are produced but which cancel similarly ill-defined terms arising from the evaluation of the partition function.

The 'connected' form factor appearing in the above expression is to be understood as follows. Using crossing symmetry, the form factor can be rewritten as

$$\begin{aligned}&\langle B_2|\mathcal{O}(0,0)|A_2\rangle_{\text{connected}} \\ &= \langle A_{b'_{i_k}}(\tilde{\theta}_{i_k})\cdots A_{b'_{i_1}}(\tilde{\theta}_{i_1})\mathcal{O}(0,0)A_{a'_{j_q}}(\theta_{j_q})\cdots A_{a'_{j_1}}(\theta_{j_1})\rangle_{\text{connected}} \\ &= \langle \mathcal{O}(0,0)A_{a'_{j_q}}(\theta_{j_q})\cdots A_{a'_{j_1}}(\theta_{j_1})A_{\bar{b}'_{i_k}}(\tilde{\theta}_{i_k}-i\pi)\cdots A_{\bar{b}'_{i_1}}(\tilde{\theta}_{i_1}-i\pi)\rangle_{\text{connected}} \\ &= f^{\mathcal{O}}_{\bar{b}'_{i_1}\cdots\bar{b}'_{i_k}a'_{j_1}\cdots a'_{j_q}}(\tilde{\theta}_{i_1}-i\pi,\cdots,\tilde{\theta}_{i_k}-i\pi,\theta_{j_1},\cdots,\theta_{j_q})_{\text{connected}},\end{aligned} \tag{2.63}$$

where the last relation holds provided we do not have $\theta_i = \tilde{\theta}_j$, $a_i = b_j$ for any i, j. If this does occur we see from the annihilation pole axiom that the form factor is not well defined, having a pole at $\theta_i = \tilde{\theta}_j$. In such cases the form factor requires regulation.

To regulate the form factor, we employ a scheme suggested by Balog [29] and used by LeClair and Mussardo [183]. We define

$$
\begin{aligned}
&f^{\mathcal{O}}_{\bar{b}'_{i_1}\cdots\bar{b}'_{i_k}a'_{j_1}\cdots a'_{j_q}}(\tilde{\theta}_{i_1}-i\pi,\cdots,\tilde{\theta}_{i_k}-i\pi,\theta_{j_1},\cdots,\theta_{j_q})_{\text{connected}}\\
&=\underset{\text{piece of}}{\text{finite}}\lim_{\eta_i\to 0} f^{\mathcal{O}}_{\bar{b}'_{i_1}\cdots\bar{b}'_{i_k}a'_{j_1}\cdots a'_{j_q}}(\tilde{\theta}_{i_1}-i\pi+i\eta_1,\cdots,\tilde{\theta}_{i_k}-i\pi+i\eta_k,\theta_{j_1},\cdots,\theta_{j_q})\,.
\end{aligned}
\tag{2.64}
$$

In taking the finite piece of $f^{\mathcal{O}}$, we discard terms proportional to η_i^{-p} as well as terms proportional to η_i/η_j. In this way the connected piece is independent of the way the various limits $\eta_i\to 0$ are taken. Balog [29] has already used this prescription to compute one point functions and successfully compare them to TBA calculations. In Ref. [29] it was argued that the delta functions leading to such terms arise from the use of infinite volume wavefunctions. If such wavefunctions are replaced instead with finite volume counterparts, the delta functions are regulated. For example, a pole in η is changed as follows

$$
\frac{1}{i\eta}=\int d\theta\,\frac{\delta(\theta)}{\theta+i\eta}\to\int d\theta\,\frac{f(\theta)}{\theta+i\eta}\,, \tag{2.65}
$$

where $f(\theta)$ is some sharply peaked function about $\theta=0$ which in the infinite volume limit evolves into a δ-function. However the principal value of this regularized integral is zero. Thus discarding the pole terms is justified in this sense. For terms that are ratios of infinitesimals, Balog also demonstrates that such terms, once regularized, disappear in the infinite volume limit.

3. Sine-Gordon Model and Spin-$\frac{1}{2}$ Quantum Magnets

The first set of applications of massive integral QFTs we will discuss involves the quantum sine-Gordon model (SGM). It describes the low energy limit of a variety of gapped "deformations" of the spin-$\frac{1}{2}$ Heisenberg chain. In order to fix notations and set the stage we first review the low-energy limit of the anisotropic spin-$\frac{1}{2}$ Heisenberg model.

3.1. *The Spin-$\frac{1}{2}$ Heisenberg Chain in a Uniform Magnetic Field*

The anisotropic spin-$\frac{1}{2}$ Heisenberg chain in a uniform "longitudinal" magnetic field H is defined by the Hamiltonian

$$
\mathcal{H}_{\rm XXZ}=J\sum_j S^x_jS^x_{j+1}+S^y_jS^y_{j+1}+\delta S^z_jS^z_{j+1}-H\sum_j S^z_j, \tag{3.1}
$$

and is exactly solvable by Bethe's ansatz [37]. In what follows we will consider only the region

$$-1 < \delta = -\cos(\gamma) \leq 1, \tag{3.2}$$

which corresponds to an "XY"-like exchange anisotropy. Ground state properties, the excitation spectrum in the thermodynamic limit, thermodynamic properties and the large-distance asymptotics of correlation functions have been determined from the Bethe ansatz solution [141, 153, 164, 270–272, 301–303]. Dynamical correlation functions of the lattice model at zero temperature and zero magnetic field have been evaluated in form of a spectral sum using the results of [152] in Refs. [1, 45, 46, 154].

3.1.1. *Excitation Spectrum of the Lattice Model*

The spectrum of low-lying excitations for the isotropic Heisenberg chain in zero field was derived from Bethe's equations [37] in Refs. [98, 99]. It was shown that for even chain lengths the spectrum is given in terms of scattering states of an even number of gapless, elementary excitations carrying spin $\frac{1}{2}$, called "spinons". There are no single-particle excitations: spinons occur only in pairs. The two-spinon continuum is shown in Fig. 3.

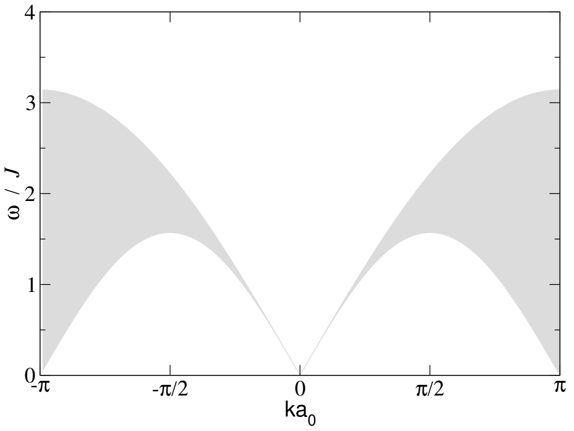

Figure 3. Two-spinon continuum in the isotropic spin-$\frac{1}{2}$ Heisenberg chain ($\delta = 1$) in zero field. The triplet $S = 1$ and singlet $S = 0$ states are degenerate.

Application of magnetic field leads to a change in the ground state properties. For any $H > 0$ there is a finite magnetization per site (see below).

At a critical field

$$H_c = J(1+\delta)\ , \tag{3.3}$$

the ground state becomes fully polarized. At H_c a phase transition between a gapped, commensurate ($H > H_c$) phase and a gapless, incommensurate ($H < H_c$) phase occurs, which is in the universality class of the commensurate-incommensurate transition [80, 127, 237, 253]. In the following we will consider only the gapless regime $H < H_c$.

In the presence of a magnetic field the spectrum is more complicated [155, 213,277]. Now single-particle excitations exist,[d] but they have spectral gaps. The most relevant excitations at low energies are two-fold parametric and are similar in nature to the two-spinon excitations in zero field. We therefore call the elementary excitations giving rise to the gapless two-particle continua for $H > 0$ spinons.[e] The two-spinon excitations with $\delta S^z = 0$ and $\delta S^z = 1$ are shown in Fig. 4. The $\delta S^z = 1$ excitation remains gapless at $P = \pi/a_0$, whereas the $\delta S^z = 0$ excitation becomes gapless at an incommensurate wave number for $H > 0$. Several variants of (3.1) are of considerable interest as they describe situations of direct experimental relevance. However, unlike the Heisenberg model itself these lattice models are not solvable by Bethe's ansatz. Interestingly, the low energy limits of these models are described by integrable massive quantum field theories, which allows for the calculation of the low-energy behavior of dynamical correlation functions. The starting point for all these considerations is the low-energy limit of the Heisenberg model (3.1), which we derive next following a well established procedure [5, 124, 125, 199].

3.1.2. *Continuum Limit*

The Heisenberg chain (3.1) is equivalent to a model of spinless fermions as can be shown by means of the Jordan–Wigner transformation

$$S^z_j = c^\dagger_j c_j - \frac{1}{2}\ ,\quad S^+_j = S^x_j + iS^y_j = c^\dagger_j\ e^{-i\pi\sum_{k<j} c^\dagger_k c_k}\ , \tag{3.4}$$

which maps (3.1) onto

$$\mathcal{H}_{\rm XXZ} = J\sum_j \frac{1}{2}\left[c^\dagger_j c_{j+1} + c^\dagger_{j+1} c_j\right] + \delta\left[c^\dagger_j c_j - \frac{1}{2}\right]\left[c^\dagger_{j+1} c_{j+1} - \frac{1}{2}\right] - H\sum_j c^\dagger_j c_j - \frac{1}{2}. \tag{3.5}$$

[d] They correspond to “string solutions” of the Bethe ansatz equations.
[e] In the literature various other terminologies have been used to denote these excitations.

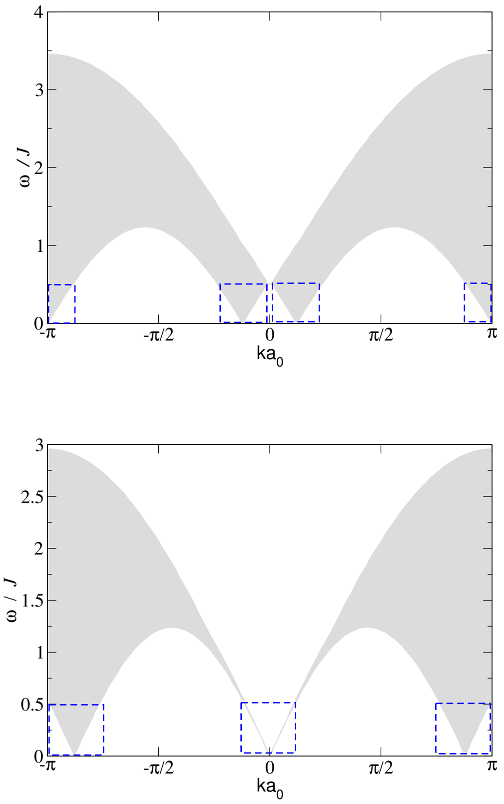

Figure 4. Two-particle continua in the isotropic spin-$\frac{1}{2}$ Heisenberg chain ($\delta = 1$) in an applied field $H = 0.5J$. (a) States with $\delta S^z = 1$, which are probed by the transverse correlation functions $\langle S_n^+(t) S_1^-(0)\rangle$ (b) States with $\delta S^z = 0$ relevant to longitudinal correlation functions $\langle S_n^z(t) S_1^z(0)\rangle$. The boxes indicate the low-energy regime, which is described by the field theory approximation.

It is instructive to analyze (3.5) for small values of δ. Denoting normal ordering by

$$:c_j^\dagger c_j: = c_j^\dagger c_j - \langle c_j^\dagger c_j\rangle, \tag{3.6}$$

we rewrite (3.5) as

$$\begin{aligned}\mathcal{H}_{\rm XXZ} = J\sum_j \frac{1}{2}\left[c_j^\dagger c_{j+1} + c_{j+1}^\dagger c_j\right] + \delta :c_j^\dagger c_j::c_{j+1}^\dagger c_{j+1}:\\ - \left[H + J\delta(1 - 2\langle c_j^\dagger c_j\rangle)\right]\sum_j c_j^\dagger c_j + \text{const.}\end{aligned} \tag{3.7}$$

Neglecting the interaction term, we may diagonalize the quadratic part of (3.7) by Fourier transform and determine the fermion number self-consistently. For small δ the low-energy degrees of freedom are then found to occur in the vicinity of $\pm k_F$, where

$$k_F^0 a_0 = \arccos\Big(\frac{H}{J}\Big)\left[1 - \frac{2\delta}{\pi\sqrt{1-H^2/J^2}}\right] + \frac{\delta}{\sqrt{1-H^2/J^2}} + \mathcal{O}(\delta^2). \quad (3.8)$$

Hence the continuum limit of (3.5) is obtained by keeping only Fourier modes with $k \approx \pm k_F^0$, i.e.

$$c_j \longrightarrow \sqrt{a_0}\left[e^{-ik_F^0 x}R(x) + e^{ik_F^0 x}L(x)\right]. \quad (3.9)$$

Substituting (3.9) into (3.5) we arrive at the low-energy fermion Hamiltonian

$$\begin{aligned}\mathcal{H} = v_F &\int dx\,\left[-iR^\dagger\partial_x R + iL^\dagger\partial_x L\right]\\ &+Ja_0\delta\int dx\ (R^\dagger R + L^\dagger L)(R^\dagger R + L^\dagger L)\\ &+Ja_0\delta\int dx\ (R^\dagger L e^{2ik_F^0 x} + \text{h.c.})(R^\dagger L e^{2ik_F^0(x+a_0)} + \text{h.c.}). \quad (3.10)\end{aligned}$$

Here $v_F = Ja_0\sin(k_F^0 a_0)$ and point splitting and normal ordering are implicit. Finally we may bosonize (3.10) using

$$R^\dagger(x) = \frac{1}{\sqrt{2\pi}}\exp\left(-\frac{i}{\sqrt{2}}\varphi'(x)\right)\ ,\quad L^\dagger(x) = \frac{1}{\sqrt{2\pi}}\exp\left(\frac{i}{\sqrt{2}}\bar\varphi'(x)\right),\ (3.11)$$

where we choose the chiral bosons φ and $\bar\varphi$ to be normalized such that

$$\begin{aligned}\big\langle\exp\big(i\alpha\varphi'(\tau,x)\big)\ \exp\big(-i\alpha\varphi'(0)\big)\big\rangle &= \frac{1}{(v\tau - ix)^{2\alpha^2}}\ ,\\ \big\langle\exp\big(i\alpha\bar\varphi'(\tau,x)\big)\ \exp\big(-i\alpha\bar\varphi'(0)\big)\big\rangle &= \frac{1}{(v\tau + ix)^{2\alpha^2}}\ . \quad (3.12)\end{aligned}$$

The bosonized form of (3.10) is

$$\begin{aligned}\mathcal{H} = \frac{v_F}{16\pi}&\int dx\left[(1+\frac{4\delta\sin(k_F^0a_0)}{\pi})(\partial_x\Phi')^2 + (\partial_x\Theta')^2\right]\\ &+\frac{J\delta\sin(2k_F^0a_0)}{\pi^2\sqrt{8}}\int dx\ \partial_x\Phi' - g\int dx\ \cos\left(\sqrt{2}\Phi' - 4k_F^0x\right), \quad (3.13)\end{aligned}$$

where $g = J\delta a_0^3/2\pi^2$ and the scalar field Φ' and its dual Θ' are defined as

$$\Phi'(x) = \varphi'(x) + \bar\varphi'(x)\ ,\quad \Theta'(x) = \varphi'(x) - \bar\varphi'(x). \quad (3.14)$$

We emphasize that the normalization condition (3.12) implies that the operator $\cos(\sqrt{2}\Phi')$ has dimension length^{-4} and hence the units in Eq. (3.13) are correct. The third term in (3.13) is important only in the vicinity of the isotropic limit $\delta \to 1$ in zero magnetic field. In this limit it is marginally irrelevant and gives rise to logarithmic corrections. These have been calculated by renormalization group improved perturbation theory in Refs. [14,15,33,34,196,198]. The second term in (3.13) is removed by shifting the field Φ'

$$\Phi' \longrightarrow \Phi' - \frac{4\sqrt{2}\delta\cos(k_F^0 a_0)}{\pi a_0}\, x\,. \tag{3.15}$$

It follows from (3.11) and (3.9) that the effect of this shift is to change the Fermi wave number to

$$k_F = k_F^0 + 2\frac{\delta H}{\pi J a_0}\ . \tag{3.16}$$

The canonical transformation

$$\begin{aligned}
\Phi' &= \left[1 + \frac{4\delta\sin(k_F^0 a_0)}{\pi}\right]^{-\frac{1}{4}} \Phi = \frac{1}{\sqrt{8}\tilde{\beta}}\Phi + \mathcal{O}(\delta^2)\ ,\\
\Theta' &= \left[1 + \frac{4\delta\sin(k_F^0 a_0)}{\pi}\right]^{\frac{1}{4}} \Theta = \tilde{\beta}\sqrt{8}\Theta + \mathcal{O}(\delta^2),
\end{aligned} \tag{3.17}$$

brings the Hamiltonian to the standard Gaussian form

$$\mathcal{H} = \frac{v}{16\pi}\int dx\, \left[(\partial_x\Phi)^2 + (\partial_x\Theta)^2\right], \tag{3.18}$$

where

$$v = v_F\left(1 + \frac{2\delta\sin(k_F a_0)}{\pi}\right) + \mathcal{O}(\delta^2). \tag{3.19}$$

Here we have made use of the fact that we are working in the small$-\delta$ limit and all formulas are valid only to lowest order in δ. Importantly, the field Θ' and hence also Θ is compactified, i.e.

$$\Theta(x) \equiv \Theta(x) + \frac{2\pi}{\tilde{\beta}}\ . \tag{3.20}$$

This is a consequence of the U(1) symmetry $c_j \longrightarrow e^{-i\alpha}c_j$ of the fermion Hamiltonian (3.5), under which Φ' is invariant whereas Θ' transforms as $\Theta' \longrightarrow \Theta' + 2\sqrt{2}\alpha$. The identification (3.20) follows by setting $\alpha = 2\pi$ and using that the corresponding $U(1)$ transformation is the identity. Similarly, the field Φ' and hence Φ is compactified,

$$\Phi \equiv \Phi + 8\pi\tilde{\beta}. \tag{3.21}$$

It turns out that the above considerations can be generalized to the entire range (3.2) of δ. This may be done by comparing the $\mathcal{O}(L^{-1})$ spectrum of the Heisenberg Hamiltonian calculated directly from the Bethe ansatz with the spectrum of the compactified boson (3.18). They are found to agree if the compactification radii fulfill (3.21), (3.20) and (3.2) and the velocity v and Fermi wave number k_F are chosen as follows. Let us introduce a dressed energy $\varepsilon(\lambda)$, dressed momentum $p(\lambda)$, dressed density $\rho(\lambda)$ and dressed charge $Z(\lambda)$ through the Fredholm integral equations

$$\begin{aligned}
\varepsilon(\lambda) - \int_{-A}^{A} \frac{d\mu}{2\pi}\ K(\lambda-\mu)\ \varepsilon(\mu) &= H - \frac{J\sin^2\gamma}{\cosh 2\lambda - \cos\gamma}\ ,\\
p(\lambda) &= \frac{2\pi}{a_0}\int_0^{\lambda} d\mu\ \rho(\mu)\ ,\\
\rho(\lambda) - \int_{-A}^{A} \frac{d\mu}{2\pi}\ K(\lambda-\mu)\ \rho(\mu) &= \frac{2\sin\gamma}{2\pi[\cosh 2\lambda - \cos\gamma]}\ ,\\
Z(\lambda) - \int_{-A}^{A} \frac{d\mu}{2\pi}\ K(\lambda-\mu)\ Z(\mu) &= 1\ ,
\end{aligned} \tag{3.22}$$

where $\delta = \cos(\gamma)$ and the integral kernel is given by

$$K(\lambda) = -2\sin 2\gamma/(\cosh 2\lambda - \cos 2\gamma)\,. \tag{3.23}$$

The integration boundary A is fixed by the condition

$$\varepsilon(\pm A) = 0\ . \tag{3.24}$$

The physical meaning of the various quantities is as follows: $\varepsilon(\lambda)$ and $p(\lambda)$ are the energy and momentum of an elementary "spinon" excitation carrying spin $S^z = \pm\frac{1}{2}$. We note that spinons can only be excited in pairs. The magnetization per site in the ground state is given in terms of the ground state root density $\rho(\lambda)$ as

$$\langle S^z_j\rangle = \frac{1}{2} - \int_{-A}^{A} d\lambda\ \rho(\lambda)\,. \tag{3.25}$$

The Fermi momentum is equal to

$$k_F = p(A) = \frac{2\pi}{a_0}\int_0^{A} d\lambda\ \rho(\lambda) = \frac{\pi}{a_0}\left[\frac{1}{2} - \langle S^z_j\rangle\right], \tag{3.26}$$

where we have used that $\rho(-\lambda) = \rho(\lambda)$. The spin velocity is equal to the derivative of the spinon energy with respect to the momentum at the Fermi points

$$v = \frac{\partial\epsilon(\lambda)}{\partial p(\lambda)}\bigg|_{\lambda=A} = \frac{\partial\epsilon(\lambda)/\partial\lambda}{2\pi\rho(\lambda)}\bigg|_{\lambda=A} a_0 \ . \tag{3.27}$$

Finally, the dressed charge is related to $\tilde{\beta}$ by

$$\tilde{\beta} = \frac{1}{\sqrt{8}Z(A)} \ . \tag{3.28}$$

In order to determine v and $\tilde{\beta}$ we solve (3.22) numerically, which is easily done to very high precision as the equations are linear. The results are shown in Fig. 5, 6 and 7.

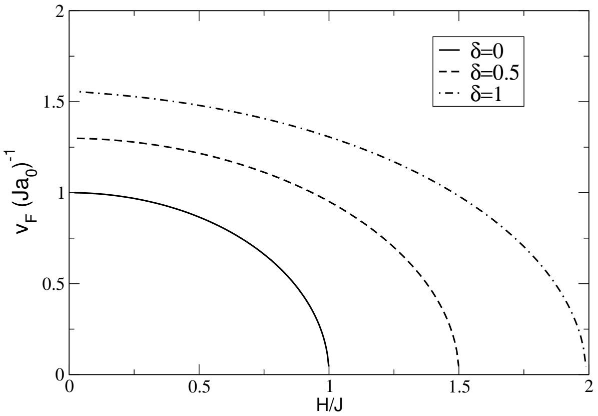

Figure 5. Spin velocity as a function of magnetic field for different values of δ

For zero magnetic field we have $k_F = \pi/2a_0$, $\tilde{\beta}^2 = \frac{1}{4\pi}\arccos(-\delta)$ and

$$v = \frac{Ja_0}{2}\frac{\sin 4\pi\tilde{\beta}^2}{1-4\tilde{\beta}^2} \, . \tag{3.29}$$

For later convenience we define a dimensionless spin velocity by

$$\tilde{v} = \frac{v}{Ja_0} \, . \tag{3.30}$$

In what range of energies do we expect the continuum limit to provide a good description of the physics of the underlying lattice model? In zero field the answer is simply that the energy at which we probe the system must

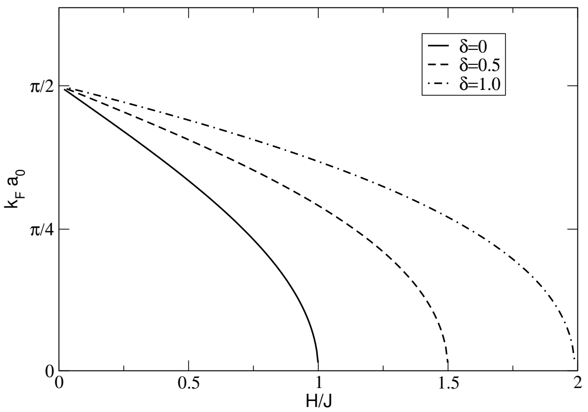

Figure 6. "Fermi momentum" k_F as a function of magnetic field for different values of δ

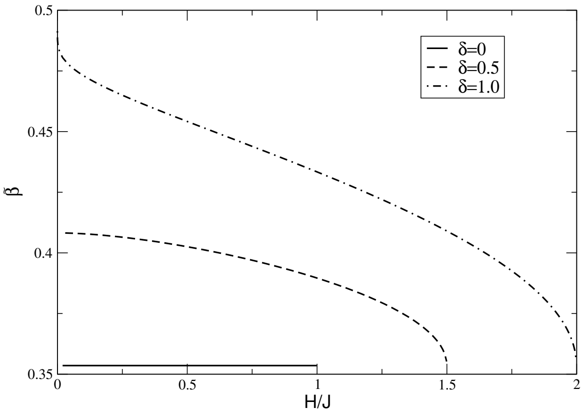

Figure 7. Parameter $\tilde{\beta}$ as a function of magnetic field for different values of δ

be small compared to the cutoff of the continuum theory, which is equal to the exchange integral J. In the presence of a magnetic field, the cutoff is actually provided by H rather than J.

3.1.3. *Operators and their Normalizations*

For small values of δ the lattice spin operators are related to the scalar fields Φ, Θ through formulas (3.4), (3.9), (3.11) and (3.17). A straightforward calculation gives

$$
\begin{aligned}
S_j^z &\sim \frac{a_0}{8\pi\tilde{\beta}}\,\partial_x\Phi - a(H)a_0^{\frac{1}{8\tilde{\beta}^2}}\sin\left(\frac{\Phi}{4\tilde{\beta}} - 2k_F x\right) + \dots\ ,\\
S_j^+ &\sim \mathcal{A}(H)a_0^{\frac{16\tilde{\beta}^2+\tilde{\beta}^{-2}}{8}}(-1)^j\left\{e^{2ik_F x}\ e^{-i(\tilde{\beta}\Theta+\frac{1}{4\tilde{\beta}}\Phi)} + e^{-2ik_F x}\ e^{-i(\tilde{\beta}\Theta-\frac{1}{4\tilde{\beta}}\Phi)}\right\}\\
&\quad +(-1)^j c(H)a_0^{2\tilde{\beta}^2}\ e^{-i\tilde{\beta}\Theta} + \dots\ . \qquad (3.31)
\end{aligned}
$$

The expressions (3.31) turn out to hold for $-1 < \delta \leq 1$ and the dots indicate operators with larger scaling dimensions, which contribute to the subleading terms in the large distance asymptotics of the spin correlation functions. In order to obtain the bosonized expression for S_j^+ it is necessary to symmetrize the Jordan–Wigner string operator as [5]

$$
e^{-i\pi\sum_{k<j}c_j^\dagger c_j} = \frac{1}{2}\left[e^{-i\pi\sum_{k<j}:c_j^\dagger c_j:+\langle c_j^\dagger c_j\rangle} + \text{h.c.}\right], \qquad (3.32)
$$

and use that $\langle c_j^\dagger c_j\rangle = 1 - \frac{k_F a_0}{\pi}$.

Interestingly, the coefficients $a(H=0)$, $c(H=0)$, $\mathcal{A}(H=0)$ are known exactly [196, 198]:

$$
\begin{aligned}
I(a,b,c) &= \left[\frac{\Gamma\left(\frac{\eta}{2-2\eta}\right)}{2\sqrt{\pi}\Gamma\left(\frac{1}{2-2\eta}\right)}\right]^a \exp\left[\int_0^\infty \frac{dt}{2t}\left[\frac{\sinh(bt)}{\sinh(ct)\cosh([1-\eta]t)} - \frac{b}{c}e^{-2t}\right]\right],\\
a(0) &= \frac{\sqrt{2}}{\pi}I\left(\frac{1}{2\eta}, 2\eta-1, \eta\right)\ , \qquad (3.33)\\
c(0) &= \frac{1}{2(1-\eta)}I\left(\frac{\eta}{2}, \eta, -1\right)\ , \qquad (3.34)\\
\mathcal{A}(0) &= \sqrt{2\pi}a(0)c(0)\frac{\Gamma\left(1+\frac{\eta}{2-2\eta}\right)}{\Gamma\left(\frac{3}{2}+\frac{\eta}{2-2\eta}\right)}, \qquad (3.35)
\end{aligned}
$$

where $\eta = 4\tilde{\beta}^2$. We note that the limit $\tilde{\beta} \to \frac{1}{2}$, which corresponds to the isotropic spin-$\frac{1}{2}$ chain $\delta \to 1$ is singular. This is because in this limit a marginally irrelevant interaction of spin currents is present in the Hamiltonian, which gives rise to logarithmic corrections in spin correlation functions. The isotropic limit $\delta \to 1$ is discussed in detail in Refs. [14, 196].

For finite magnetic fields the amplitudes have been determined numerically in [95, 131]. In Table 1 we list the results for the case of the isotropic spin-$\frac{1}{2}$ chain ($\delta = 1$ in (3.1)).

Table 1. Amplitudes a and c, dimensionless spin velocity $\tilde{v}$, coupling $\tilde{\beta}$ and magnetic field H as functions of the magnetization m for the isotropic Heisenberg chain ($\delta = 1$). The amplitudes are determined numerically except for $m = 0.5$ where exact values are shown. The figures in parentheses for a and c indicate the error on the last quoted digits.

m	a	c	$\tilde{v}$	$\tilde{\beta}$	H/J
0.02	0.591(3)	0.4937(3)	1.54271	0.46879	0.17599
0.04	0.550(5)	0.4883(2)	1.51707	0.46095	0.34214
0.06	0.520(4)	0.4863(2)	1.48415	0.45427	0.50013
0.08	0.4947(6)	0.4853(2)	1.44425	0.44812	0.65001
0.10	0.475(1)	0.4847(2)	1.39796	0.44229	0.79164
0.12	0.454(1)	0.4842(2)	1.34593	0.43670	0.92489
0.14	0.437(2)	0.4835(2)	1.28879	0.43129	1.04965
0.16	0.422(2)	0.4825(2)	1.22720	0.42604	1.16589
0.18	0.4070(7)	0.4810(2)	1.16178	0.42094	1.27360
0.20	0.3938(8)	0.4790(2)	1.09314	0.41597	1.37287
0.22	0.3813(6)	0.4764(2)	1.02184	0.41112	1.46380
0.24	0.3700(8)	0.4731(2)	0.94844	0.40639	1.54656
0.26	0.3596(7)	0.4690(2)	0.87347	0.40177	1.62134
0.28	0.3499(4)	0.4639(2)	0.79741	0.39725	1.68839
0.30	0.3406(4)	0.4578(2)	0.72074	0.39284	1.74794
0.32	0.3330(2)	0.4504(2)	0.64387	0.38852	1.80030
0.34	0.3262(2)	0.4416(2)	0.56722	0.38430	1.84575
0.36	0.3200(3)	0.4310(2)	0.49116	0.38017	1.88462
0.38	0.3145(4)	0.4183(2)	0.41602	0.37612	1.91723
0.40	0.3094(2)	0.4029(1)	0.34212	0.37216	1.94390
0.42	0.3070(8)	0.3841(1)	0.26973	0.36828	1.96497
0.44	0.3058(2)	0.3601(1)	0.19912	0.36449	1.98079
0.46	0.3062(6)	0.3284(1)	0.13049	0.36077	1.99168
0.48	0.309(1)	0.2802(1)	0.06407	0.35712	1.99797
0.50	0.3183	0	0	0.35355	2

3.1.4. *Dynamical Spin Correlation Functions*

It is now a straightforward exercise[f] to determine the dynamical spin correlation functions at low energies, i.e. in the regions of the (ω, k)-plane marked in Fig. 4. Using the bosonization dictionary (3.31) we find in imaginary time

---

[f] We exclude the limit $H \to 0$, $\delta \to 1$ from our discussion, see Refs. [14,196] for a discussion of the latter case.

$(\tau = it,\, x = ja_0)$

$$
\begin{aligned}
&\langle T_\tau\ S^+_{j+1}(\tau)\ S^-_1(0)\rangle \sim \\
&\quad \mathcal{A}^2(H) a_0^{4\tilde\beta^2+\frac{1}{4\tilde\beta^2}} (-1)^j \Big\{ e^{2ik_F x}\big\langle T_\tau\ e^{-i\left(\tilde\beta\Theta+\frac{1}{4\tilde\beta}\Phi\right)(\tau,x)} e^{i\left(\tilde\beta\Theta+\frac{1}{4\tilde\beta}\Phi\right)(0,0)}\big\rangle \\
&\qquad\qquad + e^{-2ik_F x}\big\langle T_\tau\ e^{-i\left(\tilde\beta\Theta-\frac{1}{4\tilde\beta}\Phi\right)(\tau,x)} e^{i\left(\tilde\beta\Theta-\frac{1}{4\tilde\beta}\Phi\right)(0,0)}\big\rangle \Big\} \\
&\quad + c^2(H)(-1)^j a_0^{4\tilde\beta^2}\big\langle T_\tau\ e^{-i\tilde\beta\Theta(\tau,x)}\ e^{i\tilde\beta\Theta(0,0)}\big\rangle \\
&\quad = \mathcal{A}^2(H)(-1)^j \left[\frac{a_0^2}{x^2+v^2\tau^2}\right]^{2\tilde\beta^2+1/8\tilde\beta^2} \left\{ e^{2ik_F x}\frac{v\tau+ix}{v\tau-ix} + \text{h.c.}\right\} \\
&\quad + c^2(H)(-1)^j \left[\frac{a_0^2}{x^2+v^2\tau^2}\right]^{2\tilde\beta^2} ,
\end{aligned}
\tag{3.36}
$$

$$
\begin{aligned}
\langle T_\tau\ S^z_{j+1}(\tau)\ S^z_1(0)\rangle &\sim \left[\frac{a_0}{8\pi\tilde\beta}\right]^2 \langle T_\tau\ \partial_x\Phi(\tau,x)\ \partial_x\Phi(0,0)\rangle \\
&\quad + a^2(H) a_0^{\frac{1}{4\tilde\beta^2}} \big\langle T_\tau\ \sin\big(\frac{\Phi(\tau,x)}{4\tilde\beta} - 2k_F x\big)\sin\big(\frac{\Phi(0,0)}{4\tilde\beta}\big)\big\rangle \\
&= \frac{1}{(8\pi\tilde\beta)^2}\frac{a_0^2}{x^2+v^2\tau^2} + a^2(H)\cos(2k_F x)\left[\frac{a_0^2}{x^2+v^2\tau^2}\right]^{\frac{1}{8\tilde\beta^2}} .
\end{aligned}
\tag{3.37}
$$

We see that the slowest decay of correlations occurs with an oscillating factor $(-1)^j$ in the transverse correlations and with factors $\exp(\pm 2ik_F x)$ in the longitudinal ones. Concomitantly their Fourier transforms will be most singular at these wave numbers, which in turn makes $k \approx \pm 2K_F$ and $k \approx \frac{\pi}{a_0}$ the most interesting regions in the Brillouin zone from an experimental point of view. The inelastic neutron scattering intensity is proportional to

$$
I(\omega,\boldsymbol{k}) \propto \sum_{\alpha,\gamma}\left(\delta_{\alpha\gamma} - \frac{k_\alpha k_\gamma}{\boldsymbol{k}^2}\right)\ S^{\alpha\gamma}(\omega,\boldsymbol{k})\ , \tag{3.38}
$$

where $\alpha,\gamma = x,y,z$ and the dynamical structure factor (DSF) $S^{\alpha\gamma}$ is defined by

$$
S^{\alpha\gamma}(\omega,k) = -\frac{1}{\pi}\ \text{Im}\ \chi^{\alpha\gamma}(\omega,k)\ , \tag{3.39}
$$

$$
\chi^{\alpha\gamma}(\omega,k) = -i\sum_l \int_0^\infty dt\ e^{-ikla_0+i\omega t}\langle[S^\alpha_{l+1}(t), S^\gamma_1(0)]\rangle\,. \tag{3.40}
$$

Here k denotes the component of $\boldsymbol{k}$ along the chain direction and $\chi^{\alpha\gamma}(\omega, k)$ are the components of the dynamical susceptibility. We note that in (3.38) only the symmetric combinations $S^{(\alpha\gamma)}(\omega, k) = S^{\alpha\gamma}(\omega, k) + S^{\gamma\alpha}(\omega, k)$ enter. Using a spectral representation one may show that for positive frequencies $\omega > 0$

$$S^{(\alpha\gamma)}(\omega, k) = \sum_l \int_{-\infty}^{\infty} \frac{dt}{2\pi}\ e^{-ikla_0+i\omega t} \left[\langle S^\alpha_{l+1}(t) S^\gamma_1(0)\rangle + \langle S^\gamma_{l+1}(t) S^\alpha_1(0)\rangle\right] . \tag{3.41}$$

We evaluate the retarded correlator in (3.40) by Fourier transforming the corresponding time-ordered correlation function in imaginary time and then analytically continuing to real frequencies. We arrive at the following results for the DSF in the vicinity of $2k_F$ and π/a_0 respectively

$$\begin{aligned} S^{\rm xx}(\omega, \frac{\pi}{a_0} + q) &= S^{\rm yy}(\omega, \frac{\pi}{a_0} + q) = \frac{c^2(H)}{2}\ F\big(\omega^2 - v^2q^2, 2\tilde{\beta}^2\big)\ , \\ S^{\rm zz}(\omega, 2k_F + q) &= \frac{a^2(H)}{2}\ F\Big(\omega^2 - v^2q^2, \frac{1}{8\tilde{\beta}^2}\Big)\ , \\ F(s^2, \alpha) &= \frac{\Gamma(1-\alpha)}{\Gamma(\alpha)}\, \frac{\sin(\pi\alpha)}{2\tilde{v}J} \left[\frac{(2\tilde{v}J)^2}{s^2}\right]^{1-\alpha} . \end{aligned} \tag{3.42}$$

We see that the components of the DSF exhibit power-law singularities. The exponents vary with the applied field and also depend on the exchange anisotropy. However, the transverse components are always more singular than the longitudinal one.

3.2. *Massive Perturbations and Window of Applicability of MIQFT*

As discussed above, the spin-$\frac{1}{2}$ Heisenberg chain is *quantum critical* in the sense that the elementary spinon excitations are gapless and spin correlation functions decay as power laws. In what follows we consider several perturbations of the Heisenberg chain, in which excitations have a gap and spin correlation functions decay exponentially with distance. In particular, we will determine how the DSF is changed compared to the critical form (3.42). One issue to keep in mind that the field theory approach we employ has a limited window of applicability. Field theory becomes exact in particular scaling limits of the underlying lattice models. However, in experimentally relevant situations one usually is at some distance in parameter space from the scaling limit and a practical criterion is needed to judge, whether field theory will provide good approximations to the results for the underlying lattice model. A simple such criterion is that the spectral gap should be small compared to the cutoff set by the lattice model. The latter is simply min(H, J) for the Heisenberg chain in a magnetic field.

3.3. *Field-Induced Gap Problem*

In many materials with low-symmetry crystal structure the coupling of a uniform magnetic field to spin degrees of freedom is of a tensorial nature. In the case where there are two spins per unit cell the g-tensor has generally both uniform and staggered components (see e.g. [229, 230])

$$\mathcal{H}_{\rm mag} = -\mu_B H_a \sum_j [g^u_{ab} + (-1)^j g^s_{ab}] S^b_j \,. \tag{3.43}$$

A low crystal symmetry also frequently results in the presence of a Dzyaloshinskii–Moriya (DM) [81, 210] interaction

$$H_{\rm DM} = \sum_j \mathbf{D}_j \cdot (\mathbf{S}_{j-1} \times \mathbf{S}_j) \,. \tag{3.44}$$

The direction of the DM vector $\mathbf{D}_j$ is constrained by the crystal symmetries. Of particular interest is the case when $\mathbf{D}_j$ has a staggered component, i.e. $\mathbf{D}_j = (-1)^j \mathbf{D}$. It was shown by Oshikawa and Affleck in [226] that in this case the application of a uniform magnetic field $\mathbf{H}$ leads to the generation of a staggered field perpendicular to the direction of $\mathbf{H}$. The effects of having a staggered component of the g-tensor and a staggered DM-interaction are captured by the following model [226]

$$\mathcal{H} = \sum_j J\mathbf{S}_j \cdot \mathbf{S}_{j+1} - HS^z_j - h(-1)^j S^x_j \ . \tag{3.45}$$

Here the staggered field is proportional to the uniform field

$$h = \gamma H \ , \tag{3.46}$$

where $\gamma \ll 1$ depends on the details of the material under investigation. The model (3.45) has been applied successfully to experiments on several quasi-1D spin-$\frac{1}{2}$ Heisenberg magnets: Copper Benzoate $[\mathrm{Cu(C_6D_5COO)_2 \cdot 3D_2O}]$ [16, 19, 20, 71, 72], CDC $[\mathrm{CuCl_2 \cdot 2((CD_3)_2SO)}]$ [161], Copper-Pyrimidine $[(\mathrm{PM \cdot Cu(NO_3)_2 \cdot (H_2O)_2})_n$ (PM=pyrimidine)] [104, 298, 299] and $\mathrm{Yb_4As_3}$ [166, 227]. Theoretical calculations have been carried out for the excitation spectrum [88, 191, 226], the dynamical structure factor [88, 95], the specific heat [89], the magnetic susceptibility [15, 299] and the electron-spin resonance lineshape [228].

Bosonizing the Hamiltonian (3.45) by means of the identities (3.31) yields a sine-Gordon model [226]

$$\mathcal{H} = \frac{v}{16\pi}\int dx\left[(\partial_x\Phi)^2 + (\partial_x\Theta)^2\right] - \mu(h)\int dx\cos(\beta\Theta)\,. \tag{3.47}$$

where in our normalizations $\mu(h)$ is a dimensionful quantity

$$\mu(h) \simeq h\ c(H)\ a_0^{2\beta^2-1}. \tag{3.48}$$

In our approach the velocity v and the parameter β in (3.47) are determined for the lattice Hamiltonian (3.45) with $h = 0$. This is a good approximation as long as h is small compared to H and J. For given J and H, β is then calculated from the Bethe ansatz solution of the Heisenberg model in a uniform field, see Eq. (3.28) and Fig. 7, and

$$\beta \equiv \tilde{\beta}\ . \tag{3.49}$$

Similarly, the spin velocity is given by (3.27) and Fig. 5. The parameters entering the effective SGM are summarized in Table 1.

3.3.1. *Spectrum of the SGM and Quantum Numbers*

It is useful to define a parameter

$$\xi = \frac{\beta^2}{1-\beta^2}\,. \tag{3.50}$$

The spectrum of the sine-Gordon model (3.47) in the relevant range of β consists of a soliton-antisoliton doublet and several soliton-antisoliton bound states called "breathers." There are altogether $[1/\xi]$ breathers, where $[x]$ denotes the integer part of x. The breather gaps [63, 97] can be determined for example from the Bethe ansatz solution of the massive Thirring model [38, 175] and are given by

$$\Delta_n = 2\Delta\sin\left(\frac{\pi\xi n}{2}\right),\quad n = 1,\ldots,\left[\frac{1}{\xi}\right]. \tag{3.51}$$

Here Δ is the gap for soliton and antisoliton. The parameter ξ depends on the applied uniform field H through β. We introduce labels B_n for the n$^{\rm th}$ breather, s for the soliton and $\bar{s}$ for the antisoliton. A convenient basis for the SGM (3.47) can be constructed in terms of scattering states of (anti)solitons and breathers by means of the Faddeev–Zamolodchikov algebra (see Section 2.2). The action of the charge conjugation operator C on these basis states

states follows from

$$\begin{aligned} C|0\rangle &= |0\rangle\,, \\ CA_s^\dagger(\theta)C^{-1} &= A_{\bar{s}}^\dagger(\theta)\,, \\ CA_{B_n}^\dagger(\theta)C^{-1} &= (-1)^n A_{B_n}^\dagger(\theta)\,. \end{aligned} \tag{3.52}$$

The topological charge

$$Q = \frac{\beta}{2\pi}\int_{-\infty}^{\infty} dx\ \partial_x \Theta\,, \tag{3.53}$$

is a conserved quantity in the sine-Gordon model. We will use conventions in which soliton and antisoliton have topological charges -1 and 1 respectively. Breathers have topological charge zero and so are neutral.

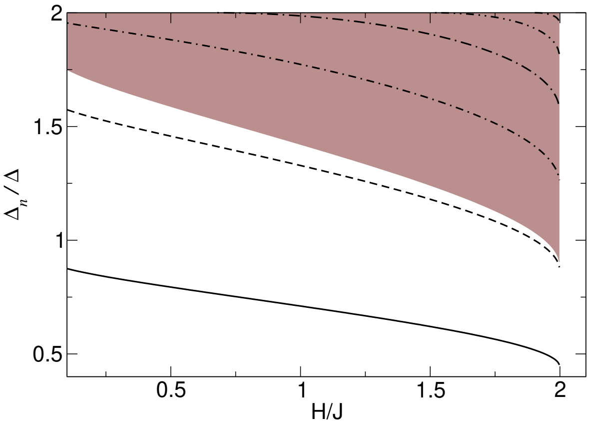

Figure 8. Breather gaps Δ_n is units of the soliton gap Δ as functions of the magnetic field. We note that Δ itself depends on H as well. The shaded area is the B_1-B_1 two-breather continuum. As the field is increased more breathers split off from the soliton-antisoliton continuum with threshold 2Δ.

The soliton gap as a function of the parameters H and h of the underlying spin chain was determined in Ref. [15] in the regime $\Delta \ll H$, where

$$\frac{\Delta}{J} \simeq \left(\frac{h}{J}\right)^{(1+\xi)/2}\left[B\left(\frac{J}{H}\right)^{\frac{1}{2}-2\beta^2}\left(2-8\beta^2\right)^{1/4}\right]^{-(1+\xi)/2}\,, \tag{3.54}$$

with $B = 0.422169$. Equation (3.54) is applicable as long as H is sufficiently smaller than J or more precisely as long as the magnetization is small. In the derivation of (3.54) both the magnetic field dependences of spin velocity and the normalization constants a and c of the spin operators in (3.31) have been neglected, which is justified in weak fields. An additional complication in weak fields is the presence of a only slightly irrelevant perturbation to the free bosonic effective Hamiltonian describing the low energy physics of the Heisenberg chain (see Eq. (3.13)). By taking this perturbation into account, renormalization group improved perturbation theory essentially leads to the result (3.54).

For magnetic fields comparable to J it is necessary to take into account the magnetic field dependences of the spin velocity and the normalization $c(H)$ of the spin operator, whereas the effects of the irrelevant perturbations to the free boson Hamiltonian may be neglected. Using the results of Ref. [317] we obtain the following expression for the gap in the regime of H comparable to J (but still $h \ll J$)

$$\frac{\Delta}{J} \simeq \frac{2\tilde{v}(H)}{\sqrt{\pi}} \frac{\Gamma(\frac{\xi}{2})}{\Gamma(\frac{1+\xi}{2})} \left[\frac{c(H)\pi}{2\tilde{v}(H)} \frac{\Gamma(\frac{1}{1+\xi})}{\Gamma(\frac{\xi}{1+\xi})} \frac{h}{J} \right]^{(1+\xi)/2} . \tag{3.55}$$

Here $\tilde{v} = v/(Ja_0)$ is the "dimensionless spin velocity".

3.3.2. *Thermodynamics*

The thermodynamics of the SGM is most efficiently studied [74] *via* the recently developed Thermal Bethe Ansatz approach [73, 164, 167, 268, 273], which circumvents problems associated with solving the infinite number of coupled nonlinear integral equations that emerge in the standard approach based on the string hypothesis [105, 106] (note that the coupling constant β in our problem is a continuously varying quantity and no truncation to a finite number of coupled equations is possible). It was shown in [74] that the free energy of the SGM can be expressed in terms of the solution of a single nonlinear integral equation for the complex quantity $\varepsilon(\theta)$ (we set $k_B = 1$)

$$\begin{aligned} \varepsilon(\theta) = -i\frac{\Delta}{T}\sinh(\theta + i\eta') &- \int_{-\infty}^{\infty} d\theta' G_0(\theta - \theta') \ln\left(1 + \exp\left[-\varepsilon(\theta')\right]\right) \\ &+ \int_{-\infty}^{\infty} d\theta' G_0(\theta - \theta' + 2i\eta') \ln\left(1 + \exp\left[-\bar{\varepsilon}(\theta')\right]\right), \end{aligned} \tag{3.56}$$

where Δ is the soliton mass and

$$G_0(\theta) = \int_0^{\infty} \frac{d\omega}{\pi^2} \frac{\cos(2\omega\theta/\pi)\sinh(\omega(\xi - 1))}{\sinh(\omega\xi)\cosh(\omega)} . \tag{3.57}$$

The free energy density is given by

$$f(T) = -\frac{T\Delta}{\pi v}\ \mathrm{Im} \int_{-\infty}^{\infty} d\theta\ \sinh(\theta + i\eta') \ln\left[1 + e^{-\varepsilon(\theta)}\right] . \tag{3.58}$$

As we are interested in the attractive regime $\gamma < 4\pi$ we have

$$0 < \eta' < \pi\xi/2\ . \tag{3.59}$$

Note that the free energy does not depend on the value of η' as long as it is chosen in the interval (3.59). The set (3.56) of two coupled nonlinear integral equations is solved by iteration. For $T \to 0$ the first iterations can be calculated analytically and the corresponding contributions to the free energy density are seen to be of the form

$$f(T) \sim -\frac{2T\Delta}{\pi v} \sum_{n=1}^{\infty} \frac{(-1)^{n+1}}{n} K_1\left(\frac{n\Delta}{T}\right) - \frac{T\Delta_1}{\pi v} K_1\left(\frac{\Delta_1}{T}\right) + \dots\ , \tag{3.60}$$

where $\Delta_1 = 2\Delta \sin\frac{\pi\xi}{2}$ is the mass of the first breather and K_1 is a modified Bessel function. The first term is the contribution of soliton-antisoliton scattering states to the free energy, whereas the second term is the contribution of the first breather. Both terms have the form characteristic of massive relativistic bosons. The contributions of the heavier breathers are found in higher orders of the iterative procedure employed in solving (3.56). The specific heat is obtained from the free energy

$$C = T\,\frac{\partial^2 f(T)}{\partial T^2}\ . \tag{3.61}$$

At low temperatures it is found to be of the form

$$C \approx \sum_{\alpha=0}^{[1/\xi]} \frac{(1+\delta_{\alpha 0})\Delta_\alpha}{\sqrt{2\pi} v} \left[1 + \frac{T}{\Delta_\alpha} + \frac{3}{4}\left(\frac{T}{\Delta_\alpha}\right)^2\right] \left(\frac{\Delta_\alpha}{T}\right)^{\frac{3}{2}} \exp\left(-\frac{\Delta_\alpha}{T}\right), \tag{3.62}$$

where $\Delta_0 \equiv \Delta$. In order to compare theoretical predictions based on the SGM with the specific heat data of [72] we need the free energy at "intermediate" temperatures and thus have to resort to a numerical solution of (3.56) by iteration. A detailed comparison of the specific heat calculated in the framework of the low-energy effective sine-Gordon theory to experimental data on Copper Benzoate was carried out in Ref. [[89]]. In Fig. 9 we show a fit of the specific heat calculated from (3.61) [89] to data taken for a particular orientation of the magnetic field on Copper Benzoate [72].

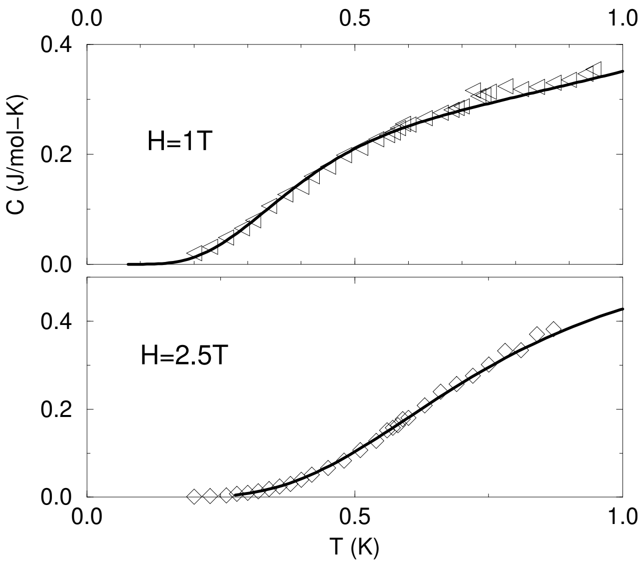

Figure 9. Specific heat as a function of temperature for fields of H=1T and H=2.5T applied along the c'' axis.

3.3.3. *Normalization of Form Factors in the Sine-Gordon Model*

The short-distance behavior of correlation function in the sine-Gordon model is governed by the operator product expansion (in imaginary time)

$$\lim_{x^2+v^2\tau^2\to 0} e^{i\alpha\Phi(\tau,x)}\ e^{i\alpha'\Phi(0,0)} = |x^2+v^2\tau^2|^{2\alpha\alpha'}\ e^{i(\alpha+\alpha')\Phi(0,0)}. \tag{3.63}$$

Given the normalization implied by (3.63) the large-distance asymptotics is [g]

$$\lim_{x^2+v^2\tau^2\to\infty} \left\langle e^{i\alpha\Phi(\tau,x)}\ e^{i\alpha'\Phi(0,0)}\right\rangle = \left\langle e^{i\alpha\Phi}\right\rangle \left\langle e^{i\alpha'\Phi}\right\rangle. \tag{3.64}$$

where the one-point functions have been determined in [195]

$$\mathcal{G}_\alpha = a_0^{2\alpha^2}\langle e^{i\alpha\Theta(0,0)}\rangle = \left(\frac{\Delta}{J\tilde{v}}\frac{\sqrt{\pi}}{2}\frac{\Gamma\left((1+\xi)/2\right)}{\Gamma(\xi/2)}\right)^{2\alpha^2}$$
$$\times \exp\left[\int_0^\infty \frac{dt}{t}\left(\frac{\sinh^2(\alpha\beta t)}{2\sinh(\frac{\beta^2}{2}t)\sinh(\frac{t}{2})\cosh[\frac{1-\beta^2}{2}t]} - 2\alpha^2 e^{-t}\right)\right]. \tag{3.65}$$

Equation (3.64) can be used to fix the overall constant factor in the form factor expansion of correlation functions.

[g] Here we do not consider the connected correlation function.

3.3.4. *Dynamical Structure Factor*

Let us now turn to the issue how the staggered field modifies the dynamical structure factor. Without a staggered field one simply has the result (3.42). At low energies the field theory description can be used to determine the dynamical spin-spin correlation functions. We substitute the decomposition (3.31) into the expression (3.40) for the dynamical susceptibility. Neglecting the contributions of rapidly oscillating terms to the integrals, we find that

$$\chi^{\rm xx}(\omega,\frac{\pi}{a_0}+q)\simeq -ic^2(H)a_0^{4\beta^2-1}\int_{-\infty}^{\infty}dx\int_0^{\infty}dt\ e^{i\omega t-iqx}\\ \times\ \langle[\cos(\beta\Theta(t,x)),\cos(\beta\Theta(0)]\rangle, \qquad (3.66)$$

$$\chi^{\rm yy}(\omega,\frac{\pi}{a_0}+q)\simeq -ic^2(H)a_0^{4\beta^2-1}\int_{-\infty}^{\infty}dx\int_0^{\infty}dt\ e^{i\omega t-iqx}\\ \times\ \langle[\sin(\beta\Theta(t,x)),\sin(\beta\Theta(0)]\rangle, \qquad (3.67)$$

$$\chi^{\rm zz}(\omega,\pm 2k_F+q)\simeq \pm\frac{a^2(H)a_0^{\frac{1}{4\beta^2}-1}}{2}\int_{-\infty}^{\infty}dx\int_0^{\infty}dt\ e^{i\omega t-iqx}\\ \times\ \left\langle\Big[\exp\left(\mp i\frac{\Phi(t,x)}{4\beta}\right),\sin\left(\frac{\Phi(0)}{4\beta}\right)\Big]\right\rangle. \qquad (3.68)$$

Using a spectral representation in terms of scattering states of solitons, antisolitons and breathers (2.2) we have e.g.

$$\chi^{\rm xx}(\omega,\frac{2\pi}{a_0}+q)=\pi c^2(H)a_0^{4\beta^2-1}\sum_{n=1}^{\infty}\sum_{\varepsilon_i}\int\frac{d\theta_1\dots d\theta_n}{(2\pi)^n n!}\\ \times|\langle 0|\cos\beta\Theta(0)|\theta_n,\dots,\theta_1\rangle_{\varepsilon_n,\dots,\varepsilon_1}|^2\\ \times\left\{\frac{\delta(q-\sum_j\frac{\Delta_{\epsilon_j}}{v}\sinh\theta_j)}{\omega-\sum_j\Delta_{\epsilon_j}\cosh\theta_j+i\epsilon}-\frac{\delta(q+\sum_j\frac{\Delta_{\epsilon_j}}{v}\sinh\theta_j)}{\omega+\sum_j\Delta_{\epsilon_j}\cosh\theta_j+i\epsilon}\right\}. \qquad (3.69)$$

Here the indices $\varepsilon_j\in\{s,\bar{s},B_1,B_2,\dots,B_{[1/\xi]}\}$ and $\Delta_s=\Delta_{\bar{s}}\equiv\Delta$, $\Delta_{B_n}\equiv\Delta_n$. Many of the form factors actually vanish for the operators we are interested in here. Using the transformation property of the scalar field Θ under charge conjugation

$$C\Theta C^{-1}=-\Theta, \qquad (3.70)$$

we observe see that by virtue of (3.52)

$$\begin{aligned} \langle 0|\cos(\beta\Theta(0))|\theta\rangle_{B_{2n-1}} &= 0\ , \\ \langle 0|\sin(\beta\Theta(0))|\theta\rangle_{B_{2n}} &= 0\ , \\ \langle 0|\sin(\beta\Theta(0))|\theta_2,\theta_1\rangle_{B_n,B_n} &= 0\ , \end{aligned} \tag{3.71}$$

and so on. On the other hand, the $\pm 2k_F$ components of S^z carry topological charge ± 1. This follows from their commutators with the operator (3.53)

$$\left[Q, \exp\left(\pm i\frac{n}{4\beta}\Phi\right)\right] = \mp n \exp\left(\pm i\frac{n}{4\beta}\Phi\right). \tag{3.72}$$

As a result the only non-vanishing form factors are of the form

$$\langle 0|e^{-\frac{i}{4\beta}\Phi(0)}|\theta\rangle_s\ ,\ \langle 0|e^{-\frac{i}{4\beta}\Phi(0)}|\theta_1,\theta_2\rangle_{s,B_m}\ ,\ \langle 0|e^{-\frac{i}{4\beta}\Phi(0)}|\theta_1,\theta_2,\theta_3\rangle_{s,s,\bar{s}}\ , \tag{3.73}$$

and so on. Combining (3.71), (3.73) and (3.68) we can identify which excited states inelastic neutron scattering experiments probe at different momentum transfers. This is summarized in Fig. 10.

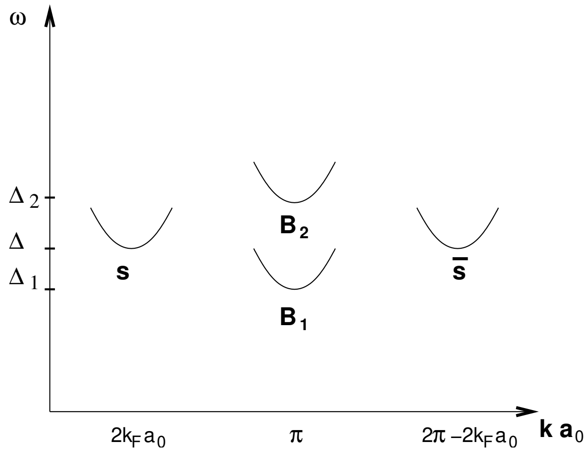

Figure 10. Schematic structure of the lowest-energy excited states relevant to neutron scattering experiments. Soliton and antisoliton occur in the vicinity of the incommensurate wave numbers $2k_F$, $2(\frac{\pi}{a_0} - k_F)$ and are seen in S^{zz}, whereas the first breather B_1 occurs in the vicinity of π/a_0 and contributes to S^{yy}. At higher energies further breather bound states as well as multi-particle scattering continua are present.

The form factors required to evaluate the first few terms in the spectral representation (3.69) have been determined in [23–25, 194, 197, 262, 264]. Determining the breather form factors via the bootstrap axiom (2.56) one obtains [88]

$$S^{\rm xx}(\omega,\frac{\pi}{a_0}+q)=\mathcal{C}_x(H)\ {\rm Re}\Biggl\{2\pi\sum_{n=1}^{[1/\xi]}Z_{2n}\ \delta(s^2-\Delta_{2n}^2)$$
$$+\frac{|F_{11}^{\cos(\beta\Theta)}[\theta(\Delta_1,\Delta_1,s)]|^2}{s\sqrt{s^2-4\Delta_1^2}}+2\frac{|F_{+-}^{\cos(\beta\Theta)}[\theta(\Delta,\Delta,s)]|^2}{s\sqrt{s^2-4\Delta^2}}+\dots\Biggr\},\quad(3.74)$$

where

$$\theta(m_1,m_2,s)={\rm arccosh}\left(\frac{s^2-m_1^2-m_2^2}{2m_1m_2}\right)\ ,\quad(3.75)$$

and the overall normalization is given by

$$\mathcal{C}_x(H)=\frac{1}{\pi}\,c^2(H)\tilde{v}(H)J\ \mathcal{G}_\beta^2\,.\quad(3.76)$$

Here $\mathcal{G}_\beta$ is given by (3.65). As we are dealing with a two point function of a Lorentz scalar, the susceptibility depends only on the Mandelstam variable

$$s=\sqrt{\omega^2-v^2q^2}.\quad(3.77)$$

The first terms in (3.74) correspond to single-particle breather states and are given by [88]

$$Z_2=\frac{2(\sin 2\pi\xi)^2}{\cot\pi\xi}\ \exp\left[-2\int_0^\infty\frac{dx}{x}\ \frac{(\sinh 2\xi x)^2\sinh x(1-\xi)}{\cosh x\ \sinh 2x\ \sinh\xi x}\right],\quad(3.78)$$
$$Z_4=\frac{2(\sin 4\pi\xi)^2}{(\cot\pi\xi)^2(\cot 3\pi\xi/2)^2}$$
$$\times\exp\left[-2\int_0^\infty\frac{dx}{x}\ \frac{(\sinh 4\xi x)^2\sinh x(1-\xi)}{\cosh x\ \sinh 2x\ \sinh\xi x}\right].\quad(3.79)$$

The soliton-antisoliton contribution is

$$|F_{+-}^{\cos(\beta\Theta)}(\theta)|^2=\frac{(2\cot\pi\xi/2\ \sinh\theta)^2}{\xi^2}\frac{\cosh\theta/\xi+\cos\pi/\xi}{\cosh 2\theta/\xi-\cos 2\pi/\xi}E(\theta),\quad(3.80)$$
$$E(\theta)=\exp\left[\int_0^\infty\frac{dx}{x}\frac{[\cosh 2x\cos 2x\theta/\pi-1]\sinh x(\xi-1)}{\cosh x\ \sinh 2x\ \sinh\xi x}\right].\quad(3.81)$$

and the B_1B_1 breather-breather contribution is

$$|F_{11}^{\cos(\beta\Theta)}(\theta)|^2 = \left[2\cos\frac{\pi\xi}{2}\sqrt{2\sin\frac{\pi\xi}{2}}\right]^4 \exp\left[-4\int_0^{\pi\xi}\frac{dx}{2\pi}\frac{x}{\sin x}\right]$$

$$\times\frac{(\sinh\theta)^2}{(\sinh\theta)^2+(\sin\pi\xi)^2}\exp\left[-4\int_0^\infty\frac{dx}{x}\frac{\cos\frac{2x\theta}{\pi}\sinh\xi x\sinh x(1+\xi)}{\sinh 2x\cosh x}\right]. \quad (3.82)$$

The next most important contribution (*i.e.* the term with the lowest threshold) in the expansion (3.74) comes from B_1B_3 breather-breather states. It will contribute at energies larger than $\Delta_1+\Delta_3$, where $\Delta_{1,3}$ are given by (3.51). In Fig. 11 we plot $S^{\rm xx}(\omega,\frac{\pi}{a_0}+q)$ as a function of $s=\sqrt{\omega^2+v^2q^2}$ for two values of the magnetization m. We see that the coherent particle peak due to the second breather carries most of the spectral weight. For $m=0.1$ the contribution due to the soliton-antisoliton continuum is considerably sharper above the threshold than for $m=0.03$. This is because the $s\bar{s}$ continuum has just given birth to the fourth breather. The latter has a very small binding energy and carries very little spectral weight. In general the $s\bar{s}$ continuum becomes singular at the threshold, whenever a new breather peak splits off from it.

Let us now turn to the yy component of the dynamical susceptibility. As the U(1) spin rotational symmetry around the axis of the uniform field H is broken by the staggered field h, $\chi^{\rm yy}$ must be different from $\chi^{\rm xx}(\omega,q)$. The form factor expansion yields

$$S^{\rm yy}(\omega,\frac{\pi}{a_0}+q) = \mathcal{C}_x(H)\ \mathrm{Re}\left\{2\pi\sum_{n=1}^{[1/\xi]} Z_{2n-1}\ \delta(s^2-\Delta_{2n-1}^2)\right.$$

$$\left.+\frac{2|F_{+-}^{\sin(\beta\Theta)}[\theta(\Delta,\Delta,s)]|^2}{s\sqrt{s^2-4\Delta^2}}+\frac{2|F_{12}^{\sin(\beta\Theta)}[\theta(\Delta_1,\Delta_2,s)]|^2}{\sqrt{(s^2-\Delta_1^2-\Delta_2^2)^2-4\Delta_1^2\Delta_2^2}}+\dots\right\}. \quad (3.83)$$

Here the breather contributions are

$$Z_1 = \frac{8(\cos\frac{\pi\xi}{2})^4}{\cot\frac{\pi\xi}{2}}\exp\left[-2\int_0^\infty\frac{dx}{x}\ \frac{\sinh\xi x\ \sinh x(1-\xi)}{\cosh x\ \sinh 2x}\right], \quad (3.84)$$

$$Z_3 = \frac{4\sin(3\pi\xi)(\sin\frac{3\pi\xi}{2})^2}{(\cot\pi\xi)^2}$$
$$\times\exp\left[-2\int_0^\infty\frac{dx}{x}\ \frac{(\sinh 3\xi x)^2\sinh x(1-\xi)}{\cosh x\ \sinh 2x\ \sinh\xi x}\right]. \quad (3.85)$$

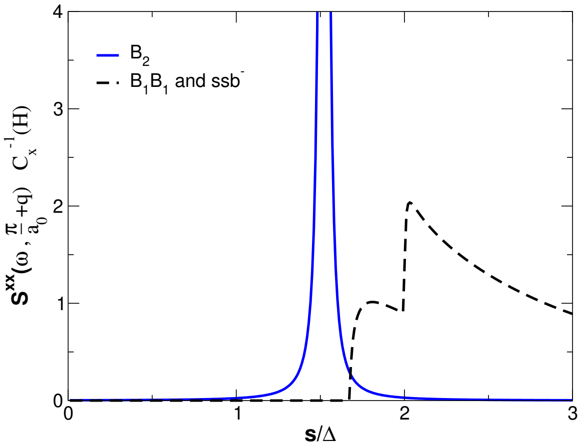

(a)

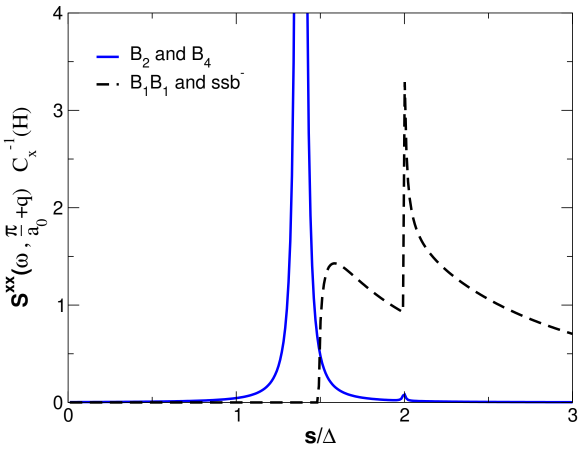

(b)

Figure 11. xx component of the dynamical structure factor for magnetizations (a) $m = 0.03$ and (b) $m = 0.1$. The delta-functions corresponding to the second breather have been broadened by a Lorentzian to make them visible.

The soliton-antisoliton contribution is

$$|F_{+-}^{\sin(\beta\Theta)}(\theta)|^2 = \frac{(2\cot\pi\xi/2\ \sinh\theta)^2}{\xi^2}\ \frac{\cosh\theta/\xi - \cos\pi/\xi}{\cosh 2\theta/\xi - \cos 2\pi/\xi}\, E(\theta)\,, \quad (3.86)$$

where $E(\theta)$ is given by (3.81). Finally we take into account the B_1B_2

breather-breather state which contributes

$$|F_{12}^{\sin(\beta\Theta)}(\theta)|^2 = \frac{\tan\pi\xi}{2}\left|\frac{\sinh^2(\theta - i\frac{\pi\xi}{2})}{\sinh^2(\theta - i\frac{\pi\xi}{2}) + \sin^2\pi\xi}\right|^2 \left[2\cos\frac{\pi\xi}{2}\sqrt{2\sin\frac{\pi\xi}{2}}\right]^6$$
$$\times \exp\left[-6\int_0^{\pi\xi}\frac{dx}{2\pi}\frac{x}{\sin x}\right]\left[1 + \frac{1}{4\cos\frac{\pi\xi}{2}(\cosh\theta + \cos\frac{\pi\xi}{2})}\right]^2$$
$$\times \exp\left[-4\int_0^{\infty}\frac{dx}{x}\frac{[\cos\frac{x\theta}{\pi}\sinh\xi x + \cosh x\xi \sinh\left(\frac{\xi x}{2}\right)]\sinh\left(x\frac{1+\xi}{2}\right)}{\sinh x\cosh\left(\frac{x}{2}\right)}\right]. \quad (3.87)$$

The next most important contribution to (3.83) is due to $B_1B_1B_1$ three breather states with a threshold at $3\Delta_1$.

The leading contributions to the longitudinal structure factor at the incommensurate wave numbers $2k_F$, $\frac{2\pi}{a_0} - 2k_F$ are due to soliton and antisoliton single-particle states. The form factor $\langle 0|e^{-\frac{i}{4\beta}\Phi(0)}|\theta\rangle_s$ is a rapidity-independent constant (as the operator is a Lorentz scalar), which has been determined by Lukyanov and Zamolodchikov Ref. [197]. A simple calculation then gives [95]

$$S^{zz}(\omega, 2k_F + q) = \mathcal{C}_z(H)\ 2\pi\ \mathcal{Z}_1\ \delta\left(\omega^2 - (vq)^2 - \Delta^2\right), \quad (3.88)$$

where $\mathcal{C}_z(H) = \frac{\tilde{v}J}{4\pi}\ a^2(H)$,

$$\mathcal{Z}_n = \left(\frac{\mathcal{C}_2}{2\mathcal{C}_1^2}\right)^{\frac{n}{2}}\left(\frac{16}{\xi\mathcal{C}_2}\right)^{\frac{n^2}{4}}\left(\frac{\sqrt{\pi}\ \Delta\Gamma\left(\frac{3}{2}+\frac{\xi}{2}\right)}{J\tilde{v}\Gamma\left(\frac{\xi}{2}\right)}\right)^{\frac{n^2}{4\beta^2}}$$
$$\times \exp\left[\int_0^\infty\frac{dt}{t}\left(\frac{\exp[-(1+\xi)nt] - 1}{2\sinh(\xi t)\sinh[(1+\xi)t]\cosh(t)} + \frac{n}{2\sinh(t\xi)} - \frac{n^2e^{-2t}}{4\beta^2}\right)\right]. \quad (3.89)$$

Here the constants $\mathcal{C}_{1,2}$ are given by [197]

$$\mathcal{C}_1 = \exp\left(-\int_0^\infty\frac{dt}{t}\frac{\sinh^2(t/2)\ \sinh[t(\xi-1)]}{\sinh(2t)\ \sinh(\xi t)\ \cosh(t)}\right), \quad (3.90)$$

$$\mathcal{C}_2 = \exp\left(4\int_0^\infty\frac{dt}{t}\frac{\sinh^2(t/2)\ \sinh[t(\xi-1)]}{\sinh(2t)\ \sinh(\xi t)}\right). \quad (3.91)$$

As was pointed out in Ref. [15], at $H = 0$ the low-energy effective theory of (3.45) is SU(2) symmetric. In our notations this implies that

$$\lim_{H\to 0}\frac{2\pi\mathcal{C}_x Z_1}{c^2(H)} = 2\lim_{H\to 0}\frac{2\pi\mathcal{C}_z\mathcal{Z}_1}{a^2(H)}\ . \quad (3.92)$$

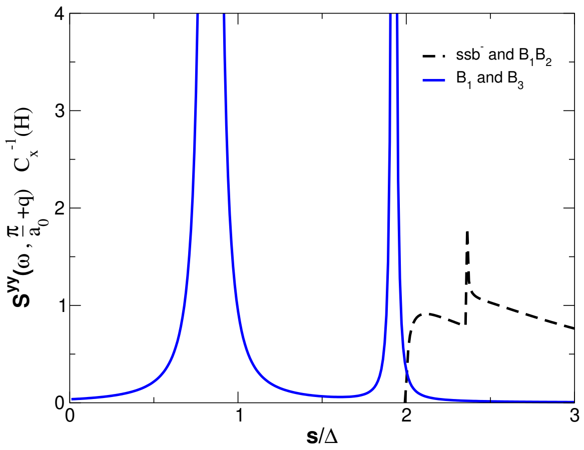

(a)

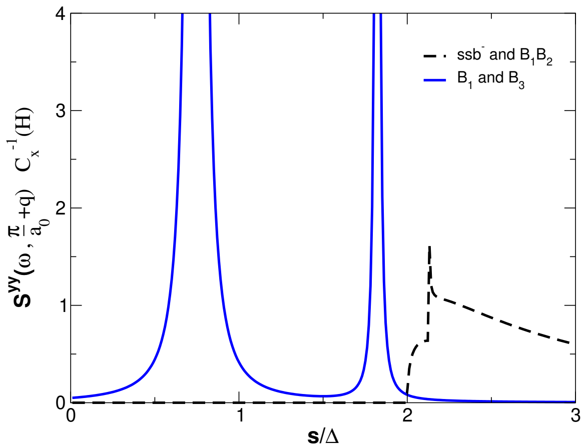

(b)

Figure 12. yy component of the dynamical structure factor for magnetizations (a) $m = 0.03$ and (b) $m = 0.1$. The delta-functions corresponding to the first and third breathers have been broadened by a Lorentzian to make them visible.

Equation (3.92) is easily verified numerically.

3.4. *Transverse-Field Model*

Some quasi-1D spin-$\frac{1}{2}$ antiferromagnets are described by Heisenberg models with exchange anisotropy. One example is Cs_2CoCl_4 [160], where the Co spin-$\frac{3}{2}$ multiplets are split by a strong single-ion anisotropy. Projecting to the low-lying spin-$\frac{1}{2}$ doublet leads to a Hamiltonian of the form (3.93) with $\delta = \frac{1}{4}$ and $H = 0$. Anisotropic Heisenberg models can also be used to describe spin chains with Dzyaloshinskii–Moriya [81, 210] interaction. The bulk DM interaction can be removed by a gauge transformation (local rotation of the coordinate system in spin space); the resulting Hamiltonian has an exchange anisotropy and twisted boundary conditions (in a ring geometry) [17, 200].

When applying a magnetic field to an anisotropic Heisenberg model we have to distinguish between two cases:

(i) the magnetic field is along the direction singled out by the anisotropy and leaves the spin rotational $U(1)$ symmetry of the Hamiltonian unchanged;

(ii) the magnetic field is at an angle to the direction singled out by the anisotropy and breaks the spin rotational $U(1)$ symmetry of the Hamiltonian.

In case (i) the model remains exactly solvable and has been discussed in section 3.1. The simplest realization of case (ii) is when the field is perpendicular to the anisotropy

$$\mathcal{H} = \sum_j J[S_j^x S_{j+1}^x + S_j^y S_{j+1}^y + \delta S_j^z S_{j+1}^z] - HS_j^x \ , \tag{3.93}$$

where $\delta < 1$. The model (3.93) has been studied in Refs. [50, 54, 75, 76]. At low fields there are both uniform and staggered ordered moments and excitations are gapped. At a critical field $H_c(\delta)$ there is quantum phase transition in the universality class of the 2D Ising model, at which the staggered magnetization vanishes. In high fields only the uniform magnetization remains and excitations are again gapped. The simplest case to deal with by field theory methods is the one where the magnetic field H is much stronger than the anisotropy $J(1-\delta)$, but is smaller than $H_c(\delta)$. The field theory limit in this case has been studied in Refs. [54, 89, 228]. It is useful to change coordinate system and rewrite the Hamiltonian (3.93) as

$$\mathcal{H}_{\rm ZXX,H} = J\sum_{j,\alpha} S_j^\alpha S_{j+1}^\alpha - H\sum_j S_j^z + (\delta-1)S_j^y S_{j+1}^y \equiv \mathcal{H}_0 + \mathcal{H}_1 \, . \tag{3.94}$$

Our strategy in the regime $H \gg J(1-\delta)$ is to bosonize at the point $\delta = 1$ at a finite value for the magnetization per site and then to treat the exchange anisotropy $\mathcal{H}_1$ as a perturbation. The continuum limit of $\mathcal{H}_0$ is constructed in section (3.1.2) and is given by a compactified boson (3.18). The perturbing Hamiltonian $\mathcal{H}_1$ can then be bosonized using (3.31). Fusion of the y-components of the staggered magnetizations gives a contribution

$$\mathcal{O}_j = S_j^y S_{j+1}^y \longrightarrow \mathcal{C}\ \cos(2\tilde{\beta}\Theta) + \dots\ . \tag{3.95}$$

In addition there is a small marginal contribution that shifts the compactification radius. For simplicity we neglect it here. Putting everything together we conclude that at low energies compared to the scale set by the applied field $H < 2J$, the effective Hamiltonian is given by a SGM

$$\mathcal{H} = \frac{v}{16\pi}[(\partial_x\Phi)^2 + (\partial_x\Theta)^2] - \mu(\delta)\ \cos(\beta\Theta)\ , \tag{3.96}$$

where

$$\beta = 2\tilde{\beta}\ . \tag{3.97}$$

The cosine term in the SGM is relevant and generates a spectral gap. As $\beta > \frac{1}{\sqrt{2}}$ (see Fig. 7) the SGM is in the *repulsive* regime and the the spectrum consists of soliton and antisoliton only. No breather bound states exist. The magnetic field dependence enters both via the prefactor and via the H-dependence of β. In order to calculate the prefactor as well as quantities like the magnetization we need to know the normalization $\mathcal{C}$ in (3.95) in the Heisenberg chain in a field, i.e. the Hamiltonian (3.94) with $\delta = 1$. In Ref. [132] $\mathcal{C}$ was estimated numerically from the large distance asymptotics of an appropriately chosen four-point function and found to be very small. An independent method for determining $\mathcal{C}$ from the uniform magnetization was suggested in [54]. The gap is given by

$$\frac{\Delta}{J} = \frac{2\tilde{v}}{\sqrt{\pi}}\frac{\Gamma\left(\frac{\beta^2}{2-2\beta^2}\right)}{\Gamma\left(\frac{1}{2-2\beta^2}\right)}\left(\frac{(1-\delta)\mathcal{C}\pi}{2\tilde{v}}\frac{\Gamma\left(1-\beta^2\right)}{\Gamma\left(\beta^2\right)}\right)^{\frac{1}{2-2\beta^2}}\ , \tag{3.98}$$

where $\tilde{v}$ is the dimensionless spin velocity $\tilde{v} = \frac{v}{Ja_0}$. As we have mentioned before, in the low field phase the staggered magnetization in x-direction is nonzero in the presence of a transverse field. One has

$$\langle(-1)^n S_n^x\rangle = c(H)\left\langle\cos\left(\frac{\beta}{2}\Theta\right)\right\rangle = c(H)\mathcal{G}_{\frac{\beta}{2}}\ , \tag{3.99}$$

where $\mathcal{G}_{\frac{\beta}{2}}$ is given by (3.65).

Next we turn to the low-energy behavior of dynamical correlation functions. We start with the transverse correlations and concentrate on momenta close to π/a_0. The staggered components of the spin operators are given by (3.31) and calculating their correlation functions reduces to the calculation of appropriate correlators in the SGM (3.96). The leading contribution to the yy-component of the dynamical structure factor is due to soliton-antisoliton two-particle intermediate states. One finds [54]

$$S^{\rm yy}(\omega,\frac{\pi}{a_0}+q)=\frac{\tilde{v}Jc^2(H)\mathcal{G}^2_{\beta/2}}{\pi\xi^2\Delta^2}\,\frac{\sqrt{s^2-4\Delta^2}}{s}\,\frac{E(\theta(M,M,s))\theta_H\left(\frac{s}{\Delta}-2\right)}{\cosh\left(\frac{\theta(M,M,s)}{\xi}\right)+\cos\left(\frac{\pi}{\xi}\right)}$$
$$+\,\text{contributions from }4,6,\dots\text{ particles.} \tag{3.100}$$

where $\theta_H(x)$ is the Heaviside function, $\theta(M,M,s)$, $\mathcal{G}_\alpha$ and $E(\theta)$ are given by(3.75), (3.65) and (3.81) respectively and $s=\sqrt{\omega^2-v^2q^2}$. The analogous result for $S^{\rm xx}(\omega,\frac{\pi}{a_0}+q)$ is

$$S^{\rm xx}(\omega,\frac{\pi}{a_0}+q)=\frac{\tilde{v}Jc^2(H)\mathcal{G}^2_{\beta/2}}{\pi\xi^2\Delta^2}\,\frac{\sqrt{s^2-4\Delta^2}}{s}\,\frac{E(\theta(M,M,s))\theta_H\left(\frac{s}{\Delta}-2\right)}{\cosh\left(\frac{\theta(M,M,s)}{\xi}\right)-\cos\left(\frac{\pi}{\xi}\right)}$$
$$+\,\text{contributions from }4,6,\dots\text{ particles.} \tag{3.101}$$

Finally we determine the longitudinal structure factor $S^{\rm zz}(\omega,k)$ in the vicinity of $k=2k_F$ and $k=\frac{2\pi}{a_0}-2k_F$. Recalling that the sine-Gordon coupling constant is given by (3.97), we see from the bosonized expressions for the lattice spin operators (3.31) that we need to consider two-point functions of $\exp\left(\pm i\frac{1}{2\beta}\Phi\right)$ in the SGM (3.96). By (3.72) these operators have topological charge ∓2 respectively. Hence the leading contribution to the zz-component of the dynamical structure factor is due to intermediate states with two solitons or two antisolitons. The corresponding form factors are readily calculated from the axioms (2.6)-(2.13). The normalization has been determined in Ref. [197]. A short calculation then gives

$$S^{\rm zz}(\omega,2k_F+k)=\frac{\tilde{v}Ja^2(H)\mathcal{Z}_2\mathcal{C}_1^2}{16\pi\Delta^2}\,\frac{\sqrt{s^2-4\Delta^2}}{s}\,E(\theta(M,M,s))\theta_H\left(\frac{s}{\Delta}-2\right)$$
$$+\,\text{contributions from }4,6,\dots\text{ particles,} \tag{3.102}$$

where $\mathcal{Z}_2$, $E(\theta)$, $\mathcal{C}_1$ are given by (3.89), (3.81) and (3.90) respectively. We see that the leading contributions to the various components of the dynamical structure factor are always due to two particles. The structure factor is entirely incoherent and always vanishes at the threshold (as β is always strictly larger than $\frac{1}{\sqrt{2}}$), which occurs at $\omega=2\Delta$.

3.5. *Dimerized Chain*

In actual materials the spin degrees of freedom are always coupled to phonons. In many cases this coupling is small and can be ignored, particularly at low temperatures. However, in quasi-1D compounds such as $CuGeO_3$ the magneto-elastic coupling leads to a phase transition, known as the spin-Peierls transition. In the low-temperature phase the lattice is then *dimerized*. This is turn leads to a modulation of the Heisenberg exchange and an appropriate model Hamiltonian is

$$\mathcal{H} = J\sum_n \left[1-(-1)^n\delta\right]\mathbf{S}_n\cdot\mathbf{S}_{n+1}\ . \tag{3.103}$$

For $\delta \ll 1$ one may study (3.103) as a perturbation of the isotropic Heisenberg chain in the field theory regime. The bosonized expression for the staggered energy density $\varepsilon_n = (-1)^n\mathbf{S}_n\cdot\mathbf{S}_{n+1}$ can be determined from the bosonized expressions of the spin operators (3.31) for zero magnetic field. The relevant piece arises from the fusion of the smooth with the staggered components and is given by [217]

$$\varepsilon(x) = \mathcal{D}\sqrt{a_0}\ \cos\Bigl(\frac{1}{2}\,\Phi(x)\Bigr). \tag{3.104}$$

The value of the constant $\mathcal{D}$ is presently not known analytically. In the aforementioned fusion procedure subleading (i.e. very irrelevant) terms in the bosonized expressions for the spin operators (3.31) contribute to the value of $\mathcal{D}$, so that it cannot be simply calculated from the known expressions (3.33), (3.34), (3.35) for $a(0)$, $c(0)$, and $\mathcal{A}(0)$. However, it was found in [225] by comparing to numerical results that $\mathcal{D}$ is well approximated by

$$\mathcal{D} \approx \frac{3}{\pi^2}\left(\frac{\pi}{2}\right)^{\frac{1}{4}}\ . \tag{3.105}$$

Bosonizing the $\delta = 0$ part of (3.103) and then using (3.104) we find that the field theory limit of the dimerized chain is

$$\mathcal{H} = \int dx\left\{\frac{v}{16\pi}\left[(\partial_x\Phi)^2 + (\partial_x\Theta)^2\right] - \mu\cos\Bigl(\frac{1}{2}\,\Phi\Bigr)\right\}, \tag{3.106}$$

where $\mu = a_0^{-\frac{1}{2}}\mathcal{D}J\delta$ and where we have dropped a marginally irrelevant interaction of spin currents present in the field theory limit of the isotropic

Heisenberg chain [h]

$$H_{\rm marg.} = \gamma \int dx \left[\cos(\Phi) + \frac{1}{16}\left[(\partial_x\Theta)^2 - (\partial_x\Phi)^2\right]\right] . \qquad (3.107)$$

Hence the dimerized chain at small Δ is described by a SGM with $\beta = \frac{1}{2}$. It is important to note that the field theory respects the spin rotational SU(2) symmetry of the original lattice Hamiltonian: the SGM (3.106) is SU(2) invariant [126]. This non-obvious fact is most easily understood using non-Abelian bosonization, see section VI of Ref. [15]. The spectrum of the SGM (3.106) consists of four particles: soliton, antisoliton and a light breather forming a SU(2) triplet with gap Δ and a heavy breather with gap $\sqrt{3}\Delta$. The latter is a SU(2) singlet. In contrast to the field induced gap problem, the nonlinear term is now the cosine of the bosonic field Φ rather than the dual field Θ. Hence the topological charge is the dual of (3.53) for $\beta = \frac{1}{2}$, which is related to the z-component of the total spin by (3.31)

$$Q = \frac{1}{4\pi}\int_{-\infty}^{\infty} dx\ \partial_x\Phi \equiv \sum_j S^z_j\ . \qquad (3.108)$$

The relation of the topological charge to the z-component of the spin agrees with our assertion that the breathers have $S^z = 0$ and soliton/antisoliton spin ∓ 1. A consequence of the SU(2) symmetry is that the following two-point functions are identical in the SGM (3.106)

$$\begin{aligned}\left\langle \cos\left(\tfrac{1}{2}\Theta(\tau,x)\right)\cos\left(\tfrac{1}{2}\Theta(0,0)\right)\right\rangle &= \left\langle \sin\left(\tfrac{1}{2}\Theta(\tau,x)\right)\sin\left(\tfrac{1}{2}\Theta(0,0)\right)\right\rangle \\ &= \left\langle \sin\left(\tfrac{1}{2}\Phi(\tau,x)\right)\sin\left(\tfrac{1}{2}\Phi(0,0)\right)\right\rangle . \qquad (3.109)\end{aligned}$$

Equations (3.109) imply various relations between form factors, which can be verified by direct calculation (see e.g. [87]). In order to determine the dynamical structure factor it is sufficient to consider the two-point function of the operator $\sin(\frac{1}{2}\Phi)$ in the SGM (3.106). Apart from the overall constant factor, the latter is the same as the result for the field induced gap problem (3.83) with H set to zero [i] and an appropriate expression substituted for the soliton gap. Using (3.105) and taking the marginally irrelevant interaction of spin currents into account in renormalization group improved perturbation

[h] The bare value of γ has been estimated e.g. in [6]
[i] At $H = 0$ we have $\beta = \frac{1}{2}$, $\tilde{v} = \frac{\pi}{2}$ as required.

theory, the soliton gap is found to be [225]

$$\frac{\Delta}{J} \approx \frac{\sqrt{\pi}\Gamma(\frac{1}{6})}{\Gamma(\frac{2}{3})}\left[\frac{3}{\pi^2}\frac{\Gamma(\frac{3}{4})}{\Gamma(\frac{1}{4})}\left[\frac{\pi}{2}\right]^{\frac{1}{4}}\delta\right]^{\frac{2}{3}}\frac{1}{\sqrt{1+\frac{2}{3}|\lambda|\ln\left|\frac{\lambda}{1.3612\delta}\right|}}\ , \tag{3.110}$$

where $\lambda \approx -0.22$. The dynamical structure factor is then given by

$$S^{\alpha\alpha}(\omega, \frac{\pi}{a_0}+q) = C\ \mathrm{Re}\Bigg\{2\pi Z_1\ \delta(s^2-\Delta^2)$$
$$+\frac{2|F_{+-}^{\sin\left(\frac{1}{2}\Theta\right)}[\theta(\Delta,\Delta,s)]|^2}{s\sqrt{s^2-4\Delta^2}}+\frac{2|F_{12}^{\sin\left(\frac{1}{2}\Theta\right)}[\theta(\Delta,\sqrt{3}\Delta,s)]|^2}{\sqrt{(s^2-4\Delta^2)^2-12\Delta^4}}+\dots\Bigg\}, \tag{3.111}$$

where Z_1, $\theta(a,b,c)$, $F_{+-}^{\sin}(\theta)$ and $F_{12}^{\sin}(\theta)$ are given by (3.84), (3.75), (3.86) and (3.87) with $\beta = \frac{1}{2}$ ($\xi = \frac{1}{3}$) respectively. We have denoted the analog of the overall factor $\mathcal{C}(H)$ in (3.83) by C. We conjecture that

$$C = \frac{J}{(2\pi)^{\frac{3}{2}}}\,\mathcal{G}_{\frac{1}{2}}^2\,, \tag{3.112}$$

where $\mathcal{G}_{\frac{1}{2}}$ is given by (3.65) with $\beta = \frac{1}{2}$ and $\tilde{v} = \frac{\pi}{2}$. We plot the DSF (3.111) in Fig. 13. The DSF is dominated by the coherent triplet modes with gap Δ given by (3.110). Starting at twice the triplet gap there is an incoherent scattering continuum. The latter is singular at its threshold 2Δ, as is the B_1B_2 scattering continuum which occurs above $\Delta + \sqrt{3}\Delta$. The heavy breather B_2 has total spin zero and is invisible to neutron scattering experiments. However, it contributes to the two-point function of energy densities $\varepsilon(x)$ and hence should be observable in Raman scattering experiments. An expression for the two-point function of energy densities was derived in [87].

3.6. *Quasi-1D Spin-$\frac{1}{2}$ Antiferromagnets in the Ordered Phase*

A generic feature of quasi-1D spin-$\frac{1}{2}$ materials is that at low temperatures they develop long range Néel order. This is a consequence of the residual coupling between the 1D chains as spontaneous symmetry breaking is forbidden in one spatial dimension. At low energies in the ordered phase the physics is dominated by Goldstone modes: if the Néel order is along the z-axis in spin space, there will be two transversely (in the xy-plane) polarized spinwave modes (one mode each for the "broken" symmetry generators S^x and S^y). Their quantum numbers are $S^z = \pm 1$. In addition to the transverse

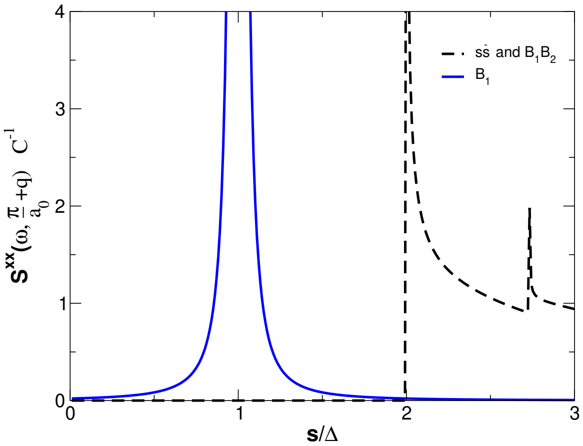

Figure 13. Dynamical structure factor of the dimerized chain. Most of the spectral weight is carried by the coherent triplet excitations, which are identified as soliton, antisoliton and the first breather in the SGM. The delta function corresponding to the coherent triplet excitation has been broadened by a Lorentzian to make it visible.

Goldstone modes there a priori also must be gapped *longitudinal* (polarized along the z-axis) excitations, which correspond to fluctuations in the size of the ordered moment.

On the other hand it is clear that at temperatures or energies that are large compared to the interchain coupling one has to recover the 1D spin chain physics.

A long-standing question is how the system crosses over from the 3D physics of the ordered phase to the 1D physics of the chains, as one varies the energy scale at which it is probed. This issue was addressed theoretically in Refs. [13,255], [87,325] and experimentally in [177] (for $KCuF_3$ [250,280,281]) and in [323, 325] (for $BaCu_2Si_2O_7$).

Our starting point is the Hamiltonian for an ensemble of weakly coupled chains. For definiteness we discuss the form appropriate for $BaCu_2Si_2O_7$ [158, 319, 320], which reads

$$H = J\sum_{i,j,n} \mathbf{S}_{i,j,n}\cdot\mathbf{S}_{i,j,n+1} \ + H',$$

$$H' = \sum_{i,j,n} J_x\ \mathbf{S}_{i,j,n}\cdot\mathbf{S}_{i+1,j,n} + J_y\ \mathbf{S}_{i,j,n}\cdot\mathbf{S}_{i,j+1,n} + J_3\ \mathbf{S}_{i,j,n}\cdot\left(\mathbf{S}_{i+1,j+1,n}+\mathbf{S}_{i+1,j-1,n}\right). \qquad (3.113)$$

where $J_x = -0.460(7)$ meV, $J_y = 0.200(6)$ meV, $2J_3 = 0.152(7)$ meV and

$J = 24.1$ meV. The Fourier transform of the inter-chain coupling is defined as

$$J'(\mathbf{p}) = J_x \cos(p_x) + J_y \cos(p_y) + J_3 \left[\cos(p_x + p_y) + \cos(p_x - p_y)\right]. \quad (3.114)$$

As some of the exchange constants are positive and some negative it is convenient to introduce new spin variables, $\widetilde{S}^\alpha$, where

$$S^x_{i,j,n} = \widetilde{S}^x_{i,j,n}\ ,\ S^\alpha_{i,j,n} = (-1)^j \widetilde{S}^\alpha_{i,j,n}\ ,\quad \alpha = y, z\,. \quad (3.115)$$

The transformation (3.115) leaves the Hamiltonians of the 1D chains invariant, but flips the signs of J_y and J_3 in the interaction of the y and z components of the spin operators in H'. In the new spin variables the interchain coupling is ferromagnetic so that we may take the staggered magnetization at $T = 0$ to be

$$\langle \tilde{S}^\alpha_{i,j,n} \rangle = \delta_{\alpha,z}\ (-1)^n\ m_0\,. \quad (3.116)$$

3.6.1. *Mean-Field Theory*

As a first step we take the long range Néel order into account in a self-consistent mean-field approximation [252, 255]. Writing

$$\tilde{S}^\alpha_{i,j,n} = \langle \tilde{S}^\alpha_{i,j,n} \rangle + \delta \tilde{S}^\alpha_{i,j,n}\ , \quad (3.117)$$

where $\delta \tilde{S}^\alpha_{i,j,n}$ denote (small) fluctuations around the expectation value, and then substituting (3.117) in H' we obtain

$$\begin{aligned} H_{\rm MF} &= \sum_{i,j} \sum_n J \tilde{\mathbf{S}}_{i,j,n} \cdot \tilde{\mathbf{S}}_{i,j,n+1} - h(-1)^n\ \tilde{S}^z_{i,j,n}\,, \\ h &= 2(J_y - J_x + 2J_3)\ m_0 \equiv J' m_0\,. \end{aligned} \quad (3.118)$$

The Hamiltonian (3.118) describes an ensemble of *uncoupled* spin-$\frac{1}{2}$ Heisenberg chains in a staggered magnetic field and is a special case of the field-induced gap problem we studied in section 3.3. At low energies, the mean-field theory Hamiltonian (3.118) reduces to a SGM for the Bose field Φ (rather than the dual field Θ as was the case in section 3.3)

$$\mathcal{H}_{\rm MF} = \int dx \left\{ \frac{v}{16\pi} \left[(\partial_x \Phi)^2 + (\partial_x \Theta)^2 \right] - \mu \cos\Big(\frac{1}{2}\,\Phi\Big) \right\}, \quad (3.119)$$

where $\mu = cha_0^{-\frac{1}{2}}$ with some constant c and[j]

$$v = \frac{\pi J a_0}{2} . \tag{3.120}$$

The form (3.119) is obtained as follows: bosonizing the Hamiltonian (3.118) in the absence of the staggered field gives a Gaussian model of the form (3.18), where the field is compactified according to $\Phi \equiv \Phi + 4\pi$. In addition there is a marginally irrelevant interaction of spin currents of the form (3.107). Bosonizing the staggered field term by means of (3.31) gives a sine-Gordon like Hamiltonian, but with a sine potential rather than a cosine. Shifting the Bose field

$$\Phi \longrightarrow \Phi - \pi , \tag{3.121}$$

while keeping the dual field unchanged and dropping the marginally irrelevant term then leads to (3.119). The shift (3.121) changes the bosonized form of the lattice spin operator S^z_j to

$$S^z_j \sim \frac{a_0}{4\pi}\, \partial_x \Phi + c a_0^{\frac{1}{2}} (-1)^j \cos\left(\frac{\Phi}{2}\right) + \dots . \tag{3.122}$$

At the particular value of β, the spectrum is formed by scattering states of four particles: soliton, antisoliton and the first breather B_1 all with gap Δ and a second breather with gap $\sqrt{3}\Delta$. As described in Ref. [15], the expectation value of the staggered magnetization can be calculated from the results of Ref. [195],

$$m_0 \simeq \frac{2^{\frac{2}{3}}}{3\sqrt{3}\pi} \left[\frac{\Gamma(\frac{3}{4})}{\Gamma(\frac{1}{4})}\right]^{\frac{4}{3}} \left[\frac{\Gamma(\frac{1}{6})}{\Gamma(\frac{2}{3})}\right]^{2} \left(\frac{h}{J}\right)^{\frac{1}{3}} \left[\ln\left(\frac{J}{h}\right)\right]^{\frac{1}{3}} . \tag{3.123}$$

Equation (3.123) is the self-consistency equation of the mean field approximation (recall that $h = m_0 J'$) and has the solution [325]

$$m_0 \simeq \frac{\sqrt{2}}{3^{\frac{7}{4}}\pi^{\frac{3}{2}}} \left[\frac{\Gamma(\frac{3}{4})}{\Gamma(\frac{1}{4})}\right]^{2} \left[\frac{\Gamma(\frac{1}{6})}{\Gamma(\frac{2}{3})}\right]^{3} \left[\frac{J'}{J} \ln\left(\frac{2.58495 J}{J'}\right)\right]^{\frac{1}{2}} . \tag{3.124}$$

We note that the constant 2.58495 should not be taken too seriously as we have ignored subleading logarithmic corrections. The result (3.124) is found to be in good agreement (for small J'/J) with a phenomenological expression obtained from quantum Monte-Carlo simulations in Ref. [247]. The soliton

[j] a_0 is the period of the spin chains that for $BaCu_2Si_2O_7$ is equal to half the lattice constant in c-direction.

gap as a function of the staggered field h has been calculated in Refs. [15,89]. Expressing h in terms of m_0 by (3.118) and then using (3.124) we obtain

$$\frac{\Delta}{J} \simeq \frac{1}{3\pi}\left[\frac{\Gamma(\frac{3}{4})}{\Gamma(\frac{1}{4})}\right]^2\left[\frac{\Gamma(\frac{1}{6})}{\Gamma(\frac{2}{3})}\right]^3\ \frac{J'}{J}\left[\ln\left(\frac{2.58495J}{J'}\right)\right]^{\frac{1}{2}}. \tag{3.125}$$

Let us now turn to the dynamical susceptibilities. A very useful observation is that because $\beta=\frac{1}{2}$ in the sine-Gordon description of the mean-field Hamiltonian (3.118), the correlation functions of the staggered magnetizations are related by the SU(2) symmetry (3.109). Hence [k,l]

$$\begin{aligned}
\langle S^x_{j+1}(t)S^x_1(0)\rangle &\simeq c^2a_0(-1)^j\big\langle\sin\big(\frac{1}{2}\Phi(t,x)\big)\sin\big(\frac{1}{2}\Phi(0,0)\big)\big\rangle\ ,\\
\langle S^y_{j+1}(t)S^y_1(0)\rangle &\simeq c^2a_0(-1)^j\big\langle\sin\big(\frac{1}{2}\Phi(t,x)\big)\sin\big(\frac{1}{2}\Phi(0,0)\big)\big\rangle\ ,\\
\langle S^z_{j+1}(t)S^z_1(0)\rangle &\simeq c^2a_0(-1)^j\big\langle\cos\big(\frac{1}{2}\Phi(t,x)\big)\cos\big(\frac{1}{2}\Phi(0,0)\big)\big\rangle\ .
\end{aligned}\tag{3.126}$$

The dynamical susceptibilities are calculated as in section 3.3.4. However, now we are interested in both the real and imaginary parts. Taking all contributions from intermediate states with at most two particles into account one finds [87]

$$\begin{aligned}
\tilde{\chi}^{\rm xx}_{\rm 1d}(\omega,\frac{\pi}{a_0}+q) \approx \tilde{C}\Bigg\{&\frac{2\pi Z_1}{s^2-\Delta^2+i\epsilon}+\int_0^\infty d\theta\frac{2|F^{\rm sin}_{+-}(\theta)|^2}{s^2-[2\Delta\cosh(\theta/2)]^2+i\epsilon}\\
&+\int_0^\infty d\theta\frac{2|F^{\rm sin}_{12}(\theta)|^2}{s^2-4\Delta^2(1+\frac{\sqrt{3}}{2}\cosh\theta)+i\epsilon}\Bigg\},
\end{aligned}\tag{3.127}$$

where $s^2=\omega^2-v^2q^2$. The functions Z_1, $F^{\rm sin}_{+-}(\theta)$ and $F^{\rm sin}_{12}(\theta)$ are given by (3.84), (3.86) and (3.87) respectively, where $\beta=\frac{1}{2}$ and hence $\xi=\frac{1}{3}$. Similarly one finds

$$\begin{aligned}
\tilde{\chi}^{\rm zz}_{\rm 1d}(\omega,\frac{\pi}{a_0}+q) \approx \tilde{C}\Bigg\{&\frac{2\pi Z_2}{s^2-3\Delta^2+i\epsilon}\ +\int_0^\infty d\theta\frac{2|F^{\rm cos}_{+-}(\theta)|^2+|F^{\rm cos}_{11}(\theta)|^2}{s^2-[2\Delta\cosh(\theta/2)]^2+i\epsilon}\\
&+\int_0^\infty d\theta\frac{|F^{\rm cos}_{22}(\theta)|^2}{s^2-[\sqrt{12}\Delta\cosh(\theta/2)]^2+i\epsilon}\Bigg\}.
\end{aligned}\tag{3.128}$$

[k] Recall that due to the shift (3.121) the staggered component of S^z_j is now the cosine rather than the sine.

[l] The same constant enters both transverse and longitudinal correlations because the spin rotational symmetry is restored at high energies.

Here Z_2, $F^{\cos}_{+-}(\theta)$ and $F^{\cos}_{11}(\theta)$ are given by (3.78), (3.80) and (3.82) respectively, where $\beta = \frac{1}{2}$ and hence $\xi = \frac{1}{3}$. The contribution from B_2B_2 two-particle states is given in [87].[m]

3.6.2. *Random Phase Approximation for the Interchain Coupling*

The mean-field approach clearly does not give a good description of the magnetic response in the ordered phase: spin excitations have a gap and there are no Goldstone modes. In order to reproduce the latter it is necessary to go beyond the mean-field approximation. It is possible to develop a perturbative expansion in the interchain coupling along the lines of [43, 44, 255] This gives

$$\chi^{\alpha\alpha}_{3\text{d}}(\omega, \mathbf{p}, k) = \frac{\tilde{\chi}^{\alpha\alpha}_{1\text{d}}(\omega, k)}{1 - 2J'(\mathbf{p})[\tilde{\chi}^{\alpha\alpha}_{1\text{d}}(\omega, q) + \Sigma^{\alpha\alpha}(\omega, \mathbf{p}, k)]} \ , \tag{3.129}$$

where $\alpha = x, y, z$. In Eq. (3.129) $\Sigma^{\alpha\alpha}$ are the self-energies that are expressed in terms of integrals involving three-point, four-point *etc* correlation functions of spin operators. The analogous expressions in the disordered phase were derived in Refs. [43, 142]. To date, the relevant multipoint correlation function have not been calculated for the SGM. Furthermore, there is no small parameter in the expansion (3.129). The reason is that the mean-field gap is generated by the interchain coupling itself and as a result the gap (3.125) is of the same order as the interchain coupling. Setting this issue aside, a simple Random-Phase Approximation in the interchain coupling (3.129) was suggested by Schulz in [255]. Its essence to simply neglect the self-energies in (3.129). In other words, one sets

$$\Sigma^{\alpha\alpha} = 0. \tag{3.130}$$

One problem is that in this approximation the transverse susceptibility will not have a zero-frequency spin wave pole at the 3D magnetic zone-center, as it should, spin waves being the Goldstone modes of the magnetically ordered state. In order for the pole to be exactly at $\omega = 0$ the full self-energy Σ^{xx} must be included. A work-around was suggested in [255]. If the RPA is a good approximation, there will almost be a zero frequency pole

$$1 \approx 2J'(0, \pi)\, \tilde{\chi}^{\text{xx}}_{1\text{d}}(0, \tfrac{\pi}{a_0}) \ . \tag{3.131}$$

The idea is to replace (3.131) by an equality

$$1 = 2J'(0, \pi)\, \tilde{\chi}^{\text{xx}}_{1\text{d}}(0, \tfrac{\pi}{a_0}) \, , \tag{3.132}$$

[m] Our normalizations are related to those of [87] by $Z = 4\pi^3\tilde{C}$

and then use (3.132) to fix the overall normalization of $\tilde{\chi}_{1d}$. Following this logic, we may carry out the integral in (3.127) numerically and obtain

$$\tilde{C} \approx 0.0645 \frac{\Delta^2}{|J'|}. \tag{3.133}$$

Now it is a simple matter to determine $\chi^{\alpha}_{3d}(\omega, \mathbf{p}, \frac{\pi}{a_0} + q)$ by evaluating the 1D susceptibilities numerically and then inserting them into (3.129).

As discussed in Refs. [87, 255], the resulting dynamic susceptibility for transverse spin fluctuations χ^{xx}_{3d}, χ^{yy}_{3d} in the coupled chains model contains a pair of spin wave excitations that disperse perpendicular to the spin chains, and are, by design, gapless. At higher energies there is an incoherent scattering continuum with threshold 2Δ, independent of the transverse momentum. This momentum independence is likely to be an artefact of the approximation made, rather than being a genuine feature of the model. The RPA result for the longitudinal susceptibility χ^{zz}_{3d} exhibits a gapped, coherent mode that disperses perpendicular to the chains as well. Above a threshold of 2Δ an incoherent scattering continuum occurs. Like for the transverse susceptibility the threshold for the continuum does not depend on the transverse momentum. Within the RPA the longitudinal mode is sharp, i.e. it has an infinite lifetime. This is certainly a feature of the approximation made: a decay of the longitudinal mode into a pair of spinwaves is permitted both by the quantum numbers of the excitations involved and phase space. Such decay processes are simply not taken into account in the RPA. The physical picture that emerges in the RPA has been found to be in good agreement with inelastic neutron scattering experiments on $KCuF_3$ [177]. There a damped longitudinal mode has been observed. It occurs approximately at the energy predicted by the RPA and its spectral weight is found to be close to the RPA result. On the other hand, the RPA does rather poorly when applied to $BaCu_2Si_2O_7$ [323, 325].

4. O(3) Non-linear Sigma Model and Gapped, Integer Spin Chains

The existence of a gap in one-dimensional, integer-spin, Heisenberg antiferromagnets was first predicted by Haldane [128]. He found that such spin chains can be mapped onto a gapped integrable field theory, the O(3) non-linear sigma model (NLSM), in the large-spin, continuum limit. It is the goal of this section to explore the properties of the O(3) NLSM and its relevant predictions for the physics of gapped spin chains.

While the O(3) NLSM is derived in a large S limit, a variety of checks imply that this behavior persists down to spin $S = 1$. A spin-1 chain with a specific $(\vec{S} \cdot \vec{S})^2$ coupling has been rigorously shown to exhibit a spin gap [4]. While at a differing value of the $(\vec{S} \cdot \vec{S})^2$ coupling, the spin chain is gapless [22, 179, 278], this critical point is believed to be unstable in the two-parameter space of couplings. Gapless behavior thus only arises as a product of fine-tuning. Numerous numerical studies carried out on spin-1 chains observe a gap [49, 67, 120, 121, 207, 208, 233, 246, 265, 274, 276, 292, 293, 300]. Experimentally, inelastic neutron scattering studies on a number of quasi-one-dimensional, spin-1 chain materials are consistent with a finite spin gap [48, 201, 202, 209, 215, 241, 267, 286, 307].

Here we will suppose that the spin chain is described by a minimal Heisenberg Hamiltonian and so ignore (for the most part) the affects of anisotropies upon the physics. These can take (at least) two forms. Easy-axis anisotropies,

$$\Delta H = D_x \sum_i (S_{xi})^2 + D_y \sum_i (S_{yi})^2 + D_z \sum_i (S_{zi})^2,$$

of varying strengths are often found in spin-1 chain materials. Furthermore, actual spin chain materials never take the form of isolated chains. Rather the chains exist in three dimensional arrays with weak but non-zero interchain couplings, J'. Thus the chains are at best quasi-one-dimensional. With a finite J', there will be some correspondingly finite Néel temperature, T_N. Below T_N the (ultra low-energy) physics, consisting of higher dimensional magnon modes, will be dramatically different than described here.

$CsNiCl_3$ was the first material for which evidence of a Haldane gap was found [48, 209, 286, 307]. While $CsNiCl_3$ has only a weak easy axis anisotropy, it does possess a a relatively large interchain coupling, $J'/J \sim .017$. Consequently Néel order is observed to set in at $T \sim 5K$. Provided however one is interested in physics at energies scales around the gap ($\Delta \sim .4J$), the absence or presence of long range order plays an unimportant role. Another material in which a Haldane gap is present is $AgVP_2S_6$ [215]. It has an extremely small interchain coupling, $J'/J \sim 10^{-5}$ and a similarly small easy axis anisotropy, $D_z/\Delta \sim 10^{-2}$. However it possesses a comparatively large gap, $\Delta \sim 320K$.

Other Haldane gap integer spin chain materials are studied experimentally, but these compounds are characterized by large easy plane anisotropies. One such material is $Ni(C_2H_8N_2)_2NO_2ClO_4$ (NENP) [201, 202, 240, 241, 308]. It has an easy-plane anisotropy given by $D_z/J \sim .16$; $D_z/\Delta \sim 2/5$ ($D_x \sim D_y \sim 0$) [308]. For NENP, the ratio $J'/J \sim 8 \times 10^{-4}$ is sufficiently small that 3D Néel order has not been observed down to temperatures $\sim$

$1.2K$. Related materials $Ni(C_5H_{14}N_2)_3(PF_6)$ (NDMAP) [122, 321, 326, 327] and $Ni(C_5H_{14}N_2)_2N_3(Cl0_4)$ (NDMAZ) [136, 137, 322] share similar easy-plane anisotropies. These latter compounds share the additional feature of field-induced antiferromagnetism [57, 136–139, 324]. The Luttinger liquid that results from magnetic fields large enough to extinguish the Haldane gap leads to quasi-long range antiferromagnetic correlations. With a small finite J', these quasi-long range correlations are promoted to full fledged long range order. The corresponding Néel temperature increases with applied magnetic fields. In this review we will not explore this phenomena nor related behavior occurring in the presence of a magnetic field (but see [9, 10, 100, 113, 117, 124, 172, 190, 204, 223, 224, 260, 275, 283]).

The physics underlying the Haldane gap is particularly robust: related systems such as two-leg spin-1/2 or Hubbard ladders also exhibit a gap to spin excitations [64, 113, 117, 172, 204]. (We will see this gapped behavior again when we discuss ladder materials in the context of SO(8) Gross–Neveu). Roughly speaking, integer-spin composites form across the rungs of the ladder making it into an effective integer-spin chain. Both the ability to fabricate these materials and their relationship to high T_c cuprate superconductors have made them the focus of intense theoretical and experimental study [26, 79, 96, 163, 169, 170, 187, 220–222, 256].

In this section we first turn to how to derive the O(3) NLSM. We will then provide a description of its spectrum, scattering matrices, and form factors. We then turn to using these form factors to compute correlators both at zero and finite temperature. Our goal at finite temperature will be to analyze whether transport in the O(3) NLSM is ballistic or diffusive.

4.1. *From Integer Spin Heisenberg Chains to the O(3) Non-linear Sigma Model*

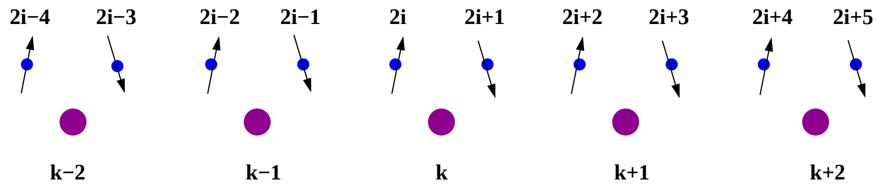

Figure 14. The Heisenberg spin chain

We begin by deriving the O(3) NLSM from the Hamiltonian of the Heisenberg spin chain [n]

$$H = J \sum_i \mathbf{S}_i \cdot \mathbf{S}_{i+1} \,, \tag{4.1}$$

where S is a spin of arbitrary size. We begin the derivation by decomposing each spin, S_i^a (a=1,2,3), in terms of two operators, n^a and M^a, via

$$S_{2i}^a = s n_{2i+1/2}^a + M_{2i+1/2}^a \,, \tag{4.2}$$

where

$$\begin{aligned} n_{2i+1/2}^a &= (S_{2i+1}^a - S_{2i}^a)/2s \,, \\ M_{2i+1/2}^a &= (S_{2i+1}^a + S_{2i}^a)/2 \,. \end{aligned} \tag{4.3}$$

Roughly speaking, the n^a and M^a operators govern antiferromagnetic and ferromagnetic fluctuations respectively. For convenience we introduce a new lattice indexed by k (see Fig. 14) with sites at $2i+1/2$ and so with twice the lattice spacing of the original lattice. Indexed in terms of this lattice, the operators, n^a and M^a, have the following commutation relations

$$\begin{aligned} \left[M_k^a, M_{k'}^b\right] &= i\epsilon^{abc} M_k^c \delta_{kk'} \,, \\ \left[M_k^a, n_{k'}^b\right] &= i\epsilon^{abc} n_k^c \delta_{kk'} \,, \\ \left[n_k^a, n_{k'}^b\right] &= i\epsilon^{abc} \frac{1}{s^2} M_k^c \delta_{kk'} \,, \end{aligned} \tag{4.4}$$

where $\delta_{kk'} = \delta_{ii'}/2$, $\delta_{ii'}$ being the Kronecker delta function on the original lattice, the factor of two taking into account the change in lattice spacing. We can also easily show that these operators obey the relations

$$\begin{aligned} \mathbf{n} \cdot \mathbf{M} &= 0 \,, \\ \mathbf{n} \cdot \mathbf{n} &= 1 + \frac{1}{s} - \frac{\mathbf{M} \cdot \mathbf{M}}{s^2} \,. \end{aligned} \tag{4.5}$$

In the large s limit we see $\mathbf{n} \cdot \mathbf{n} = 1$. Our assumption that $\mathbf{n}$ satisfies this relation in general will be the main approximation of this derivation.

We are now in position to recast the Hamiltonian. Noting that

$$\begin{aligned} \mathbf{S}_{2i} \cdot \mathbf{S}_{2i+1} &= 2\mathbf{M}_{2i+1/2} \cdot \mathbf{M}_{2i+1/2} + \text{const.} \,, \\ \mathbf{S}_{2i} \cdot \mathbf{S}_{2i-1} &= 2\mathbf{M}_{2i+1/2} \cdot \mathbf{M}_{2i+1/2} - 2s^2 \mathbf{n} \partial_x^2 \mathbf{n} + 2s(\mathbf{M} \cdot \partial_x \mathbf{n} + \partial_x \mathbf{n} \cdot \mathbf{M}) \\ &\qquad + \text{const.} \,, \end{aligned} \tag{4.6}$$

[n] This development of the O(3) NLSM follows I. Affleck's in Ref. [5].

we can write the original Hamiltonian as

$$H = J\int \frac{dx}{2}\Big\{4\mathbf{M}\cdot\mathbf{M} + 2s^2(\partial_x\mathbf{n})^2 + s(\mathbf{M}\cdot\partial_x\mathbf{n} + \partial_x\mathbf{n}\cdot\mathbf{M})\Big\}$$
$$= \frac{v}{2}\int dx\left\{g\left[\mathbf{M} + \frac{\theta}{4\pi}\partial_x\mathbf{n}\right]^2 + \frac{1}{g}(\partial_x\mathbf{n})^2\right\}, \qquad (4.7)$$

where the spin velocity, v, equals $2Js$, the coupling constant g is given by $2/s$ and the parameter, θ, the theta angle, equals $2\pi s$. In the above two equations, we have set the (original) lattice spacing to 1. To arrive at the action for the O(3) NLSM, we define the momenta conjugate to $\mathbf{n}$ as

$$\mathbf{p} = \frac{1}{g}\,\partial_t\mathbf{n} + \frac{\theta}{4\pi}\,\mathbf{n}\times\partial_x\mathbf{n}\,. \qquad (4.8)$$

This permits the Lagrangian to be written as

$$\mathcal{L} = \frac{1}{2g}\,\partial_\mu\mathbf{n}\cdot\partial^\mu\mathbf{n} - \frac{\theta}{8\pi}\epsilon^{\mu\nu}\mathbf{n}\cdot(\partial_\mu\mathbf{n}\times\partial_\nu\mathbf{n})\,, \qquad (4.9)$$

subject to the constraint that $\mathbf{n}\cdot\mathbf{n} = 1$. This model is known as the O(3) NLSM with theta angle, θ.

The theta angle plays a crucial role in determining the properties of the above Lagrangian. The term to which it serves as a coupling constant, $\epsilon^{\mu\nu}\mathbf{n}\cdot(\partial_\mu\mathbf{n}\times\partial_n u\mathbf{n})/8\pi$, counts (when integrated) the number of times the field $\mathbf{n}$ winds itself about the sphere (i.e. the second homotopy group of the sphere). As it is always an integer, this term in the Lagrangian only affects the physics if s is a half integer (and so θ is an odd multiple of π). In this case this Lagrangian describes a massless theory which at low energies is equivalent to the $SU(2)_1$ Wess-Zumino-Witten theory. If on the other hand s is integer, the theta term has no affect on the physics and the theory is one of gapped bosons. It will be this latter case in which we will be interested.

4.2. *Basic Description of the O(3) Non-linear Sigma Model*

The low energy theory of integer spin chains is then simply (setting the spin velocity to 1)

$$S = \frac{1}{2g}\int dtdx\,(\partial^\nu\mathbf{n}\cdot\partial_\nu\mathbf{n}). \qquad (4.10)$$

The field $\mathbf{n}$ describes low energy antiferromagnetic fluctuations. Fluctuations near wavevector $k\sim 0$ are described instead by

$$\mathbf{M} = \frac{1}{g}\,\mathbf{n}\times\partial_t\mathbf{n} \qquad (4.11)$$

and so are given in terms of the momentum conjugate to n. Unlike its ancestral theory, the O(3) NLSM is integrable [296,315,316]. Local conserved charges were constructed in Ref. [118,238] while non-local conserved charges were first found by Lüscher [192].

The low energy excitations in the O(3) NLSM take the form of a triplet of bosons. The bosons have a relativistic dispersion relation given by

$$E(p) = (p^2 + \Delta^2)^{1/2}.$$

Here Δ is the energy gap or mass of the bosons related to the bare coupling, g, via $\Delta \sim Je^{-2\pi/g}$. The dispersion relations of all three bosons are identical as the model has a global SU(2) symmetry. The exact eigenfunctions of the O(3) NLSM Hamiltonian are then multi-particle states made up of mixtures of the three bosons. Scattering between the bosons is described by the S-matrix [315]:

$$S^{a_3a_4}_{a_1a_2}(\theta) = \delta_{a_1a_2}\delta_{a_3a_4}\sigma_1(\theta) + \delta_{a_1a_3}\delta_{a_2a_4}\sigma_2(\theta) + \delta_{a_1a_4}\delta_{a_2a_3}\sigma_3(\theta)\,;$$

$$\begin{aligned}\sigma_1(\theta) &= \frac{2\pi i\theta}{(\theta+i\pi)(\theta-i2\pi)}\,;\\ \sigma_2(\theta) &= \frac{\theta(\theta-i\pi)}{(\theta+i\pi)(\theta-i2\pi)}\,;\\ \sigma_3(\theta) &= \frac{2\pi i(i\pi-\theta)}{(\theta+i\pi)(\theta-i2\pi)}\,.\end{aligned} \tag{4.12}$$

Here again θ parameterizes a particle's energy/momentum via $E = \Delta\cosh(\theta)$, $P = \Delta\sinh(\theta)$. These S-matrices are relativistically invariant. While we stress that this relativistic invariance is a natural feature of the low energy structure of the spin chain, we do point out for spin-1 chains, $\Delta \sim .4J$. As J serves as the cutoff for the theory, the low energy sector of the theory in this case is not unambiguously defined.

4.2.1. *Form Factors for the Staggered Magnetization Operator,* $\mathbf{n}$

We will be interested in computing correlators involving the field, $\mathbf{n}$, describing excitations near $k \sim \pi$. Form factors for the field $n(x,t)$ have been computed by both Smirnov [264] and Balog and Niedermaier [30]. However Ref. [30] presents them in a more amenable form, possible in this particular case because of the simple structure of the S-matrix of the $O(3)$ sigma model.

The staggered magnetization operator is the fundamental field in the theory. It thus has non-zero overlap with single particle excitations. By the

Z_2 symmetry, $\mathbf{n} \to -\mathbf{n}$, it also only couples to odd numbers of particles. Using the axioms of Section 2, Ref. [30] finds for the one and three particle form factors,

$$f_b^{n_a}(\theta_1) \equiv \langle 0|n_a(0,0)|A_b(\theta)\rangle = \delta_{ab}\,, \tag{4.13}$$

$$\begin{aligned} f_{bcd}^{n_a}(\theta_1,\theta_2,\theta_3) &\equiv \langle 0|n_a(0,0)|A_d(\theta_3)A_c(\theta_2)A_b(\theta_1)\rangle \\ &= -\frac{\pi^3}{2}\psi(\theta_{12})\psi(\theta_{13})\psi(\theta_{23})\Big(\delta_{ab}\delta_{cd}\theta_{23} + \delta_{ac}\delta_{bd}(\theta_{31}-2\pi i) + \delta_{ad}\delta_{bc}\theta_{12}\Big), \end{aligned}$$

where $\theta_{ij} \equiv \theta_i - \theta_j$ and $\psi(\theta)$ is defined in Eq.(4.15).

4.2.2. *Form Factors for the Magnetization Operator,* $\mathbf{M}$

We will also be interested in computing correlators involving the magnetization, $\mathbf{M}$. This field, $\mathbf{M} \equiv \mathbf{M_0}$, is part of a Lorentz two-current $(\mathbf{M}_0, \mathbf{M}_1)$. As this current is topological, both components of the current can be written in terms of a single Lorentz scalar field, $m(x,t)$,

$$\mathbf{M}_\mu(x,t) = \epsilon_{\mu\nu}\partial^\nu \mathbf{m}(x,t)\,. \tag{4.14}$$

We note that only even numbers of particles couple to the magnetization current and density operators. This is a consequence of $\mathbf{M}$ being expressible as a bilinear in the (fundamental) field $\mathbf{n}$, the field which creates the excitations.

Given Eq.(4.14), it is sufficient to compute the form factors of the scalar field $\mathbf{m}$: the form factors of $\mathbf{M}$ are then given by

$$f^{M_\mu}_{a_1\cdots a_n}(\theta_1,\cdots,\theta_n) = \epsilon_{\mu\nu}P^\nu(\theta_i)f^m_{a_1\cdots a_n}(\theta_1,\cdots,\theta_n)\,,$$

where $P^0 = \sum_i \Delta\cosh(\theta_i)$ and $P^1 = \sum_i \Delta\sinh(\theta_i)$. Ref. [30] then finds the following for the two and four particle form factors of $\mathbf{m}$:

$$f^{m_a}_{a_1a_2}(\theta_1,\theta_2) = i\frac{\pi^2}{4}\epsilon^{aa_1a_2}\psi(\theta_{12})\,, \qquad \psi(\theta) = \frac{\tanh^2(\theta/2)}{\theta}\frac{i\pi+\theta}{2\pi i+\theta}\,;$$

$$\begin{aligned} f^{m_a}_{a_1a_2a_3a_4}(\theta_1,\theta_2,\theta_3,\theta_4) = &-\frac{\pi^5}{8}\prod_{i<j}\psi(\theta_{ij})G^{m_a}_{a_1a_2a_3a_4} \\ = -\frac{\pi^5}{8}\prod_{i<j}\psi(\theta_{ij}) \times \Big(&\delta^{a_4a_3}\epsilon^{aa_2a_1}g_1(\theta_i) + \delta^{a_4a_2}\epsilon^{aa_3a_1}g_2(\theta_i) \\ &+\delta^{a_4a_1}\epsilon^{aa_3a_2}g_3(\theta_i) + \delta^{a_3a_2}\epsilon^{aa_4a_1}g_4(\theta_i) \\ &+\delta^{a_3a_1}\epsilon^{aa_4a_2}g_5(\theta_i) + \delta^{a_2a_1}\epsilon^{aa_4a_3}g_6(\theta_i)\Big); \end{aligned}$$

$$\begin{pmatrix} g_1(\theta_i) \\ g_2(\theta_i) \\ g_3(\theta_i) \\ g_4(\theta_i) \\ g_5(\theta_i) \\ g_6(\theta_i) \end{pmatrix} = i \begin{pmatrix} -i\pi({\theta_{32}}^2 + {\theta_{31}}^2 - i\pi\theta_{32} - i\pi\theta_{31} + 2\pi^2) \\ (\theta_{32} - i\pi)\theta_{31}(\theta_{31} - i\pi) \\ (\theta_{32} - i\pi)(\theta_{32} + i2\pi)(i\pi - \theta_{31}) \\ \theta_{32}\theta_{31}(3\pi i - \theta_{31}) \\ \theta_{32}(\theta_{32} - i\pi)\theta_{31} \\ 2\pi i(i\pi - \theta_{32})\theta_{31} \end{pmatrix} \tag{4.15}$$

$$+i(\theta_{43}-i\pi)\begin{pmatrix} -4\pi^2 - i\pi(\theta_{32}+\theta_{31}) - (\theta_{32}-\theta_{31})^2 \\ -2\pi^2 - 3\pi i\theta_{31} + {\theta_{31}}^2 \\ -4\pi^2 + i\pi(\theta_{32} - 2\theta_{31}) - {\theta_{32}}^2 \\ 2\pi^2 + i\pi(\theta_{32} + 2\theta_{31}) - 2\theta_{32}\theta_{31} \\ -i\pi(2\theta_{32} + \theta_{31}) + 2\theta_{32}\theta_{31} \\ -2\pi^2 + i\pi(\theta_{32} - 3\theta_{31}) \end{pmatrix} + i(\theta_{43}-i\pi)^2 \begin{pmatrix} 0 \\ 0 \\ 0 \\ -\theta_{32} \\ \theta_{31} - 2\pi i \\ \theta_{32} - \theta_{31} \end{pmatrix}.$$

The reader should note however that we use a different particle normalization than Ref. [30] and so the above presented results differ by an overall multiplicative constant.

4.3. *Zero Temperature Correlators*

In this section we consider the zero temperature dynamic spectral functions of the spin operator near $k \sim 0$ and $k \sim \pi$. These spectral functions govern the response in inelastic neutron scattering experiments.

4.3.1. $k \sim 0$ *Magnetization Correlations*

This problem was first studied theoretically in Ref. [11]. From this work, we expect at $k \sim 0$ to see a two-magnon continuum. A high resolution study mapping out this continuum has been carried out in Ref. [310]. Observing the two-magnon continuum is a difficult task as the scattering function vanishes at small momentum (as we will demonstrate).

The spectral function for an integer spin chain near $k \sim 0$ is given by

$$S(\omega, k) = -\frac{1}{\pi}\,\mathrm{Im}\left[\int_{-\infty}^{\infty} dx \int_{-\infty}^{\infty} d\tau e^{i(-i\omega+\epsilon)\tau - ikx}\big(-\langle T(M^3(x,\tau)M^3(0,0))\rangle\big)\right]. \tag{4.16}$$

Here $\langle T(M^3M^3)\rangle$ is an imaginary time-ordered correlator. We evaluate this correlator using two particle form-factors. As the next form factor that contributes is a four-particle one, our result will be exact for energies, $\omega < 4\Delta$. Moreover we can expect the contribution to the overall spectral weight of the four-particle form factors and beyond to be small.

The time-ordered correlator evaluated to the two-particle level equals

$$\begin{aligned} G(x,\tau) &= -\Theta(\tau)\langle M^3(x,\tau)M^3(0,0)\rangle - \Theta(-\tau)\langle M^3(0,0)M^3(x,\tau)\rangle \\ &= -\Theta(\tau)\frac{1}{2}\int d\hat{\theta}_1 d\hat{\theta}_2 \sum_{a_1,a_2=1}^{3} |f^{M^3}_{a_1a_2}(\theta_1\theta_2)|^2 e^{-m\tau(c(\theta_1)+c(\theta_2))+imx(s(\theta_1)+s(\theta_2))} \\ &\quad - \Theta(-\tau)\frac{1}{2}\int d\hat{\theta}_1 d\hat{\theta}_2 \sum_{a_1,a_2=1}^{3} |f^{M^3}_{a_1a_2}(\theta_1\theta_2)|^2 e^{m\tau(c(\theta_1)+c(\theta_2))-imx(s(\theta_1)+s(\theta_2))}, \end{aligned} \tag{4.17}$$

where $\hat{\theta} \equiv \theta/(2\pi)$, $c(\theta) \equiv \cosh(\theta)$, and $s(\theta) \equiv \sinh(\theta)$. If we now take Fourier transforms in space and time, make the necessary analytic continuation in ω, and use the results for the form factors in the previous section, we find

$$\begin{aligned} S(\omega > 0, k) &= k^2 \frac{\pi^3}{16} \frac{1}{\sqrt{\omega^2 - k^2}} \frac{1}{\sqrt{\omega^2 - k^2 - 4\Delta^2}} \frac{\tanh^4(\theta_{12}/2)}{\theta_{12}^2} \frac{\theta_{12}^2 + \pi^2}{4\pi^2 + \theta_{12}^2}, \\ \theta_{12} &= \cosh^{-1}\Big(\frac{\omega^2 - k^2 - 2\Delta^2}{2\Delta^2}\Big). \end{aligned} \tag{4.18}$$

We have only given the spectral function for $w > 0$. This response function of an incoherent two magnon continuum is plotted in Fig. 15. We can observe there the lack of spectral weight at small momentum [11]. Ref. [310] compares these theoretical predictions with a neutron scattering study of $CsNiCl_3$.

4.3.2. $k \sim \pi$ *Magnetization Correlations*

We now consider the dynamic response function for wavevectors near π. While at $k = 0$ the response is governed by the magnetization operator, $\mathbf{M}$, here at $k = \pi$ the relevant operator is $\mathbf{n}$. We expect then that the response will be dominated by a coherent single mode (the magnon). Beyond single magnon excitations exists a three magnon continuum. The continuum's contribution to the response function has been studied in the context of the O(3) NLSM in Ref. [90, 140] where it was found to be small. This accords with the intuition built up in Section 2.5 of this review that higher particle form-factors make negligible contributions to their corresponding spectral function.

The computation of the dynamic response function in terms of the O(3)

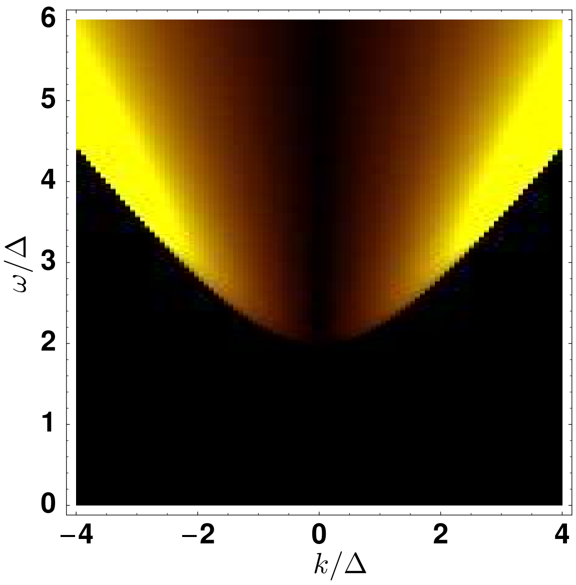

Figure 15. A plot of two magnon contribution to the spectral weight of the spin-spin correlator around $k = 0$ in the $O(3)$ NLSM. This plot is exact (within the confines of this model) for energies less than 4Δ.

NLSM amounts to computing

$$S(\omega, k) = -\frac{1}{\pi}\int_{-\infty}^{\infty} dx \int_{-\infty}^{\infty} d\tau e^{i\omega\tau - ikx}\big(- \langle T(n^3(x,\tau)n^3(0,0))\rangle\big)|_{\omega\to -i\omega+\epsilon}. \tag{4.19}$$

We compute contributions to this correlator up to and including three magnon form-factors. The next contribution comes at five magnons and so this result will be exact for frequencies, ω, up to 5Δ. The time-ordered correlator evaluated to the three-particle level is given by

$$\begin{aligned} G(x,\tau) &= -\Theta(\tau)\langle n^3(x,\tau)n^3(0,0)\rangle - \Theta(-\tau)\langle n^3(0,0)n^3(x,\tau)\rangle \\ &= -\Theta(\tau)\Big\{ \int d\hat\theta \sum_{a_1=1}^{3} |f^{n_3}_{a_1}(\theta)|^2 e^{-m\tau c(\theta)+imxs(\theta)} \\ &+\frac{1}{3!}\int d\hat\theta_1 d\hat\theta_2 d\hat\theta_3 \sum_{a_1,a_2,a_3=1}^{3} |f^{n_3}_{a_1a_2a_3}(\theta_1,\theta_2,\theta_3)|^2 e^{\sum_{i=1}^{3}(-m\tau c(\theta_i)+imxs(\theta_i))}\Big\} \\ &- (\tau, x\to -\tau,-x). \end{aligned} \tag{4.20}$$

If we again Fourier transform, using the form-factor results of the previous-section we find for positive frequencies [90]

$$\begin{aligned}
S(\omega > 0, \pi + k) &= S_1(\omega, k) + S_3(\omega, k) \\
&= \frac{1}{\sqrt{k^2+\Delta^2}}\delta(\omega - \sqrt{k^2+\Delta^2}) \\
&+ \frac{2\pi^4}{3}\int_0^{z_0} \left(3\pi^2 + 3z^2 + Y^2\right)\left|\psi(2z)\psi(z+Y)\psi(z-y)\right|^2 \\
&\times \frac{1}{\sqrt{(\omega^2 - k^2 - \Delta^2 - 4\Delta^2\cosh^2(z))^2 - 16\Delta^4\cosh^2(z)}}\,, \quad (4.21)
\end{aligned}$$

where

$$\begin{aligned}
z_0 &= \cosh^{-1}[(x-1)/2]\,, \\
Y &= \cosh^{-1}\left(\frac{x^2 - 1 - 4\cosh^2(z)}{4\cosh(z)}\right), \\
x^2 &= \frac{\omega^2 - q^2}{\Delta^2}\,. \quad (4.22)
\end{aligned}$$

The δ-function term, $S_1(\omega, k)$, in the above expression for $S(\omega, k)$ corresponds to the coherent one magnon contribution. The next term, $S_3(\omega, k)$, arises from the incoherent three magnon continuum. From Lorentz invariance, both are a function of $s = \sqrt{w^2 + k^2}$.

We can evaluate the three magnon contribution numerically. The result is plotted in Fig. 16 as a function of s. It is zero for $\omega < 3\Delta$. At threshold, i.e. $\omega - 3\Delta$ small and positive, $S(\omega, k+\pi)$ behaves as $(\omega - 3\Delta)^3$. We see that it peaks at around $s \sim 6\Delta$. Furthermore it is clear that its contribution to the response function is small. We can make this observation more qualitative. If we define

$$I_i(k+\pi) = \int_0^{30\Delta} d\omega S_i(\omega, k+\pi)\,, \quad (4.23)$$

we find that

$$\frac{I_3(\pi)}{I_1(\pi)} = 0.018\,. \quad (4.24)$$

Thus 98% of the total weight at wavevector π is found in the coherent one magnon contribution [90, 140].

While the three magnon continuum's contribution to the spectral function is small, we do note that there are reports of its observation in the Haldane gapped material, $CsNiCl_3$ [157, 159]. These reports suggest that the three magnon continuum is larger than computed in the O(3) NLSM. Ref. [157] finds instead that the ratio in Eq. (4.12) is given by $I_3(\pi)/I_1(\pi) \sim 0.1$. That the O(3) NLSM might underestimate the three magnon weight is not an impossibility. It is a low energy description of an integer spin chain. Given the spin gap, Δ, equals $0.4J$ where J, the spin-spin interaction strength, is an effective UV-cutoff, we would not necessarily expect accurate predictions for energies beyond $\omega > J$. This possibility is supported by the calculation of the response function using another low energy description of the integer spin chain, that of three Majorana fermions [90, 285]. There we have $\frac{I_3(\pi)}{I_1(\pi)} \sim .2$. However one must greet any attempt to describe physics in the Majorana description at energies larger than J with the same skepticism as the O(3) NLSM.

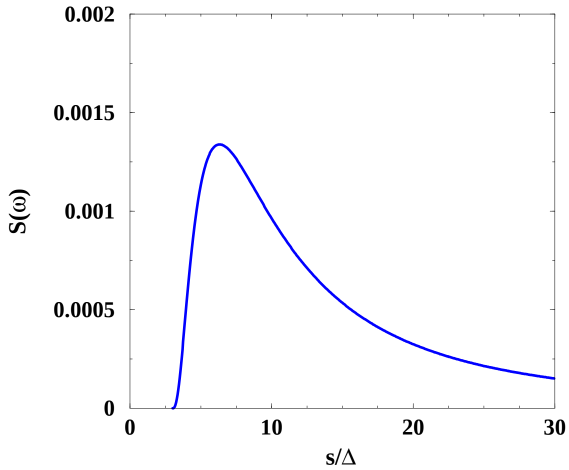

Figure 16. A plot of the three magnon contribution to the spectral weight of the spin-spin correlator near wavevector π in the $O(3)$ NLSM as a function of s.

4.4. *Low Temperature Properties of Correlation Functions*

In this section we show that finite temperature correlation functions admit low temperature expansions as discussed in Section 2. We begin by computing the finite DC susceptibility of the system. As we can access this quantity exactly through other means, we are able to test the methodology. We will find that the form factors reproduce precisely the known exact results. We then turn to computing the NMR relaxation rate as well as the finite field spin conductance. These quantities both probe the nature of transport in integer spin chains as described by the O(3) NLSM. We will thus be able to argue that transport here is ballistic not diffusive.

4.4.1. *Magnetization*

The susceptibility, χ, at $H = 0$ can be computed from the magnetization-magnetization operator using a Kubo formula,

$$\begin{aligned} \chi_(H=0) &= C(\omega=0,k=0)\,, \\ C(\omega,k) &= \left[\int_{-\infty}^{\infty} dx \int_0^{\beta} d\tau e^{iw_n\tau} e^{ikx} \langle T(M_0^3(x,\tau)M_0^3(0,0))\rangle\right]_{\omega_n\rightarrow -i\omega+\delta}. \end{aligned} \tag{4.25}$$

To evaluate this correlator we first expand out the thermal trace,

$$\begin{aligned} \langle M_0^3(x,\tau)M_0^3(0,0)\rangle &= \frac{1}{\mathcal{Z}}\,\mathrm{Tr}(e^{-\beta H}\mathcal{O}(x,t)\mathcal{O}(0,0)) \\ &= \frac{\sum_{ns_n} e^{-\beta E_{s_n}}\langle n,S_n|\mathcal{O}(x,t)\mathcal{O}(0,0)|n,S_n\rangle}{\sum_{nS_n} e^{-\beta E_{s_n}}\langle n,S_n|n,S_n\rangle}\,. \end{aligned} \tag{4.26}$$

Here $|n, S_n\rangle$ is a state of n excitations with spins described by $S_n = \{s_1, \cdots, s_n\}$. In writing the above we have suppressed sums over the energy and momenta of the excitations. A term in the thermal trace with n excitations is weighted by a factor of $e^{-n\beta\Delta}$. Thus, as discussed in Section 2, at low temperatures it is a good approximation to truncate this trace. For this computation we keep only terms with one and two excitations, i.e. $n = 1, 2$. To evaluate the matrix elements appearing in Eq. (4.16), we insert a resolution of the identity in between the two fields. As we only consider matrix elements involving one and two excitations from the thermal trace, we thus have

$$\begin{aligned} \langle s_1|M_0^3(x,\tau)M_0^3(0,0)|s_1\rangle &= \sum_{mS_m}\langle s_1|M_0^3(x,\tau)|mS_m\rangle\langle mS_m|M_0^3(0,0)|s_1\rangle \\ &= \sum_{s_1'}\langle s_1|M_0^3(x,\tau)|s_1'\rangle\langle s_1'|M_0^3(0,0)|s_1\rangle + \cdots\,, \\ \langle s_1s_2|M_0^3(x,\tau)M_0^3(0,0)|s_2s_1\rangle &= \sum_{mS_m}\langle s_1s_2|M_0^3(x,\tau)|mS_m\rangle \\ &\qquad\times\langle mS_m|M_0^3(0,0)|s_2s_1\rangle \\ = \Bigg(\sum_{s_1's_2'}\langle s_1s_2|M_0^3(x,\tau)|s_1's_2'\rangle&\langle s_2's_1'|M_0^3(0,0)|s_2s_1\rangle\Bigg) + \cdots\,. \end{aligned} \tag{4.27}$$

In the above we have truncated the sum arising from the resolution of the identity. With the first matrix element of the thermal trace, we only keep terms from the resolution of identity with one excitation. We are interested in the behavior of the susceptibility at $\omega = 0$ and this term provides the only contribution [173]. Similarly, the only term arising from the second matrix element of the thermal trace contributing to the DC susceptibility comes from keeping the term from the resolution of the identity involving two excitations. We can then evaluate $C(\omega, k)$ with the result

$$C(\omega, k) = C_1(\omega, k) + C_2(\omega, k)\,. \tag{4.28}$$

For $C_1(\omega, k)$, we then have the corresponding expression

$$\begin{aligned}
C_1(x,\tau) &= \sum_{s_1 s_2} \int \frac{d\theta}{2\pi}\frac{d\theta_1}{2\pi}\, e^{-\Delta\beta\cosh(\theta)} \langle A_{s_1}(\theta)|M_0^3(x,\tau)|A_{s_2}(\theta_1)\rangle \\
&\qquad\qquad \times \langle A_{s_2}(\theta_1)|M_0^3(0,0)|A_{s_1}(\theta)\rangle \\
&= \sum_{s_1 s_2} \int \frac{d\theta}{2\pi}\frac{d\theta_1}{2\pi}\, e^{-\Delta\beta\cosh(\theta)} e^{-\tau\Delta(\cosh(\theta_1)-\cosh(\theta))+ix\Delta(\sinh(\theta_1)-\sinh(\theta))} \\
&\quad \times \langle M_0^3(0,0)|A_{s_2}(\theta_1)A_{s_1}(\theta - i\pi)\rangle \langle M_0^3(0,0)|A_{s_1}(\theta)A_{s_2}(\theta_1 - i\pi)\rangle \\
&= \sum_{s_1 s_2} \int \frac{d\theta}{2\pi}\frac{d\theta_1}{2\pi}\, e^{-\Delta\beta\cosh(\theta)} e^{-\tau\Delta(\cosh(\theta_1)-\cosh(\theta))+ix\Delta(\sinh(\theta_1)-\sinh(\theta))} \\
&\qquad\qquad \times f^{M_0^3}_{s_1 s_2}(\theta - i\pi, \theta_1) f^{M_0^3}_{s_2 s_1}(\theta_1 - i\pi, \theta).
\end{aligned} \tag{4.29}$$

We have used crossing symmetry in the second line. From Section 4.2.2, the form factor $f^{M_0^3}_{aa_1}(\theta, \theta_1)$ is given by

$$f^{M_0^3}_{aa_1}(\theta, \theta_1) = i\frac{\pi^2\Delta}{4}\epsilon^{3aa_1}(\sinh(\theta) + \sinh(\theta_1))\psi(\theta - \theta_1). \tag{4.30}$$

Then upon Fourier transforming the above in x and τ and continuing $\omega_n \to -i\omega + \delta$, we obtain

$$C_1(\omega = 0, k = 0) = \frac{\beta\Delta}{\pi}\int d\theta \cosh(\theta) e^{-\beta\Delta\cosh(\theta)} = \frac{2\beta\Delta}{\pi}K_1(\beta\Delta), \tag{4.31}$$

where K_1 is a modified Bessel function. This has the expected small temperature behavior, $C_1(\omega = 0, k = 0) \sim T^{-1/2}e^{-\beta\Delta}$.

On the other hand $C_2(\omega = 0, k = 0)$ is given by

$$\begin{aligned}
C_2(x,\tau) = \frac{1}{4}\sum_{s_1 s_2 s_3 s_4} &\int \frac{d\theta_1}{2\pi}\frac{d\theta_2}{2\pi}\frac{d\theta_3}{2\pi}\frac{d\theta_4}{2\pi} \\
&\times \langle A_{s_1}(\theta_1)A_{s_2}(\theta_2)|M_0^3(x,\tau)|A_{s_3}(\theta_3)A_{s_4}(\theta_4)\rangle \\
&\times \langle A_{s_4}(\theta_4)A_{s_3}(\theta_3)|M_0^3(0,0)|A_{s_2}(\theta_2)A_{s_1}(\theta_1)\rangle \\
&- C_1(x,\tau)\sum_a \int \frac{d\theta}{2\pi}\, e^{-\beta\Delta\cosh(\theta)} \langle A_a(\theta)|A_a(\theta)\rangle.
\end{aligned} \tag{4.32}$$

The last term is disconnected (proportional to $C_1(x,\tau)$) and will ultimately cancel (good, as it is proportional to $\delta(0)$). The four particle matrix elements appearing in the above take the form (as per Section 2.7.1)

$$\begin{aligned}
&\langle A_{s_1}(\theta_1)A_{s_2}(\theta_2)|M_0^3(x,\tau)|A_{s_3}(\theta_3)A_{s_4}(\theta_4)\rangle\\
&\qquad= \delta_{s_1s_4}2\pi\delta(\theta_1-\theta_4)f^{M_0^3}_{\bar{s}_2,s_3}(\theta_2-i\pi,\theta_3)\\
&\qquad+\delta_{s_3's_2'}2\pi\delta(\theta_3-\theta_2)S^{s_1's_2'}_{s_1s_2}(\theta_{12})S^{s_3's_4'}_{s_3s_4}(\theta_{34})f^{M_0^3}_{\bar{s}_1',s_4'}(\theta_1-i\pi,\theta_4)\\
&\qquad+\delta_{s_2's_4}2\pi\delta(\theta_2-\theta_4)S^{s_1's_2'}_{s_1s_2}(\theta_{12})f^{M_0^3}_{\bar{s}_1',s_3}(\theta_1-i\pi,\theta_3)\\
&\qquad+\delta_{s_1s_3'}2\pi\delta(\theta_1-\theta_3)S^{s_3's_4'}_{s_3s_4}(\theta_{34})f^{M_0^3}_{\bar{s}_2,s_4'}(\theta_2-i\pi,\theta_4)\\
&\qquad+f^{M_0^3}_{\bar{s}_2,\bar{s}_1,s_4,s_3}(\theta_2-i\pi,\theta_1-i\pi,\theta_4,\theta_3)_{\rm c}\,,
\end{aligned}\tag{4.33}$$

where f_c refers to a connected form-factor. Substituting this expression into the above and using the form factors of Section 4.2.2, we find

$$\begin{aligned}
C_2(\omega=0,k=0) &= -\frac{6\beta\Delta}{\pi}K_1(2\beta\Delta)\\
&+\frac{2\beta\Delta}{\pi}\int d\theta_1 d\theta_2 e^{-\beta\Delta(\cosh(\theta_1)+\cosh(\theta_2))}\cosh(\theta_1)\frac{11\pi^2+2\theta_{12}^2}{\theta_{12}^4+5\pi^2\theta_{12}^2+4\pi^4}\\
&=-\frac{6\beta\Delta}{\pi}K_1(2\beta\Delta)+\frac{22\beta\Delta}{\pi^3}K_0(\beta\Delta)K_1(\beta\Delta)+\mathcal{O}\Big(\frac{T}{\Delta}e^{-2\beta\Delta}\Big),
\end{aligned}\tag{4.34}$$

where $\theta_{12}=\theta_1-\theta_2$ and K_n are standard modified Bessel functions. The first term in C_2 is a 'disconnected' contribution related to C_1. The second term is a connected contribution and as such is genuinely distinct from C_1.

It is possible in the case of the $O(3)$ sigma model to arrive at exact expressions (in the form of coupled integral equations) for the zero-field susceptibility [284, 296]. These equations, in their most compact form, appear as

$$\begin{aligned}
\chi(H=0) &= -\frac{\Delta}{2\pi}\int d\theta\cosh(\theta)\frac{\partial_H^2\epsilon(\theta)|_{H=0}}{1+e^{\beta\epsilon(\theta)}}\,,\\
\epsilon(\theta) &= \Delta\cosh(\theta)-T\int d\theta'\log(1+e^{\beta\epsilon_2(\theta')})s(\theta-\theta')\,,\\
\epsilon_n(\theta) &= T\int d\theta' s(\theta-\theta')\Big\{\log(1+e^{\beta\epsilon_{n-1}(\theta')})\\
&\qquad\qquad+\log(1+e^{\beta\epsilon_{n+1}(\theta')})+\delta_{2n}\log(1+e^{\beta\epsilon(\theta')})\Big\}\,,\\
H &= \lim_{n\to\infty}\frac{\epsilon_n(\lambda)}{n}\,.
\end{aligned}\tag{4.35}$$

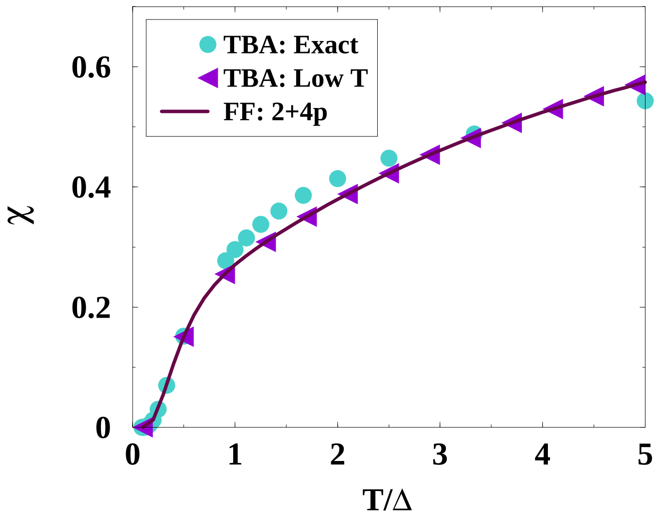

Figure 17. Plots of the zero-field susceptibility computed both from the TBA equations and from the form factor expansion. The first of these is an exact numerical solution of the TBA equations for the O(3) non-linear sigma model. The second is arrived at from a small temperature expansion in powers of $e^{-\beta\Delta}$ of these same equations. The final plot gives the form factor computation of the susceptibility. We have truncated the form factor expansion at the four particle level.

These equations admit a closed form low temperature expansion. The details of this expansion may be found in Ref. [284]. Here we just quote the results

$$\chi = \frac{2\beta\Delta}{\pi} K_1(\beta\Delta) - \frac{6\beta\Delta}{\pi} K_1(2\beta\Delta)$$
$$+\frac{2\beta\Delta}{\pi}\int d\theta_1 d\theta_2 e^{-\beta\Delta(\cosh(\theta_1)+\cosh(\theta_2))}\cosh(\theta_1)\,\frac{11\pi^2+2\theta_{12}^2}{\theta_{12}^4+5\pi^2\theta_{12}^2+4\pi^4}\,. \quad (4.36)$$

Remarkably, we see this expansion agrees exactly with the corresponding expression derived with the aid of form factors. Thus the form factor expansion at finite temperature meets an important test.

In Fig. 17 are plotted the susceptibilities computed via an exact numerical analysis of the TBA equations, a low temperature expansion of the same equations, and a computation based upon the two and four particle form factors. We see that as indicated previously that the form factor computation and the low temperature expansion match exactly. Moreover these two computations track the exact susceptibility over a considerable range of temperatures despite the fact these computations are truncated low temperature expansions.

4.4.2. *NMR Relaxation Rate*

In this section we compute the NMR relaxation rate, $1/T_1$. We are interested in computing this rate in order to compare it to the experimental data found in Ref. [269] on the relaxation rate of the quasi one-dimensional spin chain, $AgVP_2S_6$. For temperatures in excess of $100K$ (the gap, Δ, in this compound is on the order of $320K$), the experimental data [269] shows the relaxation rate to have an inverse dependence upon $\sqrt{H}$,

$$1/T_1 \propto \frac{1}{\sqrt{H}} \, .$$

This dependence is nicely reproduced by the semi-classical methodology in Refs. [66, 243]. Moreover the semi-classical computation reproduces the activated behavior of $1/T_1$ in this same temperature regime,

$$1/T_1 \propto e^{-3\beta\Delta/2}.$$

We are interested in determining whether a calculation in the fully quantum O(3) NLSM can reproduce these results. To this end we compute $1/T_1$ using a form factor expansion. Sagi and Affleck [245] have already done such a computation to lowest order in $e^{-\beta\Delta}$. But they do not find the above behavior. Rather they see

$$1/T_1 \propto \log(H)\, , \qquad 1/T_1 \propto e^{-\beta\Delta}.$$

We continue this computation one further step, computing to $\mathcal{O}(e^{-2\beta\Delta})$. Given the behavior, $1/T_1 \sim H^{-1/2}$, appears only as T is increased beyond 100K (i.e. $T/\Delta \sim 1/3$), it is not unreasonable to suppose higher order terms in a low temperature expansion of $1/T_1$ are needed to see this singularity.

To proceed with the computation of $1/T_1$, we review its constituent elements. $1/T_1$ can be expressed in terms of the spin-spin correlation function [245],

$$1/T_1 = \sum_{\substack{\alpha=1,2\\ \beta=1,2,3}} \int \frac{dk}{2\pi} A_{\alpha\beta}(k) A_{\alpha\gamma}(-k) \langle M_0^\beta M_0^\gamma \rangle (k, \omega_N)\, , \tag{4.37}$$

where $\omega_N = \gamma_N H$ is the nuclear Lamour frequency with γ_N the nuclear gyromagnetic ratio and the $A_{\alpha\beta}$ are the hyperfine coupling constants. In the above we assume H is aligned in the 3-direction. The above integral is dominated by values of k near 0 [245]. Moreover in the relevant experiment, the hyperfine couplings are such that only $\langle M_0^1 M_0^1 \rangle$ contributes. Hence

$$1/T_1 \propto \langle M_0^1 M_0^1 \rangle (x = 0, \omega_N \sim 0)\, . \tag{4.38}$$

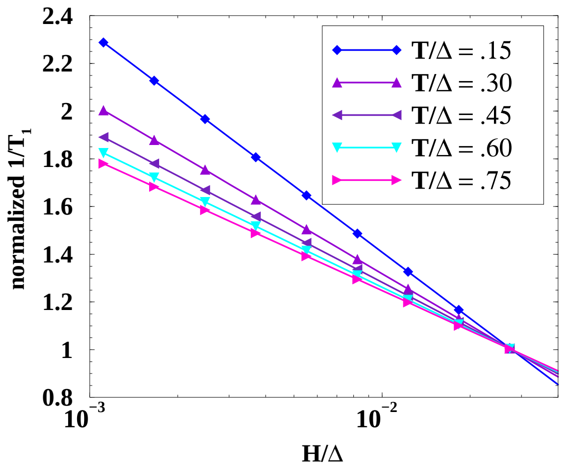

Figure 18. In this log-linear plot we present the form factor computation of the NMR relaxation rate, $1/T_1$, as a function of H for a variety of temperatures. We plot a normalized rate, the ratio of $1/T_1(H)$ with $1/T_1(H=\Delta/36)$.

We now proceed to compute $\langle M_0^1 M_0^1\rangle$.

To compute $\langle M_0^1 M_0^1\rangle$, we again employ a form factor expansion. Akin to the computation of the susceptibility and the spin conductance, this computation amounts to a low temperature expansion of $\langle M_0^1 M_0^1\rangle$,

$$\langle M_0^1 M_0^1\rangle = a_1 e^{-\beta\Delta} + a_2 e^{-2\beta\Delta} + \cdots ,$$

where we are able to compute a_1 and a_2. For the details of this computation we refer the reader to Ref. [173]. We find there

$$\langle M_0^1 M_0^1\rangle(x=0,\omega=0) = \Bigg(\frac{2\Delta}{\pi}\, e^{-\beta\Delta}\big(\log(\frac{4T}{H}) - \gamma\big) - \frac{6\Delta}{\pi}\, e^{-2\beta\Delta}\big(\log(\frac{2T}{H}) - \gamma\big)$$
$$+\Delta e^{-2\beta\Delta}\big(\log(\frac{4T}{H}) - \gamma\big)\sqrt{\frac{2\pi}{\beta\Delta}}\Big(24\pi + \frac{17}{\pi^3}\Big)\Bigg)\big(1 + \mathcal{O}(H/T) + \mathcal{O}(T/\Delta)\big)\,, \tag{4.39}$$

where $\gamma = .577\ldots$ is Euler's constant. We are interested in the regime $H \ll T \ll \Delta$ (the regime where it is expected spin diffusion produces singular behavior in $1/T_1$). The terms that we have dropped do not affect this behavior. In principle there is no difficulty in writing down the exact expression (to $\mathcal{O}(e^{-2\beta\Delta})$); it is merely unwieldy. This expression for $1/T_1$ is plotted in Fig. 18 for a variety of values of the ratio T/Δ.

We see that we do not obtain the same behavior as found in Refs. [66, 243]. Going to the next order in $\mathcal{O}(e^{-2\beta\Delta})$ produces a behavior in $1/T_1$ as

$H \to 0$ identical to the lower order computation of $\mathcal{O}(e^{-\beta\Delta})$: we again find a logarithmic behavior consistent with ballistic transport. An alternative comparison we might make to the results of Refs. [66, 243] is to perform a low temperature expansion (in $\mathcal{O}(e^{-\beta\Delta})$) of the semi-classical computation of $\langle M_0^1 M_0^1\rangle(x = 0, \omega = 0)$. Doing so by treating $Te^{-\beta\Delta}/H$ as a small parameter, we find

$$\langle M_0^1 M_0^1\rangle(x=0,\omega=0) \propto \Delta e^{-\beta\Delta}\Big(\log(\frac{4T}{H}) - \gamma + \Big(\frac{\pi}{4} - \frac{1}{2}\Big)\frac{T^2}{\pi H^2}\, e^{-2\beta\Delta} + \mathcal{O}(e^{-3\beta\Delta})\Big)\,. \tag{4.40}$$

We see that the low temperature expansion of the semi-classical result agrees to leading order with our computation but afterward differs. It possesses no term of $\mathcal{O}(e^{-2\beta\Delta})$. The next term rather appears at $\mathcal{O}(e^{-3\beta\Delta})$ and possesses a $1/H^2$ divergence. That the small H behavior should be $1/\sqrt{H}$ does suggest the importance of summing up terms. But the lack of a term of $\mathcal{O}(e^{-2\beta\Delta})$ in the semi-classical result nonetheless hints that the two results are genuinely different.

4.5. *Drude Weight of Spin Conductance at Finite Field*

In this section we compute the spin conductivity, σ_s. The spin conductivity gives the response of the spin chain to a spatially varying magnetic field. It is defined via

$$j_1(x,t) = \sigma_s \nabla H\,, \tag{4.41}$$

and so can be expressed in terms of a Kubo formula,

$$\mathrm{Re}\,\sigma_s(k,\omega) = -\frac{1}{k}\int dxdt e^{ikx+i\omega t}\,\mathrm{Im}\langle j_0(x,t)j_1(0,0)\rangle_{\mathrm{retarded}}\,. \tag{4.42}$$

In the notation used in this paper the spin current j_1 is synonymous with M_1^3 (for a field in the 3-direction), the Lorentz current counterpart of the uniform magnetization, $M_0^3 \equiv j_0$. We will focus primarily on computing the Drude weight, D, of $\mathrm{Re}\,\sigma_s$, i.e. computing the term in $\sigma_s(k,\omega)$ of the form

$$\sigma_s(k=0,\omega) = D\delta(\omega)\,. \tag{4.43}$$

However we are able to compute σ_s for general k, ω. We find that for $\omega \ll 2\Delta$, $k = 0$, the spin conductivity is described solely by the Drude weight. In particular, we find no indication of a regular contribution to $\sigma_s(k = 0, \omega)$.

To evaluate σ_s, we employ the identical form factor expansion to that used in computing the susceptibility. And like the susceptibility, our result is an exact low temperature expansion of D,

$$D = \sum_n D_n e^{-n\beta\Delta}.$$

Here we will compute D_1 and D_2 exactly. As the details of the computation are nearly identical to that of the susceptibility, we merely write down the results,

$$\begin{aligned}
D(H=0) &= \beta\Delta \int d\theta e^{-\beta\Delta\cosh(\theta)} \frac{\sinh^2(\theta)}{\cosh(\theta)} (1 - 3e^{-\beta\Delta\cosh(\theta)}) \\
&\quad + 2\beta\Delta \int d\theta_1 d\theta_2 e^{-\beta\Delta(\cosh(\theta_1)+\cosh(\theta_2))} \frac{\sinh^2(\theta_2)}{\cosh(\theta_2)} \frac{11\pi^2 + 2\theta_{12}^2}{\theta_{12}^4 + 5\pi^2\theta_{12}^2 + 4\pi^4} \\
&\quad + \mathcal{O}(e^{-3\beta\Delta}) \\
&= e^{-\beta\Delta}\sqrt{\frac{2\pi}{\beta\Delta}}\left(1 + \mathcal{O}\left(\frac{T}{\Delta}\right)\right) \\
&\quad - e^{-2\beta\Delta}\sqrt{\frac{1}{\beta\Delta}}\left(\frac{3}{2}\sqrt{\pi} - \frac{11}{\pi}\sqrt{\frac{T}{\Delta}} + \mathcal{O}\left(\frac{T}{\Delta}\right)\right) + \mathcal{O}(e^{-3\beta\Delta}). \qquad (4.44)
\end{aligned}$$

This expression, like the susceptibility, involves only the two and four particle form factors. We plot this result in Fig. 4.5 as a function of T/Δ.

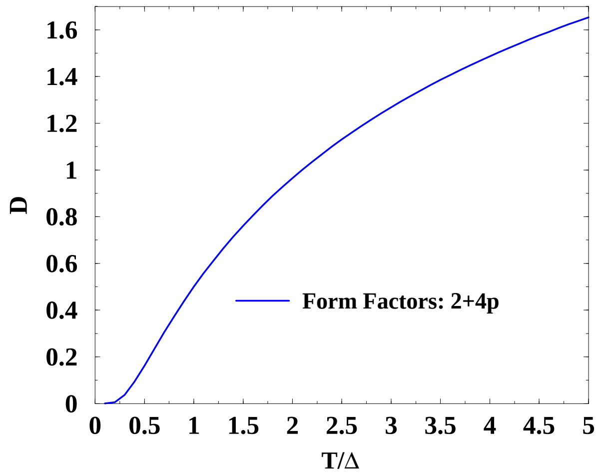

Figure 19. In this plot we present the form factor computation of the zero field ($H = 0$) Drude weight, D, of the spin conductance.

We observe that $D(H = 0) \neq 0$. This is in accordance with Ref. [111] where D is computed using an argument involving the finite size scaling of the thermodynamic Bethe ansatz equations. (We do note that the computation of D at $H = 0$ in Ref. [111] appears only as a note added in proof and so is decidedly sketchy. However the equations governing D developed in Ref. [111] are manifestly positive with the consequence D cannot vanish.) But our results do differ from the semi-classical computation of Ref. [244] where it was found that D vanishes at $H = 0$. We find as well no additional regular contributions to $\sigma_s(\omega, k = 0)$ near $\omega = 0$ – only the Drude term is present in contrast to Refs. [66, 243]. (There will, however, be regular contributions at higher frequencies, in particular for $\omega > 2\Delta$, which persist even in the zero temperature limit).

We have only given the spin conductivity at $H = 0$. However it is extremely straightforward to generalize the form factor computation to finite H. As H couples to the total spin, a conserved quantity, the form factors, $f^{\mathcal{O}}(x,t)$, of an operator, $\mathcal{O}(x,t)$, carrying spin s, are altered via the rule

$$f^{\mathcal{O}}(t) \to e^{iHst} f^{\mathcal{O}}(t)\,.$$

(In the case of the spin conductance, the spin currents, $j_\mu = M^3_\mu$, carry no spin and so are not altered at all.) The only remaining change induced by a finite field is to the Boltzmann factor appearing in the thermal trace. If an excitation with rapidity, θ, carries spin s, its Boltzmann factor becomes

$$e^{-\beta(\Delta\cosh(\theta) - sH)}.$$

For example we find D as a function of H (to $\mathcal{O}(e^{-\beta\Delta})$) to be

$$D(H) = \beta\Delta\cosh(\beta H) \int d\theta\, e^{-\beta\Delta\cosh(\theta)}\, \frac{\sinh^2(\theta)}{\cosh(\theta)}\,. \tag{4.45}$$

Again this in agreement with Ref. [111]. Indeed Ref. [111] computes $D(H)$ at large H/T (but $H \ll \Delta$) to be

$$D = \frac{\beta\Delta}{4\pi}\, e^{\beta H} \int d\theta\, \frac{\sinh^2(\theta)}{\cosh(\theta)}\, e^{-\beta\Delta\cosh(\theta)} + \mathcal{O}(e^{-2\beta\Delta})\,. \tag{4.46}$$

Up to a factor of 2π, this expression is in exact agreement with 4.46. In this particular case our derivation of $D(H)$ agrees with the semi-classical computation [244] (provided $T \ll H \ll \Delta$). The symmetries in the semi-classical model that lead $D(H = 0)$ to vanish are broken for finite H.

4.6. *Transport: Ballistic or Diffusive*

We have compared our transport calculations to the semi-classical computations in Refs. [66, 243]. The essence of this method lies in treating the spin-chain as a Maxwell-Boltzmann gas of spins which interact with one another through the low energy limit of the scattering of the O(3) NLSM,

$$S_{ab}^{cd}(\theta = 0) = -\delta_{ad}\delta_{cb}\,. \tag{4.47}$$

In contradistinction to the semi-classical computation, we have found that the Drude weight of the spin conductance is finite in the limit of zero external field. Our results for the NMR relaxation rate, $1/T_1$, indicate a similar discrepancy. We, like Ref. [245], find that $1/T_1$ is characterized by ballistic logarithms. These logarithms are relatively robust: they continue to appear at higher orders in the low temperature expansion. We do not, however, see diffusive behavior in the relaxation rate, i.e. $1/T_1 \sim 1/\sqrt{H}$, nor does our low temperature expansion match the low temperature expansion of the semi-classical computation of the correlator.

To come to some sort of judgment between the form-factor and the semi-classical approaches, an understanding is needed of the differences between our computations of the spin conductance and the NMR relaxation rate. In the case of the first quantity, it is likely this difference is real and not an artefact of our methodology. The data that goes into the spin conductance is identical to that needed to compute the susceptibility and we know that we can match the low temperature expansion of the susceptibility with a similar expansion coming from the exact free energy. Moreover we know that the Drude weight of $\sigma_s(H = 0)$ has been found to be finite from an approach [111] independent of ours.

In generic systems, the Drude weight, D, at finite temperatures will be zero. It is then the integrability of the O(3) NLSM and the attendant existence of an infinite number of conserved quantities that leads to a finite weight. The existence of these quantities can be directly related to a finite D. As discussed in Refs. [55, 328, 329], D is bounded from below via an inequality developed by Mazur:

$$D \geq c \sum_n \frac{\langle JQ_n\rangle}{\langle Q_n^2\rangle}\,, \tag{4.48}$$

where J is the relevant current operator, Q_n are a set of orthogonal conserved quantities, i.e. $\langle Q_n Q_m\rangle = \delta_{nm}\langle Q_n^2\rangle$, and c is some constant. For a finite Drude weight, we then require that at least one matrix element, $\langle JQ_n\rangle$, does not vanish. While we do no direct computations, we can obtain an indication of whether the matrix elements vanish by examining the symmetries of the model. Under the discrete (Z_2) symmetries of the O(3) NLSM, the spin current, J, transforms via

$$Z_2(J) \to \pm J\,.$$

In order that the matrix element, $\langle JQ_n\rangle$, not vanish we require that

$$Z_2(Q_n) \to \pm Q_n\,.$$

The Z_2 symmetries in the O(3) NLSM include $n_a \to -n_a$, $a = 1, 2, 3$, parity, and time reversal. The spin current we are interested in transforms under rotations as a pseudo-vector. Thus any charge, Q_n, coupling to the current must also transform as such. From the work by Lüscher [192], there is at least one conserved pseudo-vectorial quantity such that $\langle JQ_n\rangle$ does not vanish due to the action of one of the above Z_2 symmetries. For the sake of completeness we exhibit it. Rewriting the magnetization and spin current, $M_{0,1}$, explicitly as antisymmetric tensors,

$$M^{ab}_\mu = n^a\partial_\mu n^b - n^b\partial_\mu n^a\,, \quad \mu = 0, 1\,,$$

the conserved quantity takes the form,

$$Q^{ab}(t) = \sum_c \int dx_1 dx_2\, \mathrm{sgn}(x_1 - x_2) M^{ac}_0(t, x_1) M^{cb}_0(t, x_2) - \int dx M^{ab}_1(t, x)\,.$$

While the first term of Q^{ab} does not contribute to the matrix element, $\langle JQ^{ab}\rangle$, as it is bilinear in the currents, M^{ab}, the second term does. We point out that Q^{ab} is an exotic object inasmuch as it is a *non-local* conserved quantity. As pointed out in Ref. [192], it is the first in a series of non-local charges.

While the structure of the conserved quantities in the O(3) NLSM seem to be consistent with the existence of a finite Drude weight, this is not the case in the semi-classical approach. The dynamics of the semi-classical approximation used in Refs. [66, 243] are also governed by an infinite number of conserved quantities. Importantly however, these are different than those appearing in the fully quantum model. In particular, the semi-classical approximation does not admit non-local conserved quantities. As shown in Refs. [66, 243], the structure of the Z_2 symmetries in the semi-classical approach is such that all matrix elements, $\langle JQ_n\rangle$, vanish. It would thus seem the absence of a Drude weight in the semi-classical case is a consequence of differences in the symmetries between the semi-classical and fully quantum models.

To understand the discrepancies in the case of the NMR relaxation rate, $1/T_1$, is not as simple. However if we believe that the spin conductance demonstrates finite temperature ballistic behavior, it is hardly surprising to find the NMR relaxation rate characterized by ballistic logarithms. Again the difference between the fully quantum treatment and the semi-classical approach will lie in the differences between the models' conserved quantities. Nonetheless one possibility that we must consider is that merely going to $\mathcal{O}(e^{-2\beta\Delta})$ in the computation of $1/T_1$ is insufficient. It is possible that we need to perform some resummation of contributions from all orders to see the desired singular behavior, $1/T_1 \sim 1/\sqrt{H}$. While this would belie our experience with computing the susceptibility and the spin conductance via the correlators, the data that goes into the two computations is not exactly identical. Thus the possibility that the low temperature expansion of $1/T_1$ is not well controlled cannot be entirely ruled out.

The differences in the nature of the conserved quantities between the O(3) NLSM and the semi-classical model of Refs. [66,243] suggest the latter is not equivalent to the O(3) NLSM, even at low energies. An indication of this lack of equivalency may lie in the universal nature of the ultra low energy S-matrix. This quantity is the primary input of the semi-classical model. The semi-classical model imagines a set of classical spins interacting via

$$S^{cd}_{ab}(\theta = 0) = -\delta_{ad}\delta_{cb}\,,$$

i.e. in the scattering of two spins, the spins exchange their quantum numbers. However this specification may be insufficient to adequately describe the O(3) NLSM. Even beyond the quantum interference effects which are neglected by the semi-classical treatment, it is not clear that the zero-momentum S-matrix is enough to determine the model.

In this light it is instructive to consider the sine-Gordon model in its repulsive regime. The sine-Gordon model is given by the action,

$$S = \frac{1}{16\pi}\int dxdt\,\left(\partial_\mu\Phi\partial^\mu\Phi + \lambda\cos(\beta\Phi)\right), \tag{4.49}$$

where β falls in the range $0 < \beta < 1$. The model is generically gapped. Its repulsive regime occurs in the range, $1/2 < \beta^2 < 1$. The model's spectrum in this same range then consists solely of a doublet of solitons carrying U(1) charge. It is repulsive in the sense that the solitons have no bound states. The sine-Gordon model has a similar low energy S-matrix to the O(3) NLSM,

$$S^{cd}_{ab}(\theta = 0) = -\delta_{ad}\delta_{cb}\,,$$

where here the particle indices range over $\pm$, the two solitons in the theory. Thus we might expect that sine-Gordon model to possess identical low energy behavior over its entire repulsive regime.

This is likely to be in general untrue. For example we might consider the behavior of the single particle spectral function. We might thus want to compute a correlator of the form

$$\langle \psi_+(x,t)\psi_-(0,0)\rangle \, ,$$

where $\psi_\pm$ are Mandelstam fermions given by

$$\psi_\pm(x,t) = \exp\Bigg(\pm \frac{i}{2}\Big(\frac{1}{\sqrt{2}\beta} + \sqrt{2}\beta\Big)\phi_L(x,t) \mp \frac{i}{2}(\frac{1}{\sqrt{2}\beta} - \sqrt{2}\beta)\phi_R(x,t)\Bigg) \, ,$$
$$\phi_{L/R} = \frac{1}{2}\Bigg(\Phi(x,t) \pm i\int_{-\infty}^{x} dy \partial_t \Phi(y,t)\Bigg) \, . \tag{4.50}$$

As these fields depend explicitly upon β, it is hard to see how the properties of the above correlator, even at low energies could be independent of this same quantity. More generally, β determines the compactification radius of the boson in the model and so is related in a fundamental way to the model's properties.

It is useful to point out that Mandelstam fermions are the unique fields that create/destroy solitons that carry Lorentz spin 1/2, i.e. a spin that is independent of β. They would then be the only fields with a chance of matching any semi-classical computation. However there are other soliton creation fields, for example,

$$e^{\pm i\phi_{L,R}/(\sqrt{2}\beta)},$$

for which one could determine the corresponding spectral density. As these fields carry spin that varies as a function of β, their spectral functions will depend upon more than the ultra low energy soliton S-matrix. In general, the semi-classical treatment of the sine-Gordon model cannot capture its full quantum field content.

As with the O(3) NLSM, the conductance of the fully quantum model differs from that of the semi-classical treatment. If one were to compute the conductance at finite temperature in the sine-Gordon model one would again find a finite Drude weight, D, while the semi-classical approach yields $D = 0$ [114]. The notion of under-specificity appears here again. The semi-classical approach for the sine-Gordon model equally well describes the Hubbard model at half-filling (the solitons are replaced by particle/hole excitations in the half-filled band). But it fails to give the correct Drude weight.

An analysis of finite size corrections to the free energy in the presence of an Aharonov–Bohm flux [110] again finds a finite Drude weight in the half-filled Hubbard model at finite temperature.

Interestingly however, there are certain properties at low energies that seem to be independent of β. For example, if one were to compute the low temperature static charge susceptibility, the term of $\mathcal{O}(e^{-\beta\Delta})$ would be independent of β. However at the next order, $\mathcal{O}(e^{-2\beta\Delta})$, this would almost certainly cease to be true. And the energy/temperature ranges we are interested in exploring do not permit dropping terms of $\mathcal{O}(e^{-2\beta\Delta})$.

It is important to stress we do not question the agreement between the semi-classical model and experiment. What we do question is whether the fully quantum O(3) NLSM exhibits spin diffusivity. If we are then to understand spin diffusion in terms of the O(3) NLSM, it is possible we need to include additional physics such as an easy axis spin anisotropy (weakly present in the experimental system, $AgVP_2S_6$), inter-chain couplings, or a spin-phonon coupling (as done in [111]).

Beyond these, another mechanism that might lead to diffusive behavior are small integrable breaking perturbations of the O(3) NLSM. Generically any physical realization of a spin chain will possess such perturbations, even if arbitrarily small. Such perturbations may introduce the necessary ergodicity into the system, ergodicity that is absent in the integrable model because of the presence of non-trivial conserved charges, and so lead to diffusive behavior. As discussed in the semi-classical context by Garst and Rosch [114], such perturbations introduce an additional time scale, τ, governing the decay of conserved quantities in the problem. For times, $t < \tau$, the behavior of the system is ballistic and the original conserved quantities do not decay. For times, $t > \tau$, the behavior is then diffusive. Consequently the Drude weight in the purely integrable model is transformed into a peak in $\sigma(\omega)$ at $\omega \sim 1/\tau$.

Now the difference in the physics between the O(3) NLSM and its semi-classical variant is not that of integrable breaking perturbations. As demonstrated in Refs. [66, 243], their semi-classical model is classically integrable. However as discussed above the models do possess different conserved charges. It might then seem for certain transport quantities, the semi-classical model cures the lack of ergodicity present in its quantum counterpart.

5. U(1) Thirring Model and Quasi One Dimensional Mott Insulators

The Mott metal-insulator transition [115, 211, 212] is a zero temperature ("quantum") phase transition between a gapless metallic phase and a gapped insulating one. It occurs at some critical ratio of the strength of the electron-electron interaction "U" to the kinetic energy, which is usually measured in terms of the tunneling amplitude t of an appropriate tight-binding model. In practice U/t can be varied by applying pressure to a crystal, which results in a better overlap between the orbitals of the conduction band and leads to an increase in t. In high-energy physics the Mott transition corresponds to the phenomenon of dynamical mass generation.

The intrinsic difficulty in describing the Mott transition quantitatively in the general case is that it occurs when the kinetic and potential energies are of the same order of magnitude. This regime is difficult to access from either the "band" limit, where one diagonalizes the kinetic energy first and then takes electron-electron interactions into account perturbatively, or the "atomic" limit, in which the electron-electron interaction is diagonalized first and the electron hopping is taken into account perturbatively. Interestingly, the Mott transition on lattices where tunneling along one direction is much larger than along all others can be understood in some detail by employing methods of integrable quantum field theory. The systems under consideration can be thought of in terms of weakly coupled chains of electrons and will be referred to as *quasi one dimensional Mott insulators*. When the band is half-filled and the interchain tunneling is switched off, Umklapp processes dynamically generate a spectral gap M and we are dealing with an ensemble of uncoupled 1D Mott insulating chains. The same Umklapp scattering mechanism can generate gaps at *any* commensurate filling e.g. quarter filling, but only if the interactions are sufficiently strong. There are two questions we want to address: (i) What is the dynamical response of the uncoupled Mott-insulating chains system and (ii) What are the effects of a weak interchain tunneling. As far as point (i) is concerned we will concentrate on the optical conductivity and the single particle spectral function. Results are also available for the density-density response function [61] and the dynamical structure factor [40]. Examples of materials that are believed to fall into the general category of quasi-1D Mott insulators are the Bechgaard salts [47] and chain cuprates like $SrCuO_2$, Sr_2CuO_3 [o] or $PrBa_2Cu_3O_7$. They have been found to exhibit very rich and unusual physical properties

[o] More precisely, these compounds are considered to be charge-transfer insulators.

such as spin-charge separation [112, 162, 165, 206, 309, 311].

5.1. *Lattice Models of Correlated Electrons*

The simplest models used in the description of one dimensional Mott insulators are "extended" Hubbard models of the form

$$\hat{H} = -t\sum_{n,\sigma}\left[c^\dagger_{n,\sigma}c_{n+1,\sigma} + \text{h.c.}\right] + U\sum_k n_{k,\uparrow}n_{k,\downarrow} + \sum_{j\geq 1} V_j \sum_k n_k n_{k+j}\ , \quad (5.1)$$

where $n_{k,\sigma} = c^\dagger_{k,\sigma}c_{k,\sigma}$ and $n_k = n_{k,\uparrow} + n_{k,\downarrow}$ are electron number operators. The electron-electron interaction terms mimic the effects of a screened Coulomb interaction. Two cases are of particular interest from the point of view of application to, for example, the Bechgaard salts [47]:

(1) half filling (one electron per site);
(2) quarter filling (one electron per two sites).

We will discuss both these cases and emphasize similarities and differences in their dynamical response.

5.2. *Field Theory Description of the Low Energy Limit*

The field theory limit is constructed by keeping only the low-energy modes in the vicinity of the Fermi points $\pm k_F$. We may express the lattice electron annihilation operator in terms of the slowly varying (on the scale of the lattice spacing a_0) right and left moving electron fields $R(x)$ and $L(x)$,

$$c_{l,\sigma} \longrightarrow \sqrt{a_0}\left[\exp(ik_F x)\ R_\sigma(x) + \exp(-ik_F x)\ L_\sigma(x)\right]. \quad (5.2)$$

Here $k_F = \pi/2a_0$ for the half-filled band and $x = la_0$. The resulting fermion Hamiltonian can then be bosonized by standard methods [119]. In order to make our presentation reasonably self-contained we review the relevant steps in the half-filled case next.

5.2.1. *Half Filled Band*

Using (5.2) in (5.1) we arrive at the following low-energy effective Fermion theory

$$\begin{aligned}\mathcal{H} = \sum_\sigma v_F \int dx\ :\Big[L_\sigma^\dagger\ i\partial_x L_\sigma - R_\sigma^\dagger\ i\partial_x R_\sigma\Big]: - \frac{g_0}{6}\int dx\ :\big[\mathbf{J}\cdot\mathbf{J} + \bar{\mathbf{J}}\cdot\bar{\mathbf{J}}\big]:\\ -g_s\int dx\ :\mathbf{J}\cdot\bar{\mathbf{J}}: + \frac{g_c^\perp + g_c^\parallel - 2g_0}{6}\int dx\ :\big[\mathbf{I}\cdot\mathbf{I} + \bar{\mathbf{I}}\cdot\bar{\mathbf{I}}\big]:\\ +\int dx\left[\frac{g_c^\perp}{2} :(I^+\bar{I}^- + I^-\bar{I}^+): + g_c^\parallel :I^z\bar{I}^z:\right].\end{aligned} \tag{5.3}$$

Here $v_F = 2ta_0$ is the Fermi velocity,

$$g_0 = 2Ua_0,\quad g_s = g_c^\perp = 2a_0(U-2V_1+2V_2),\quad g_c^\parallel = 2a_0(U+6V_1+2V_2), \tag{5.4}$$

and $\mathbf{J}$, $\mathbf{I}$ are the chiral components of SU(2) spin and pseudospin currents,

$$\begin{aligned}\bar{I}^z &= \frac{1}{2}:\Big(L_\uparrow^\dagger L_\uparrow + L_\downarrow^\dagger L_\downarrow\Big):,\quad \bar{I}^+ = (\bar{I}^-)^\dagger = L_\uparrow^\dagger L_\downarrow^\dagger\ ,\\ I^z &= \frac{1}{2}:\Big(R_\uparrow^\dagger R_\uparrow + R_\downarrow^\dagger R_\downarrow\Big):,\quad I^+ = (I^-)^\dagger = R_\uparrow^\dagger R_\downarrow^\dagger\ ,\\ \bar{J}^z &= \frac{1}{2}:\Big(L_\uparrow^\dagger L_\uparrow - L_\downarrow^\dagger L_\downarrow\Big):,\quad \bar{J}^+ = (\bar{J}^-)^\dagger = L_\uparrow^\dagger L_\downarrow\ ,\\ J^z &= \frac{1}{2}:\Big(R_\uparrow^\dagger R_\uparrow - R_\downarrow^\dagger R_\downarrow\Big):,\quad J^+ = (J^-)^\dagger = R_\uparrow^\dagger R_\downarrow\ .\end{aligned} \tag{5.5}$$

Here ":" denotes normal ordering of point-split expressions [3]. The "kinetic" terms in the Hamiltonian (5.3) can be expressed as normal ordered bilinears of currents as well [3, 62, 119]

$$\begin{aligned}\frac{2\pi}{3}\int dx\ :[\mathbf{I}\cdot\mathbf{I} + \mathbf{J}\cdot\mathbf{J}]: &= -\int dx\left[\sum_\sigma :R_\sigma^\dagger\ i\partial_x\ R_\sigma:\right],\\ \frac{2\pi}{3}\int dx\ :[\bar{\mathbf{I}}\cdot\bar{\mathbf{I}} + \bar{\mathbf{J}}\cdot\bar{\mathbf{J}}]: &= \int dx\left[\sum_\sigma :L_\sigma^\dagger\ i\partial_x\ L_\sigma:\right].\end{aligned} \tag{5.6}$$

Using (5.6) the Hamiltonian (5.3) can now be split into two parts, corresponding to the spin and charge sectors respectively

$$\begin{aligned}
\mathcal{H} &= \mathcal{H}_c + \mathcal{H}_s \ , \\
\mathcal{H}_c &= \frac{2\pi v_c'}{3}\int dx \ \ :\left[\mathbf{I}\cdot\mathbf{I}+\bar{\mathbf{I}}\cdot\bar{\mathbf{I}}\right]: \\
&\quad + \int dx\left[\frac{g_c^{\perp}}{2}:(I^+\bar{I}^- + I^-\bar{I}^+): + g_c^{\parallel}:I^z\bar{I}^z:\right], \\
\mathcal{H}_s &= \frac{2\pi v_s}{3}\int dx \ \ :\left[\mathbf{J}\cdot\mathbf{J}+\bar{\mathbf{J}}\cdot\bar{\mathbf{J}}\right]: - g_s\int dx \ \ :\mathbf{J}\cdot\bar{\mathbf{J}}: \ .
\end{aligned} \tag{5.7}$$

Here $v_s = v_F - Ua_0/2\pi$ and $v_c' = v_F + (U+4V_1+4V_2)a_0/2\pi$. The Hamiltonian (5.7) with $v_s = v_c'$ and $g_s = 0$ is known as the U(1) Thirring model in the literature. As we will see the difference in velocities can be accommodated and as will show now the current-current interaction in the spin sector is marginally irrelevant and will only lead to logarithmic corrections at low energies. The 1-loop renormalization group equation for g_s is

$$r\,\frac{\partial g_s}{\partial r} = -\frac{g_s^2}{2\pi} \ . \tag{5.8}$$

Hence g_s diminishes under renormalization and the current-current interaction in the spin sector is marginally irrelevant. In order to keep things simple we will drop it from now on. Keeping it would lead to logarithmic corrections in many of the formulas below. The Hamiltonian (5.7) can now be bosonized using

$$\begin{aligned}
L_\sigma^\dagger(x) &= \frac{\eta_\sigma}{\sqrt{2\pi}}e^{if_\sigma\pi/4}\exp\left(-\frac{i}{2}\bar{\phi}_c\right)\exp\left(-\frac{if_\sigma}{2}\bar{\phi}_s\right), \\
R_\sigma^\dagger(x) &= \frac{\eta_\sigma}{\sqrt{2\pi}}e^{if_\sigma\pi/4}\exp\left(\frac{i}{2}\phi_c\right)\exp\left(\frac{if_\sigma}{2}\phi_s\right),
\end{aligned} \tag{5.9}$$

where η_a are Klein factors with $\{\eta_a, \eta_b\} = 2\delta_{ab}$ and where $f_\uparrow = 1$, $f_\downarrow = -1$. [p] The canonical Bose fields $\Phi_{s,c}$ and their respective dual fields $\Theta_{s,c}$ are given by

$$\Phi_a = \phi_a + \bar{\phi}_a \ , \qquad \Theta_a = \phi_a - \bar{\phi}_a \ , \ a = s, c \ , \tag{5.10}$$

[p] The phase factors in (5.17) have been introduced in order to ensure the standard bosonization formulas for the staggered magnetizations.

where the chiral boson fields ϕ_a and $\bar{\phi}_a$ fulfill the following commutation relations

$$[\phi_a(x), \bar{\phi}_a(y)] = 2\pi i \ , \quad a = c, s. \tag{5.11}$$

We choose a normalization such that for $|x-y| \longrightarrow 0$ the following operator product expansion holds ($a = s, c$)

$$\exp\left(i\alpha\Phi_a(x)\right)\exp\left(i\beta\Phi_a(y)\right) \longrightarrow |x-y|^{4\alpha\beta}\exp\left(i\alpha\Phi_a(x)+i\beta\Phi_a(y)\right). \tag{5.12}$$

Applying the bosonization identities we obtain the following bosonic form of the low energy effective Hamiltonian (we recall that we have set $g_s = 0$)

$$\begin{aligned}
\mathcal{H}_c &= \frac{v_c'}{16\pi}\int dx\, \left[(\partial_x\Phi_c)^2 + (\partial_x\Theta_c)^2\right] \\
&\quad -\frac{g_c^{\perp}}{(2\pi)^2}\int dx\ \cos(\Phi_c) + \frac{g_c^{\parallel}}{(8\pi)^2}\int dx\, \left[(\partial_x\Phi_c)^2 - (\partial_x\Theta_c)^2\right] \ , \\
\mathcal{H}_s &= \frac{v_s}{16\pi}\int dx\, \left[(\partial_x\Phi_s)^2 + (\partial_x\Theta_s)^2\right].
\end{aligned} \tag{5.13}$$

Finally we carry out a canonical transformation on the charge boson

$$\Phi_c \longrightarrow \beta\Phi_c \ , \qquad \Theta_c \longrightarrow \frac{1}{\beta}\Theta_c \ , \tag{5.14}$$

where

$$\beta = \left[\frac{1 - g_c^{\parallel}/4\pi v_c'}{1 + g_c^{\parallel}/4\pi v_c'}\right]^{\frac{1}{4}}. \tag{5.15}$$

The transformation property of the dual field follows from the fact that $-\partial_x\Theta_c$ is the momentum conjugate to Φ_c. In terms of the rescaled fields the charge sector takes the form of a sine-Gordon model

$$\mathcal{H}_c = \frac{v_c}{16\pi}\int dx\, \left[(\partial_x\Theta_c)^2 + (\partial_x\Phi_c)^2\right] - \frac{g_c^{\perp}}{4\pi^2}\int dx\, \cos\beta\Phi_c \ , \tag{5.16}$$

where $v_c = (v_c' + g_c^{\parallel}/4\pi)\beta^2$. The entire procedure we have been following can be summarized as follows. We first project the lattice Hamiltonian to the low-energy degrees of freedom using (5.2) and then bosonize the resulting fermion Hamiltonian by means of the identities

$$L^\dagger_\sigma(x) = \frac{\eta_\sigma}{\sqrt{2\pi}} e^{if_\sigma\pi/4} \exp\left(-\frac{i}{4}\left[\beta\Phi_c - \frac{1}{\beta}\Theta_c\right]\right) \exp\left(-\frac{if_\sigma}{4}\left[\Phi_s - \Theta_s\right]\right),$$
$$R^\dagger_\sigma(x) = \frac{\eta_\sigma}{\sqrt{2\pi}} e^{if_\sigma\pi/4} \exp\left(\frac{i}{4}\left[\beta\Phi_c + \frac{1}{\beta}\Theta_c\right]\right) \exp\left(\frac{if_\sigma}{4}\left[\Phi_s + \Theta_s\right]\right). \quad (5.17)$$

The Hamiltonian (5.16) exhibits spin-charge separation: $\mathcal{H}_{\rm c,s}$ describe collective charge and spin degrees of freedom respectively, which are independent of one another. The pure Hubbard model corresponds to the limit $\beta \to 1$ and the effect of V_j is to decrease the value of β. From the form (5.16) we can deduce a number of important properties. Firstly, the spin sector is gapless and is described by a free bosonic theory. Hence correlation functions involving (vertex operators of) the spin boson Φ_s and its dual field Θ_s can be calculated by standard methods [119]. Excitations in the spin sector are scattering states of gapless, chargeless spin $\frac{1}{2}$ objects called *spinons*. The charge sector of (5.16) is a SGM. Here excitations in the regime $\beta > \frac{1}{\sqrt{2}}$ are scattering states of gapped charge $\pm e$ soliton and antisoliton excitations respectively. In the context of the half-filled Mott insulator these are also known as *holon* and *antiholon*. Soliton and antisoliton have massive relativistic dispersions with velocity $v_{\rm c}$ and single-particle gap Δ,

$$E(P) = \sqrt{\Delta^2 + v_{\rm c}^2 P^2}\ . \quad (5.18)$$

For $V_j = 0,\ j \geq 3$ the gap can be determined by renormalization group methods

$$\Delta \approx \frac{8t}{\sqrt{2\pi}} \sqrt{g(1+x)} \left(\frac{1-x}{1+x}\right)^{(gx+2)/4gx}, \quad (5.19)$$

where we have fixed the constant factor by comparing to the exact result for the Hubbard model [186], and where

$$x = \left[1 - \left(\frac{U - 2V_1 + 2V_2}{U + 6V_1 + 2V_2}\right)^2\right]^{1/2},$$
$$g = (U + 6V_1 + 2V_2)/2\pi t\ . \quad (5.20)$$

We note that the gap vanishes on the critical surface $U - 2V_1 + 2V_2 = 0$ separating the Mott-insulating phase with gapless spin excitations from another phase with a spin gap.

In the regime $0 < \beta < 1/\sqrt{2}$, soliton and antisoliton attract and can form bound states. In the SGM these are known as "breathers" and correspond to excitons in the underlying extended Hubbard lattice model. There are

$$N = \left[\frac{1-\beta^2}{\beta^2}\right] \tag{5.21}$$

different types of excitons, where $[x]$ in (5.21) denotes the integer part of x. The exciton gaps are given by

$$\Delta_n = 2\Delta \sin(n\pi\xi/2)\ , \quad n = 1, \ldots, N\ , \tag{5.22}$$

where we have defined

$$\xi = \frac{\beta^2}{1-\beta^2}\ . \tag{5.23}$$

We note that in the weak coupling analysis summarized above β cannot be appreciably smaller than 1. However, numerical Dynamical Density Matrix Renormalization Group (DDMRG) computations [91, 145] indicate that the U(1) Thirring model description remains valid in an extended region of parameter space where U, V_1, V_2 are not small compared to t, but the model is still in a Mott insulating phase. A rough criterion for the applicability of the U(1) Thirring model to the description of the low-energy physics is that the charge gap should be small compared to the electronic band width $4t$. When applying the U(1) Thirring model in the extended region of parameter space, the gap Δ and the parameter β have to be determined numerically.

5.2.2. *Quarter Filled Band*

In the quarter filled case there are no simple Umklapp processes that can open a gap in the charge sector. As a result the quarter-filled extended Hubbard model is metallic in the weak coupling regime, i.e. both charge and spin sectors are gapless. However, integrating out the high energy degrees or freedom in a path-integral formulation generates “double Umklapp” processes involving four electron creation and annihilation operators each [116, 305]. For small U, V_j these processes are irrelevant, but increasing U, V_j decreases their scaling dimension. This suggests that for sufficiently large U, V_j the double Umklapp terms eventually become relevant and open up a Mott gap in the charge sector. Such a scenario is indeed supported by numerical computations [234]. Assuming that a bosonized description remains valid beyond the weak coupling region, the low-energy effective Hamiltonian is identical to (5.16). However, the relations between the Fermi operators and the Bose fields are different

$$L^\dagger_\sigma(x) = \frac{\eta_\sigma}{\sqrt{2\pi}}\, e^{if_\sigma\pi/4} \exp\left(-\frac{i}{4}\left[\frac{\beta}{2}\Phi_c - \frac{2}{\beta}\Theta_c\right]\right) \exp\left(-\frac{if_\sigma}{4}\left[\Phi_s - \Theta_s\right]\right),$$

$$R^\dagger_\sigma(x) = \frac{\eta_\sigma}{\sqrt{2\pi}}\, e^{if_\sigma\pi/4} \exp\left(\frac{i}{4}\left[\frac{\beta}{2}\Phi_c + \frac{2}{\beta}\Theta_c\right]\right) \exp\left(\frac{if_\sigma}{4}\left[\Phi_s + \Theta_s\right]\right). \quad (5.24)$$

Although the low-energy effective Hamiltonian is the same as for the half-filled Mott insulator, the physical properties in the quarter-filled case are rather different. Firstly, the insulating state emerging for sufficiently large U, V_j at quarter filling is generated by a different physical mechanism (double Umklapp scattering) as compared to half filling (Umklapp scattering) and concomitantly is referred to as a $4k_F$ charge-density wave insulator in the literature [216]. We adopt this terminology here. Secondly, the quantum numbers of elementary excitations in the charge sector are different. Like for the half-filled case the elementary excitations in the charge sector are a soliton/antisoliton doublet, but now they carry *fractional charge* $\pm\frac{e}{2}$. A simple way to see this is to recall that the conserved topological charge in the SGM is defined as

$$Q = \frac{\beta}{2\pi}\int_{-\infty}^{\infty} dx\ \partial_x\Phi_c\ . \quad (5.25)$$

The soliton has topological charge -1 and the antisoliton $+1$. A simple calculation shows that the right moving fermion creates two solitons

$$QR^\dagger_\sigma(x)|0\rangle = -2R^\dagger_\sigma(x)|0\rangle\ . \quad (5.26)$$

This implies that fermion number 1 corresponds to topological charge 2 and hence solitons have fractional charge. The elementary excitations in the spin sector are again a pair of gapless, chargeless spin $\pm\frac{1}{2}$ spinons.

5.3. *Correlation Functions*

Due to spin charge separation a general local operator $\mathcal{O}(t,x)$ can be represented as a product of a charge and a spin piece $\mathcal{O} = \mathcal{O}_c\mathcal{O}_s$. As a result correlation functions factorize as well,

$$\langle 0|\mathcal{O}^\dagger(\tau,x)\,\mathcal{O}(0)|0\rangle = {}_c\langle 0|\mathcal{O}^\dagger_c(\tau,x)\,\mathcal{O}_c(0)|0\rangle_c\ {}_s\langle 0|\mathcal{O}^\dagger_s(\tau,x)\,\mathcal{O}_s(0)|0\rangle_s\,, \quad (5.27)$$

where $|0\rangle_{s,c}$ are the vacua in the spin and charge sectors respectively. Correlation functions in the spin sector are easily evaluated as we are dealing with a free theory. In what follows we only need correlators of vertex operators, which in our normalizations are given by

$$
\begin{aligned}
{}_s\langle \exp\left(i\alpha\varphi_s(\tau,x)\right)\exp\left(-i\alpha\varphi_s(0)\right)\rangle_s &= \frac{1}{(v_s\tau - ix)^{2\alpha^2}}\ ,\\
{}_s\langle \exp\left(i\alpha\bar\varphi_s(\tau,x)\right)\exp\left(-i\alpha\bar\varphi_s(0)\right)\rangle_s &= \frac{1}{(v_s\tau + ix)^{2\alpha^2}}\ . \qquad (5.28)
\end{aligned}
$$

5.3.1. *Correlation Functions in the Charge Sector*

As the charge sector of the U(1) Thirring model is equal to a SGM, we may use the form factor approach to determine the charge pieces of correlation functions. In the parameter regime of interest the spectrum of the SGM consists of soliton, antisoliton and several breather bound states, which we denote by labels $s, \bar{s}, B_1, B_2, \dots B_N$. Energy and momentum are then parametrized in terms of the rapidity variable θ as

$$
E_\alpha(\theta) = \Delta_\alpha \cosh\theta\ , \quad P_\alpha(\theta) = \frac{\Delta_\alpha}{v_{\rm c}}\sinh\theta\ , \qquad (5.29)
$$

where

$$
\Delta_s = \Delta_{\bar{s}} \equiv \Delta\ , \quad \Delta_{B_n} \equiv \Delta_n\ , \qquad (5.30)
$$

and the breather gaps, Δ_n, are given by (5.22).

5.4. *Optical Conductivity*

The optical conductivity was calculated in Refs. [59,60,91,143]. In the field-theory limit, the electrical current operator is related to the fermion current J by

$$
J_{\rm el}(\tau,x) = -ea_0 J(\tau,x) = -i\,\frac{ea_0\mathcal{A}}{2\pi}\,\partial_\tau\phi_{\rm c}\ , \qquad (5.31)
$$

where $\mathcal{A}$ is a non-universal constant. For $U, V_j \ll t$ we have $\mathcal{A} \approx 1$. The expression for the current operator is the same for the half-filled and the quarter filled bands. As seen from Eq. (5.31), the current operator does not couple to the spin sector. This shows that spinons do not contribute to the optical conductivity in the field theory limit. Hence, the calculation of the optical conductivity has been reduced to the evaluation of the retarded current-current correlation function in the charge sector. The real part of the optical conductivity ($\omega > 0$) has the following spectral representation

$$\mathrm{Re}\ \sigma(\omega) = \frac{2\pi^2 e^2}{a_0^2\omega}\sum_{n=1}^{\infty}\sum_{\epsilon_i}\int \frac{d\theta_1\dots d\theta_n}{(2\pi)^n n!}\left|f^J(\theta_1\dots\theta_n)_{\epsilon_1\dots\epsilon_n}\right|^2 \times\ \delta\Big(\sum_k \frac{\Delta_{\epsilon_k}}{v_{\rm c}}\sinh\theta_k\Big)\ \delta(\omega - \sum_k \Delta_{\epsilon_k}\cosh\theta_k)\ . \quad (5.32)$$

In Refs. [23,109,156,193,194,264] integral representations for the form factors of the current operator $J(\tau, x)$ in the SGM were derived. Using these results we can determine the first few terms of the expansion (5.32). From (5.32) it is easy to see for any given frequency ω only a finite number of intermediate states will contribute: the delta function forces the sum of single-particle gaps $\sum_j \Delta_{\epsilon_j}$ to be less than ω. Expansions of the form (5.32) are usually found to exhibit a rapid convergence, which can be understood in terms of phase space arguments [53,214]. Therefore we expect that summing the first few terms in (5.32) will give us good results over a large frequency range.

Using the transformation property of the current operator under charge conjugation one finds that many of the form factors in (5.32) actually vanish. In particular, only the "odd" breathers $B_1, B_3, \dots$ (assuming they exist, i.e., β is sufficiently small) couple to the current operator. The first few non-vanishing terms of the spectral representation (5.32) are

$$\mathrm{Re}\ \sigma(\omega) = \left(\frac{Ae}{2a_0}\right)^2 v_c \left[\sum_{n=1}^{[(1+\xi)/2\xi]}\sigma_{B_{2n-1}}(\omega) + \sigma_{s\bar{s}}(\omega) + \sigma_{B_1B_2}(\omega) + \dots\right]. \quad (5.33)$$

Here $\sigma_{B_n}(\omega)$, $\sigma_{s\bar{s}}(\omega)$ and $\sigma_{B_1B_2}(\omega)$ are the contributions of the odd breathers, the soliton-antisoliton continuum and the B_1B_2 breather-breather continuum respectively. The latter of course exists only if $\xi \le \frac{1}{2}$. We find

$$\begin{aligned}\sigma_{B_{2n-1}}(\omega) &= \pi\ f_{2n-1}\delta(\omega - \Delta_{2n-1})\\ f_m &= \frac{2\xi^2}{\tan\left(\frac{m\pi\xi}{2}\right)}\prod_{n=1}^{m-1}\tan^2\left(\frac{\pi n\xi}{2}\right)\\ &\quad\times\exp\left[-2\int_0^\infty \frac{dt}{t}\frac{\sinh\big(t(1-\xi)\big)}{\sinh(t\xi)\cosh(t)}\frac{\sinh^2(mt\xi)}{\sinh 2t}\right]\ . \quad (5.34)\end{aligned}$$

The soliton-antisoliton contribution is [59]

$$\sigma_{s\bar{s}}(\omega) = \frac{4\sqrt{\omega^2 - 4\Delta^2}\ \Theta(\omega - 2\Delta)}{\omega^2[\cos\left(\frac{\pi}{\xi}\right) + \cosh\left(\frac{\theta_0}{\xi}\right)]} \times \exp\left(\int_0^\infty \frac{dt}{t} \frac{\sinh(t(1-\xi))\left[1 - \cos\left(\frac{2t\theta_0}{\pi}\right)\cosh 2t\right]}{\sinh(t\xi)\cosh(t)\sinh 2t}\right), \quad (5.35)$$

where $\theta_0 = 2\text{arccosh}(\omega/2\Delta)$. The result for the B_1B_2 breather-breather continuum is given in Ref. [91]. As a function of the parameter β, the optical conductivity behaves as follows.

- $1 \geq \beta^2 > 1/2$:

  In this regime the optical spectrum consists of a single "band" corresponding to (multi) soliton-antisoliton states above a threshold $\Delta = 2\Delta$. The absorption band increases smoothly above the threshold Δ in a universal square root fashion

$$\sigma(\omega) \propto \sqrt{\omega - \Delta} \quad \text{for} \quad \omega \to \Delta^+ \ . \quad (5.36)$$

  In Fig. 20 we plot the leading contributions for the case $\beta^2 = 0.9$. Clearly, the four-particle contribution is negligible at low frequencies.

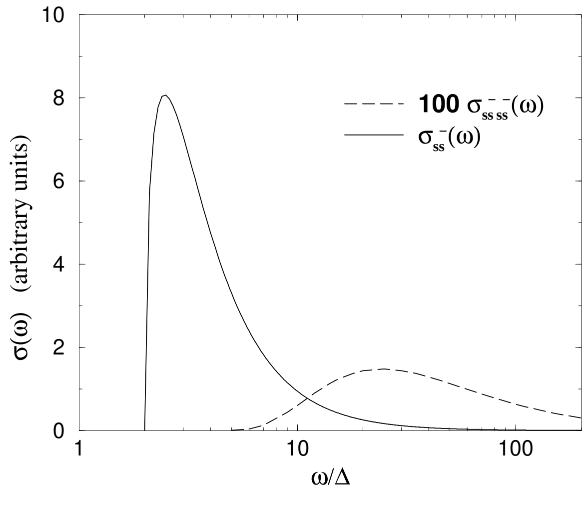

Figure 20. Optical conductivity for $\beta^2 = 0.9$. Shown are the dominant contributions at low frequencies: the soliton-antisoliton part $\sigma_2(\omega)$ and the two soliton - two antisoliton contribution $\sigma_4(\omega)$.

- $1/2 \geq \beta^2 > 1/3$:

  Here the optical spectrum contains one band and one excitonic breather peak below the optical gap $\Delta = 2\Delta$ at the energy $\omega_{B_1} = \Delta_1$. The optical weight is progressively transferred from the band to the breather as β^2 decreases down to $1/3$. The absorption band again increases in a square-root fashion (5.36) above the threshold for all values of β^2 except $\beta^2 = 1/2$, where the breather peak merges with the band. In this case $\sigma(\omega)$ shows a square-root divergence at the absorption threshold

$$\sigma(\omega) \propto \frac{1}{\sqrt{\omega - \Delta}} \quad \text{for} \quad \omega \to \Delta^+ \ (\beta^2 = 1/2) \ . \tag{5.37}$$

The field theory results discussed here have been compared to DDMRG computations (see e.g. Ref. [144] and references therein) computations of $\sigma(\omega)$ for extended Hubbard models in Refs. [91, 143, 145] and good agreement has been found in the appropriate regime of parameters. We note that the DDMRG method can also deal with parameter regimes in the underlying lattice model, to which field theory does not apply. Let us discuss the above results from the point of view of an application to optical conductivity measurements in the Bechgaard salts [130,258,288]. There it is found that up to 99% of the total spectral weight is concentrated in a finite-frequency feature, which has been attributed to Mott physics of the type discussed here [258]. A comparison of (5.33) to the experimental data gives satisfactory agreement at high frequencies, but the detailed peak structure at low frequencies is not reproduced [59]. A likely source for these differences is the interchain tunneling.

5.5. ***Spectral Function***

5.5.1. *Half-Filled Mott Insulator*

The zero-temperature spectral function of the half-filled Mott insulator has been studied in many previous works. There have been extensive numerical studies on finite size *t-J* and Hubbard models e.g. Refs. [31, 162, 259, 306]. The limit where the single-particle gap is much larger than the bandwidth was treated in Refs. [231,232,235]. This regime is complementary to the case we address here. The weak-coupling limit we are interested in was studied in Refs. [266, 289, 295], where a conjecture for the spectral function was put forward. Here we derive these results by means of an exact, systematic method. In what follows we will for simplicity fix $\beta = 1$, i.e. deal with the Hubbard model only.

5.5.2. *Zero Temperature*

The single particle Green's function is calculated by following the steps outlined above [92]. The creation and annihilation operators for right and left moving fermions factorize into spin and charge pieces upon bosonization (5.17). The spin part is easily calculated: in imaginary time we have

$$\left\langle e^{-\frac{if\sigma}{4}[\Phi_s+\Theta_s]}\ e^{\frac{if\sigma}{4}[\Phi_s+\Theta_s]}\right\rangle = \frac{1}{\sqrt{v_s\tau - ix}}\ . \tag{5.38}$$

The correlation function in the charge sector is calculated by means of the form factor bootstrap approach. Taking into account only processes involving one soliton we obtain

$$\left\langle e^{-\frac{i}{4}[\Phi_c+\Theta_c]}\ e^{\frac{i}{4}[\Phi_c+\Theta_c]}\right\rangle \simeq \frac{Z_0}{\sqrt{v_c\tau - ix}}\exp\left(-\frac{\Delta}{v_c}\sqrt{x^2+v_c^2\tau^2}\right), \tag{5.39}$$

where $Z_0 \approx 0.9218$ [197]. The form of (5.39) is fixed by the transformation properties of the operator $\exp(-\frac{i}{4}\left[\Phi_c+\Theta_c\right])$ under Lorentz transformations. The corrections to (5.39) involve intermediate states with three particles and are negligible at long distances/low energies [77]. The imaginary time Green's functions of left and right moving electrons are then given by

$$-\langle T_\tau\ R_\sigma(\tau,x)R^\dagger_\sigma(0,0)\rangle \simeq -\frac{Z_0}{2\pi}\,\frac{\exp\left[-\Delta\sqrt{\tau^2+x^2v_c^{-2}}\right]}{\sqrt{v_s\tau - ix}\sqrt{v_c\tau - ix}}\ , \tag{5.40}$$

$$-\langle T_\tau\ L_\sigma(\tau,x)L^\dagger_\sigma(0,0)\rangle \simeq -\frac{Z_0}{2\pi}\,\frac{\exp\left[-\Delta\sqrt{\tau^2+x^2v_c^{-2}}\right]}{\sqrt{v_s\tau + ix}\sqrt{v_c\tau + ix}}\ . \tag{5.41}$$

Fourier transforming and analytically continuing to real frequencies (we suppress the spin index σ in the formulas below) we arrive at the following result for the retarded single-particle Green's function

$$\begin{aligned} G^{(R)}(\omega,k_F+q) \simeq{}& -Z_0\sqrt{\frac{2v_c}{v_c+v_s}}\,\frac{\omega+v_cq}{\sqrt{\Delta^2+v_c^2q^2-\omega^2}} \\ &\times\left[\left(\Delta+\sqrt{\Delta^2+v_c^2q^2-\omega^2}\right)^2-\frac{v_c-v_s}{v_c+v_s}(\omega+v_cq)^2\right]^{-\frac{1}{2}}\ . \end{aligned} \tag{5.42}$$

We note that the charge velocity v_c is larger than the spin velocity v_s. The spectral function is obtained from the imaginary part of the single particle

Green's function (5.42). In the case $v_s = v_c = v$ it takes the simple form

$$A(\omega, k_F + q) = -\frac{1}{\pi}\mathrm{Im}G^{(R)}(\omega, k_F + q) = \frac{Z_0\ \Delta}{\pi|\omega - vq|}\ \frac{\Theta\big(|\omega| - \sqrt{\Delta^2 + v^2q^2}\big)}{\sqrt{\omega^2 - \Delta^2 - v^2q^2}}\ . \tag{5.43}$$

In Fig. 21 we plot the spectral function in the case $v_s = 0.8v_c$ and $\beta = 1$ in a series of constant q scans. There is a continuum of states above the

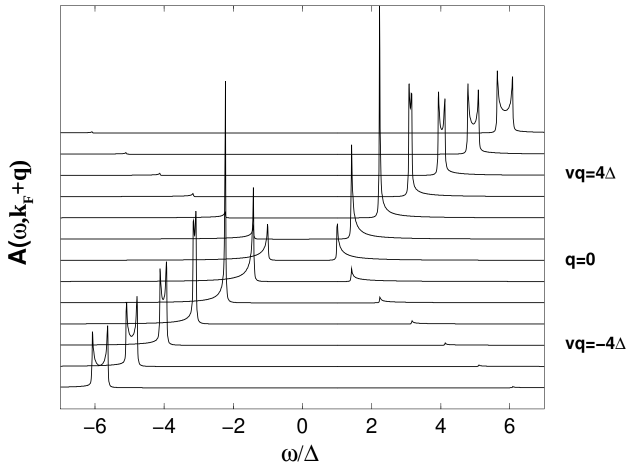

Figure 21. Spectral function for a half-filled Mott insulator with $v_s = 0.8511v_c$ and $\beta = 1$, corresponding to the half-filled Hubbard model with $U = t$.

Mott gap, which is smallest at k_F. The most striking feature is the presence of two distinct "peaks" dispersing with velocities v_s and v_c respectively. Most of the spectral weight is concentrated in these features, which are a direct manifestation of Spin-Charge Separation. The higher (lower) energy feature corresponds to the situation where the momentum carried by the spin (charge) sector is held constant. Concomitantly the high/low energy feature is referred to as antiholon/spinon peak. Neither peak is sharp but has intrinsic width (more precisely, they correspond to square root divergences). The threshold at $\omega > 0$ in the vicinity of k_F is [92]

$$E_{\mathrm{thres}}(k_F + q) = \begin{cases} \sqrt{\Delta^2 + v_c^2q^2} & \text{if } q \le Q\,, \\ v_sq + \Delta\sqrt{1-\alpha^2} & \text{if } q \ge Q\,, \end{cases} \tag{5.44}$$

where

$$\alpha = \frac{v_s}{v_c}\ , \quad Q = \frac{v_s\Delta}{v_c\sqrt{v_c^2 - v_s^2}}\ . \tag{5.45}$$

We see that for $q < Q$ the threshold follows the antiholon dispersion, whereas for $q > Q$ it follows the (linear) spinon dispersion (shifted by a constant).

5.5.3. *Finite Temperature $T \ll \Delta$*

It is possible to extend the results for the spectral function to small temperatures $T \ll \Delta$ [94] by the method described in Ref. [173] and summarized in section 2.7. As $T \ll \Delta$ the effects of temperature on the charge piece of the correlation function are small, but the spin piece can be affected quite strongly because the spinons are gapless. The spectral function in the vicinity of k_F can be represented as

$$\begin{aligned} A(\omega, k_F + q) \approx \mathcal{A}\int_{-\infty}^{\infty} dz\ e^{z/2}\Big[&\tilde{g}_s(\omega - \Delta c(z), q - \frac{\Delta}{v_c}s(z)) \\ &+ e^{-\Delta c(z)/T}\tilde{g}_s(\omega + \Delta c(z), q + \frac{\Delta}{v_c}s(z)) + \left\{\begin{matrix}\omega\to-\omega\\ q\to -q\end{matrix}\right\}\Big], \end{aligned} \tag{5.46}$$

where $\mathcal{A} = \sqrt{\frac{\pi\Delta}{v_c}}\frac{Z_2}{(2\pi)^3}$, $c(z) = \cosh z$, $s(z) = \sinh z$ and

$$\tilde{g}_s(\omega, q) = \sqrt{\frac{8\pi v_s}{T}}\mathrm{Re}\left[\sqrt{-2i}B\left(\frac{1}{4} - i\frac{\omega + v_s q}{4\pi T}, \frac{1}{2}\right)\right]\delta(\omega - v_s q)\,. \tag{5.47}$$

In Fig. 22 we plot the spectral function for $v_s = 0.5v_c$ and $\beta = 1$ at a temperature of 0.05 times the single particle gap. A significant temperature dependence of the "charge" peak is apparent. It gets damped rather strongly at temperatures that are still small compared to the gap. This may make an unambiguous detection of SC-separation by ARPES more difficult as the experiments are done at elevated temperatures (room temperature for Sr_2CuO_3) in order to avoid charging effects.

5.5.4. *Quarter-Filled CDW Insulator*

The single-particle Green's function in the quarter-filled case can be determined by the same method [93]. The spin sector is again gapless and the spin part of the Green's function is easily determined. The charge piece is analyzed by means of the form factor bootstrap approach. The difference to the half-filled case is that the charge piece of the single-electron operator (5.24) now couples to at least two (anti)solitons. Neglecting contributions

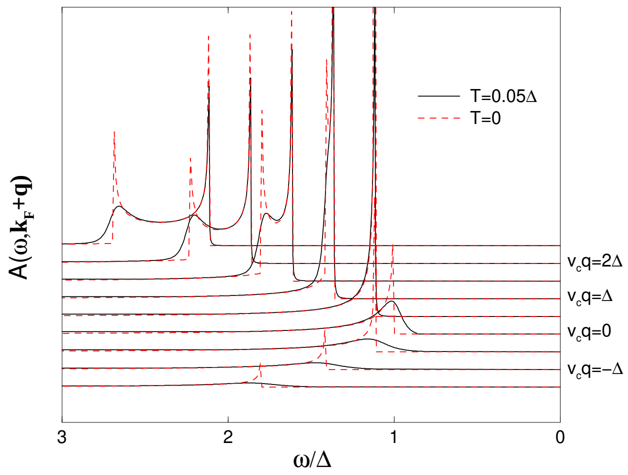

Figure 22. Spectral function for a half-filled Mott insulator with $v_s = 0.5v_c$, $T = 0$ (dotted) and $T = 0.05\Delta$ (solid). The different curves are constant-q scans with $v_c q/\Delta = -1.5, -1, \ldots 2.5$ (from bottom to top), which have been offset.

of four or more particles in the charge sector we obtain the following result for the single-particle Green's function in the vicinity of k_F [93]

$$G^{(R)}(\omega, k_F + q) = -\mathcal{C}\sqrt{\frac{2}{1+\alpha}} \int_{-\infty}^{\infty} d\theta\ \frac{E(2\theta)\sinh^2(\theta)}{\sqrt{\cosh(\theta)}} \frac{\omega + v_c q}{\sqrt{c^2(\theta) - s^2}} \times \left[\left(c(\theta) + \sqrt{c^2(\theta) - s^2}\right)^2 - \frac{1-\alpha}{1+\alpha}(\omega + v_c q)^2\right]^{-\frac{1}{2}}, \quad (5.48)$$

where $E(\theta)$ is given in (3.81), $s^2 = \omega^2 - v_c^2 q^2$, $c(\theta) = 2\Delta\cosh\theta$, and $\alpha = v_s/v_c$. $\mathcal{C}$ is a numerical constant. In Fig. 23 we plot the spectral function $A(\omega, k_F + q)$ as a function of ω for $v_s = 0.8v_c$ and different values of q. We observe that the spectral function is rather featureless and there are no singularities. Furthermore, in contrast to the half-filled Mott insulator discussed above, there are no dispersing features associated separately with v_c and v_s. The absence of any distinct features is clearly related to the fact that the electron has "fallen apart" into at least three pieces.

Just above the threshold at $s^2 = \omega^2 - v^2 q^2 = 4\Delta^2$ one finds for $v_c = v_s$

$$A(\omega, q) \propto \frac{1}{|\omega - vq|}\left(\frac{s}{2\Delta} - 1\right). \quad (5.49)$$

Thus the spectral weight increases linearly with $s - 2\Delta$ above the threshold.

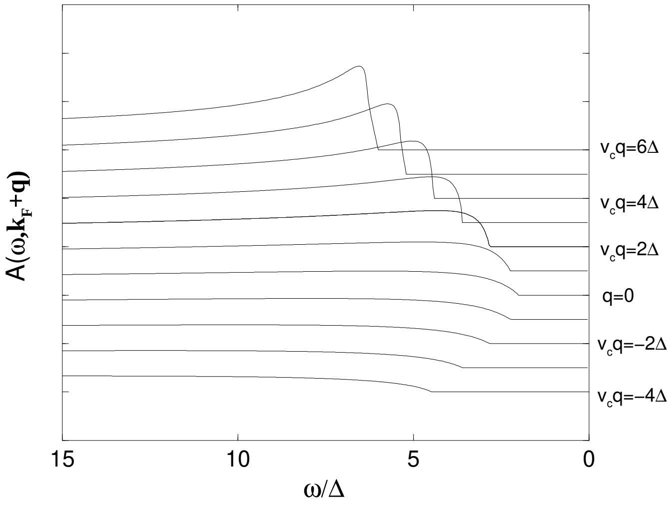

Figure 23. $A(\omega, k_F + q)$ as a function of ω/Δ for $v_s = 0.8v_c$. The curves for different q are offset.

The tunneling density of states is

$$\begin{aligned}\rho(\omega) &= -\frac{1}{\pi}\int_{-\pi}^{\pi}\frac{dk}{2\pi}\text{Im }G^{(R)}(\omega,k)\\ &= \frac{2\mathcal{C}}{\pi\sqrt{v_c v_s}}\int_0^{\text{arccosh}(\omega/2\Delta)} d\theta\ \frac{E(2\theta)\sinh^2(\theta)}{\sqrt{\cosh\theta}}\ ,\end{aligned} \tag{5.50}$$

and displays a roughly linear increase after an initial $(\omega - 2\Delta)^{3/2}$ behavior just above the threshold at $\omega = 2\Delta$.

Let us now turn to a comparison with experiments. $PrBa_2Cu_3O_7$ (P123) is a quarter-filled quasi-1D cuprate, to which the theory presented here may have some relevance. The ARPES data for P123 (Fig. 3 of [206]) show a single, very broad, dispersing feature that is asymmetric around k_F. If we interpret the underlying increase in intensity in the data as background, the signal has a form similar to Fig. 23. In order to assess whether the theory presented here is indeed relevant to P123, it would be interesting to extract a value $\Delta_{\rm PE}^{(\frac{1}{4})}$ for the gap from the ARPES data and compare it to gaps seen in optical measurements $\Delta_{\rm opt}^{(\frac{1}{4})}$ and the thermal activation gap $\Delta_{\rm T}^{(\frac{1}{4})}$ extracted e.g. from the dc conductivity. The theory presented here predicts

$$\Delta_{\rm opt}^{(\frac{1}{4})} = 2\Delta_{\rm T}^{(\frac{1}{4})} = \Delta_{\rm PE}^{(\frac{1}{4})}\ . \tag{5.51}$$

This is in contrast to the case of the half-filled Mott insulator, where one has

$$\Delta_{\rm opt}^{(\frac{1}{2})} = 2\Delta_{\rm T}^{(\frac{1}{2})} = 2\Delta_{\rm PE}^{(\frac{1}{2})} \ . \tag{5.52}$$

5.6. *A Remark on Luttinger's Theorem*

In all cases we have discussed, the Green's functions have branch cuts but no poles. In particular there are no poles at zero frequency and hence no Fermi surface. Nevertheless Luttinger's theorem holds as we will now show following [94]. Luttinger's theorem reads [2, 82]

$$\frac{N}{V} = 2\int_{G(0,k)>0} \frac{d^Dk}{(2\pi)^D}\,, \tag{5.53}$$

where N is the total number of electrons, V is the volume and the integration is over the interior of the region defined by either singularities or zeroes of the single-particle Green's function. The former is the case for a Fermi liquid whereas the latter is the case at hand. The interest in the equality (5.53) derives from the fact that it implies that the integral on the right hand side is independent of electron-electron interactions. In a Fermi liquid this means that the volume of the Fermi surface is unaffected by interactions. The Green's functions we have discussed above all fulfill (5.53) by virtue of them having zeroes at the position of the non-interacting Fermi surface.

The mechanism underlying this fact can be understood as follows. For simplicity let us concentrate on the Lorentz invariant case, where $v_s = v_c$. Then

- As the spin sector is gapless, we have $\langle R_\sigma(\tau,x) L^\dagger_\sigma(0)\rangle = 0$;
- Lorentz invariance of the low-energy effective theory implies that

$$\langle \Psi_\sigma(\tau,x)\Psi^\dagger_\sigma(0)\rangle \sim \exp(\pm i\phi)\mathcal{R}(r); \quad \Psi = R, L\,. \tag{5.54}$$

  Here r and ϕ are polar coordinates and $\mathcal{R}$ denotes the radial part of the correlation function.

As we are dealing with an insulating state we have $\mathcal{R}(r) \propto \exp(-\Delta r)$ at large distances and hence $\int dr\ \mathcal{R}(r)r$ is finite. Thus

$$G(0, \pm k_F) = \int_{-\pi}^{\pi} d\phi\ \exp(\pm i\phi) \int dr\ \mathcal{R}(r)r = 0\,. \tag{5.55}$$

For a metallic state the r integral would diverge and the Green's function would have a singularity rather than a zero.

5.7. *Interchain Tunneling*

Let us now consider a quasi one dimensional situation of Hubbard chains weakly coupled by a long-ranged interchain tunneling

$$H = \sum_l H^{(l)} + \sum_{l\neq m;n;\sigma} t_\perp^{lm}\ c^{(l)\dagger}_{n,\sigma} c^{(m)}_{n,\sigma} + \text{h.c.}\,,$$
$$H^{(l)} = -t\sum_{n,\sigma} c^{(l)\dagger}_{n,\sigma} c^{(l)}_{n+1,\sigma} + \text{h.c.} + U\sum_n n^{(l)}_{j,\uparrow} n^{(l)}_{j,\downarrow}\ . \tag{5.56}$$

We allow the interchain tunneling to be long-ranged in order to be able to carry out a controlled expansion in the case where the Fourier transform $\tilde{t}_\perp(\vec{k})$ of the interchain tunneling becomes of the same order as the 1D Mott gap Δ (see the discussion below). For simplicity we take $t_\perp$ long-ranged only in the direction perpendicular to the chains, although it is straightforward to generalize all formulas to an interchain tunneling of the form

$$\sum_{l\neq m;n;p;\sigma} [t_\perp]^{lm}_{np}\ c^{(l)\dagger}_{n,\sigma} c^{(m)}_{p,\sigma} + \text{h.c.}\ . \tag{5.57}$$

5.7.1. *Expansion Around Uncoupled Chains*

Following the analogous treatment for the case of coupled Luttinger liquids [18, 44, 291] we take the interchain tunneling into account in a perturbative expansion. The building blocks of this expansion are the n-point functions of fermion operators for uncoupled chains, which are represented pictorially in Fig. 24. The full single-particle Green's function is given in terms of

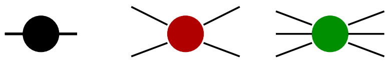

Figure 24. Elements of the diagrammatic perturbation theory in the interchain tunneling.

a diagrammatic expansion, the first few terms of which are shown in Fig. 25

Unlike for Luttinger liquids it is extremely difficult to determine four-point functions for 1D Mott insulators. On the other hand, it is straightforward to sum all diagrams involving only two-point functions of uncoupled chains. This approximation is known as RPA and goes back a long way [252]. The small parameter making RPA a controlled approximation for any form of the interchain tunneling is the ratio of the interchain tunneling to the Mott gap (at zero temperature) [44]. This is because the only energy scale entering the n-point functions is the dynamically generated gap Δ. Dimensional

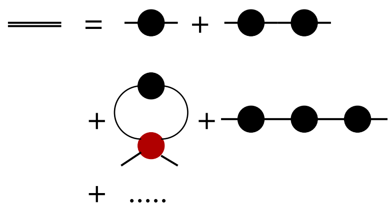

Figure 25. Diagrammatic expansion for the single-particle Green's function of coupled chains.

analysis then shows that the diagrams neglected in RPA are suppressed by powers of $t_\perp/\Delta$. Within RPA the single-particle Green's function is given by

$$G_{\rm 3D}(\omega,q,\vec{k}) = \frac{G_{1D}(\omega,q)}{1-t_\perp(\vec{k})\ G_{1D}(\omega,q)}\ ,$$
$$t_\perp(\vec{k}) = \sum_m t_\perp^{lm}\exp(i\vec{k}\cdot[\vec{R}_l-\vec{R}_m])\ . \qquad (5.58)$$

The RPA Green's function $G_{\rm 3D}(\omega,q,\vec{k})$ has the interesting property that it has a pole, which corresponds to a bound state of an antiholon and a spinon with the quantum numbers of an electron. For small interchain tunneling this bound state still has a gap. Fig. 26 is a density plot of $G_{\rm 3D}(\omega,q,\vec{k})$ as a function of ω and q for a fixed value of $\vec{k}$ and hence a fixed value of $t_\perp(\vec{k})$. At energies above the Mott gap there is a continuum of states, which is similar in nature to the result for uncoupled chains. In the Mott gap the coherent electronic mode is visible.

5.7.2. *Formation of a Fermi surface*

As long as the "binding energy" of the electronic bound state is small, RPA is a controlled approximation for any form of the interchain tunneling [44]. However, in the most interesting situation when the gap of the bound states becomes very small, RPA becomes uncontrolled; there is no longer any small expansion parameter for a generic $t_\perp(\vec{k})$. An exception is the case of a long-ranged interchain tunneling: here the support of $t_\perp(\vec{k})$ becomes very small, so that any integration over the transverse momentum generates a small volume factor proportional to the inverse range of the hopping. Recalling that RPA takes into account all terms not involving any integrations over the transverse hopping (i.e. "loops"), we conclude that RPA is the leading term in a controlled loop expansion. Increasing $t_\perp(\vec{k})$ in RPA reduces the gap of the electronic bound state, until it eventually vanishes and electron and

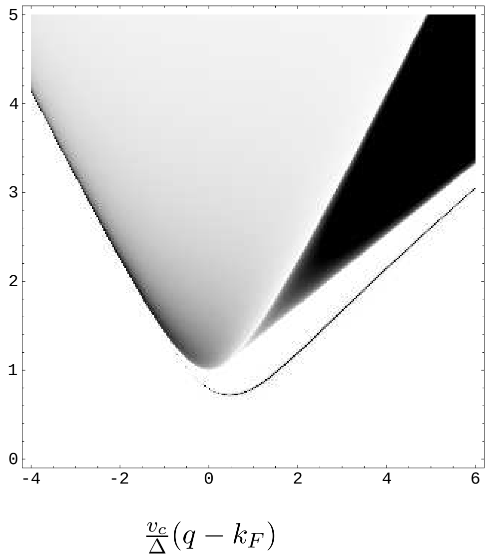

Figure 26. The spectral function for fixed momentum perpendicular to the chains $\vec{k}$. The electronic bound state is visible as a delta-function peak below the antiholon-spinon continuum

hole pockets are formed: we have crossed over from weakly coupled 1D Mott insulators to an anisotropic Fermi liquid. As an example, let us consider a 2D square lattice with interchain tunneling between nearest neighbor chain only. Here RPA is an uncontrolled approximation, but we still find it instructive to discuss its predictions. In this case electron pockets are formed in the

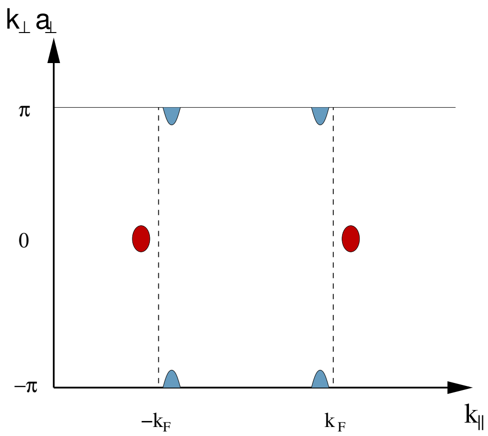

Figure 27. Fermi surface predicted by the RPA for a 2D square lattice with nearest-neighbor interchain tunneling.

vicinity of the points $(\pm k_F, \mathbf{0})$ and hole pockets form around $(\pm k_F, \pm\pi)$. In the particle-hole symmetric case the volume of the electron pockets is precisely the same as the volume of the hole pockets.

6. Hubbard Ladders and Carbon Nanotubes: SO(8) Gross–Neveu model

In this section we address another set of examples of quasi one-dimensional interacting electronic systems, two-leg Hubbard ladders and single-walled carbon nanotubes.

Two-leg ladders have been the focus of much theoretical (i.e. [26–28, 32, 64, 65, 96, 117, 146, 147, 169, 170, 187, 188, 218, 242, 254, 257, 290, 294]) and experimental activity (i.e. [133–135, 147, 180, 203, 251]). At half-filling they are Mott insulators, exhibiting gaps to all excitations, and in particular, a spin gap. They are typical examples of 'spin-liquids'. Upon doping, the gaps to all excitations except for those with charge-two survive [26,96,169,187,188,257]. The gapless charge modes induce quasi long-range superconducting pairing correlations, with approximate d-wave symmetry, reminiscent of underdoped cuprate superconductors.

Carbon nanotubes are novel materials whose mechanical and electronic properties promise potential for new technological applications [83]. They are formed by wrapping graphite sheets into cylinders of nanoscale dimensions. They support electronic excitations, which, for a prominent member of the nanotube family, the armchair (n, n) type, can be described by the same theoretical model as that used for the two-leg Hubbard ladders [27, 174, 187, 188, 219]. Even though these systems would be one-dimensional band metals in the absence of interactions, they become Mott insulators at half-filling due to the presence of short-ranged electronic interactions, which play an important role due to their one-dimensional nature. [q] It is these interaction effects that we analyze exactly in this section using form factors. After experimental techniques had been developed to fabricate long single-walled nanotubes with high yields in the laboratory, this field of material science has seen a explosive development [41, 78, 239, 297]. Electronic properties can be measured relatively easily by attaching metallic leads [279] or by tunneling into these materials with scanning tunneling microscope (STM) tips. The practical feasibility of such tunneling experiments from an STM tip into an individual single-walled nanotube placed upon a gold substrate

[q] If forward scattering interactions are assumed predominant, the metallic nanotube is a Luttinger liquid, not a Mott insulator [85, 86, 148, 184, 188, 257].

(screening long-range Coulomb forces) has been demonstrated in a number of experimental reports [149, 150, 287, 297].

As said, both systems, two-leg ladders and single-walled armchair nanotubes, would be one-dimensional metals in the absence of electron interactions. These are described theoretically (on scales much smaller than the non-interacting band width) by two species of spinful massless Dirac fermions in $(1+1)$ dimensions. (These two species have equal Fermi velocities due to particle-hole symmetry present at half-filling.) For the ladder compounds, the two species arise in an obvious way from the two legs of the ladder, whereas for the nanotubes they arise from the particular band structure of the underlying hexagonal graphite lattice, characterized by two Fermi points in the Brillouin zone [27, 174]. These massless Fermi surface excitations interact with short-range interactions whose detailed nature is determined by non-universal microscopic considerations.

A remarkable low energy feature of these system was observed by Lin, Balents, and Fisher [188]. These authors argued that within an 1-loop RG any such model with generic, non-chiral, short range interactions flows at half-filling into a theory with an immense symmetry, namely the $SO(8)$ symmetric Gross–Neveu model. This model not only has a large $SO(8)$ global symmetry, which encompasses an one-dimensional version of $SO(5)$ advocated by S. C. Zhang [318], but in addition has an infinite number of hidden conservation laws, which are a consequence of the integrability of this model.

Motivated by this work, we study in this section the low energy properties of nanotubes and two-leg ladders through computing correlation functions via form factors in SO(8) Gross–Neveu. In order to be pedagogical, we initiate our discussion by explaining why the low energy excitation spectrum of armchair carbon nanotubes and Hubbard ladders (four Dirac fermions) are identical. We then move on by reviewing the RG argument (and its limitations) by which these systems flow onto the SO(8) Gross–Neveu model. Having done this, we consider the excitation spectrum of SO(8) Gross–Neveu together with the connection between the fields in the theory and the original lattice operators. Finally we compute a number of physically relevant correlation functions for these systems.

6.1. *Armchair Carbon Nanotubes and Hubbard Ladders: Identical Low Energy Behavior*

We begin by showing that the set of low energy excitations in a non-interacting Hubbard ladder is equivalent to the low energy sector in an

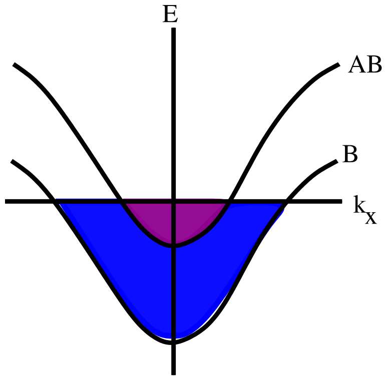

Figure 28. The bonding and anti-bonding bands of a Hubbard ladder.

armchair carbon nanotube [188, 189]. The Hubbard ladder Hamiltonian is

$$H_0 = -\sum_{x,\alpha}\Big(\; t a^\dagger_{1\alpha}(x+1)a_{1\alpha}(x) + t a^\dagger_{2\alpha}(x+1)a_{2\alpha}(x) \\ + t_\perp a^\dagger_{1\alpha}(x)a_{2\alpha}(x) + \text{h.c.}\Big). \tag{6.1}$$

Here the $a_l/a^\dagger_l$ are the electron annihilation/creation operators for the electrons on rung l of the ladder, x is a discrete coordinate along the ladder, and $\alpha = \uparrow, \downarrow$ describes electron spin. t and $t_\perp$ describe respectively hopping between and along the ladder's rung. The first step in the map is to reexpress the a's of H_0 in terms of bonding/anti-bonding pairs,

$$c_{j\alpha} = \frac{1}{\sqrt{2}}(a_{1\alpha} + (-1)^j a_{2\alpha})\,. \tag{6.2}$$

With this transformation, the Hamiltonian can be diagonalized in momentum space in terms of two bands, the bonding (B) and anti-bonding bands (AB). Their dispersions are given by

$$E_{B/AB}(k_x) = -2t\cos(k_x) \mp t_\perp\,. \tag{6.3}$$

These bands are pictured as half-filled in Fig. 28. Working at this filling, particle-hole symmetry dictates that the Fermi velocities, v_{Fj}, of the two bands, $j = 1, 2$, are equal. As we are interested in the low energy behavior of the theory, the $c_{j\alpha}$'s are linearized about the Fermi surface, k_{Fj},

$$c_{j\alpha} \sim c_{Rj\sigma}e^{ik_{Fj}x} + c_{Lj\sigma}e^{-ik_{Fj}x}, \tag{6.4}$$

where L, R correspond to right and left moving modes. With this H_0 becomes,

$$H_0 = v_F \int dx \sum_{j\alpha} \left[c^\dagger_{Rj\sigma} i\partial_x c_{Rj\sigma} - c^\dagger_{Lj\sigma} i\partial_x c_{Lj\sigma} \right]. \tag{6.5}$$

Thus the lower energy description of a non-interacting Hubbard ladder is that of four Dirac fermions (once spin degeneracy is taken into account). We now show that the low energy spectrum of a non-interacting armchair carbon nanotube is exactly the same.

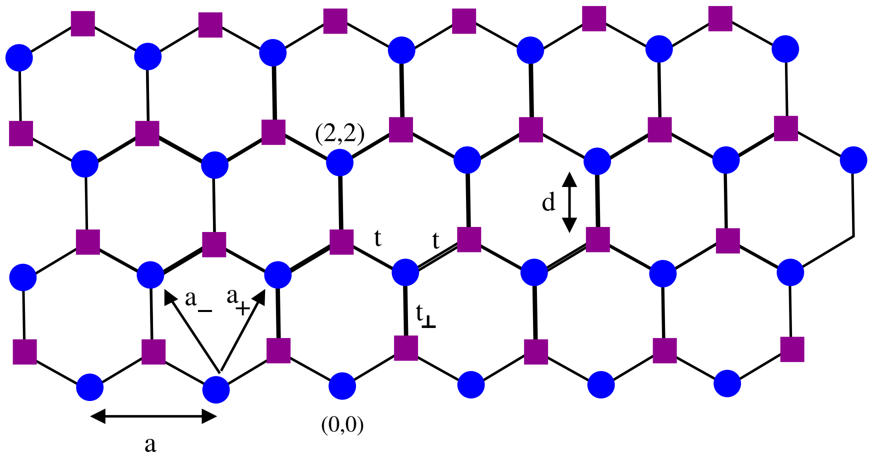

Figure 29. The graphite lattice is composed of two interpenetrating triangular lattices.

A single-walled armchair carbon nanotube is made by rolling up a sheet of graphite [123, 205, 248]. As such we first focus upon the graphite lattice, picture in Fig. 29. This lattice consist of two interpenetrating triangular lattices marked as blue circles and violet squares in Fig. 29. A tight-binding hopping model of electrons on this lattice is described by the Hamiltonian

$$H = \sum_{\mathbf{r}\in\mathbf{R},\sigma} \Big\{ - t a^\dagger_{1\sigma}(\mathbf{r}) a_{2\sigma}(\mathbf{r}+\mathbf{a}_- + \mathbf{d}) - t a^\dagger_{1\sigma}(\mathbf{r}) a_{2\sigma}(\mathbf{r}+\mathbf{a}_+ + \mathbf{d}) \\ - t_\perp a^\dagger_{1\sigma}(\mathbf{r}) a_{2\sigma}(\mathbf{r}+\mathbf{d}) + \text{h.c.} \Big\}. \tag{6.6}$$

Here $\mathbf{R}$ is the set of lattice vectors generated by the bases a_- and a_+ where $a_\pm = a(\pm 1/2, \sqrt{3}/2)$. The two triangular lattices are displaced by a vector $d = a(0, 1/\sqrt{3})$. Here again $a_{\mathbf{r}}/a^\dagger_{\mathbf{r}}$ create and destroy an electron at site $\mathbf{r}$.

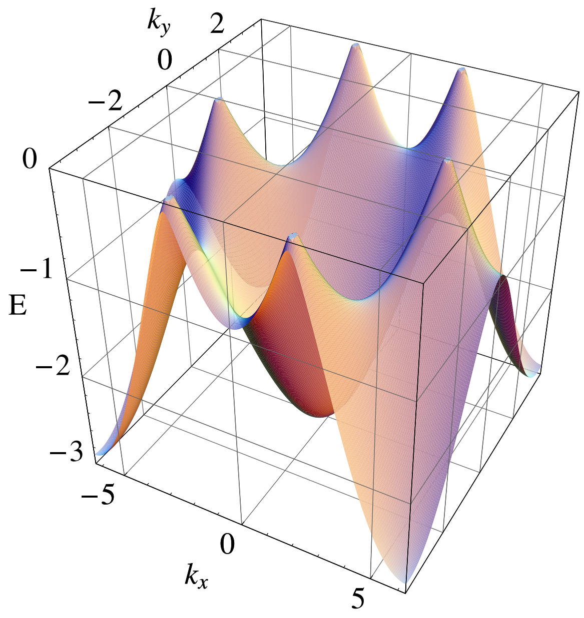

Figure 30. The dispersion of the bonding band of graphite.

In the absence of interactions, it is possible to diagonalize this Hamiltonian. One looks for eigenfunctions of the form

$$|\psi_{\mathbf{k}\sigma}\rangle = \sum_{\mathbf{r}\in\mathbf{R}} (a^\dagger_{1\sigma} + \beta(\mathbf{k}) a^\dagger_{2\sigma}) e^{i\mathbf{k}\cdot\mathbf{r}} \,. \tag{6.7}$$

Solving $H|\psi_{k\sigma}\rangle = E(\mathbf{k})|\psi_{k\sigma}\rangle$, one then finds a solution of the form

$$\begin{aligned}
\Gamma(\mathbf{k}) &= 2t\cos(k_x a/2) e^{ik_y a/\sqrt{12}} + t_\perp e^{-ik_y a/\sqrt{3}} \,, \\
E(\mathbf{k}) &= \pm|\Gamma(\mathbf{k})| \,, \\
\beta^2(\mathbf{k}) &= \Gamma(\mathbf{k})\Gamma^*(\mathbf{k}) \,.
\end{aligned} \tag{6.8}$$

The two signs in the above equation for the energy correspond to the bonding and antibonding bands. We plot the dispersion of the bonding band in Fig. 30.

We see that the dispersion is characterized by a series of cones whose tips extend to zero energy. The positions of these tips are known as Dirac points. The Dirac points are located at $\mathbf{k} = (\pm 4\pi/3a, 0)$ (and equivalent reciprocal lattice vectors). In Fig. 31 we mark with violet squares the position of the Dirac points in reciprocal space provided $t = t_\perp$. At half-filling the bonding band is completely filled and there will be a set of low energy excitations.

These excitations, however, have a vanishing density of states at the Fermi surface. Consequently graphite is known as a semi-metal.

At this point we want to consider the effects of rolling up the sheet of graphite on the low energy spectrum. These effects will change depending on how this is done. We will only be interested when the sheet is rolled up such that an (N, N) armchair carbon nanotube is obtained. This tube has a circumference of $\sqrt{3}aN$. Referring to Fig. 29, a $(2, 2)$ tube can be obtained by rolling the sheet so that the two lattice points labelled $(0, 0)$ and $(2, 2)$ are identified. When the sheet is rolled up, momentum transverse to the direction of the resulting tube will be quantized. For an armchair tube, k_y momentum is quantized. For an (N, N) tube, there will be N distinct allowed values of k_y given by

$$\begin{aligned} k_y &= \frac{2\pi}{\sqrt{3}a}\frac{n}{N}, \quad n = 0, \pm 1, \pm 2, \cdots, \pm\frac{(N-1)}{2}, \qquad \text{N odd,} \\ k_y &= \frac{2\pi}{\sqrt{3}a}\frac{n}{N}, \quad n = 0, \pm 1, \pm 2, \cdots, \pm\frac{(N-2)}{2}, N/2, \quad \text{N even.} \end{aligned} \tag{6.9}$$

The allowed values of discrete k_y-momentum are shown in Fig. 31 for a $(3, 3)$ tube.

When the tube is rolled up, one generically expects the hopping parameters to change. If once $t = t_\perp$, we then expect $t \neq t_\perp$. With such a change, the Dirac points are shifted. How these Dirac points are shifted is pictured in Fig. 31 for a $(3, 3)$ tube supposing that $t_\perp$ is now less than t. We see the shift involves only k_x and not k_y. Thus rolling up an armchair nanotube leaves the Dirac points (and so the presence of low energy excitations) in the allowed spectrum. The linearization of the spectrum about each of the two Dirac points gives a single Dirac fermion. Thus with spin degeneracy, the low energy spectrum of an armchair carbon nanotube is four Dirac fermions, identical to that of a Hubbard ladder.

6.2. *Weak Coupling Flow Onto SO(8) Gross–Neveu*

There exist a number of treatments of interactions in carbon nanotubes. As carbon nanotubes are quasi-one dimensional, a number of authors have employed bosonization, in combination with the renormalization group, to understand the effects of correlations [85, 86, 96, 148, 188, 257]. We will be interested in treatments of half-filled nanotubes with short range interactions where all excitation are gapped as opposed to nanotubes with long range, unscreened Coulomb interactions. In the latter case, the nanotubes are Luttinger liquids [85, 86, 148, 184, 188, 257]. In particular, we will focus upon

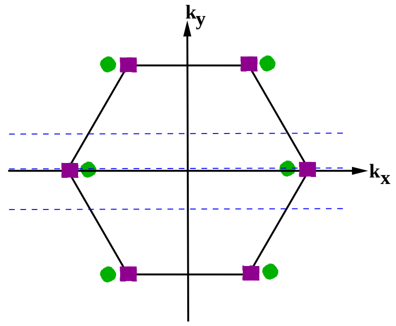

Figure 31. The Brillouin zone for the graphite lattice. Pictured are Dirac points for both the case $t = t_\perp$ (violet squares) and $t > t_\perp$ (green circles). The blue dashed lines mark the allowed values of quantized k_y-momenta for a $(3,3)$ armchair carbon nanotube. For the armchair tubes, the Dirac points always lie at an allowed $\mathbf{k}$ value.

Ref. [188] where it was shown that weak interactions lead the interacting electrons to flow in an RG sense onto the SO(8) Gross-Neveu model.

To set up this analysis, we consider the low-energy, non-interacting Hamiltonian for the ladders/tubes

$$H_0 = v_F \int dx \sum_{\sigma} \sum_{j=1,2} \left[c^\dagger_{Rj\sigma} i\partial_x c_{Rj\sigma} - c^\dagger_{Lj\sigma} i\partial_x c_{Lj\sigma} \right]. \tag{6.10}$$

We now consider adding all possible allowed interactions to this Hamiltonian. To organize this addition, we introduce various $SU(2)$ scalar and vector currents:

$$\begin{aligned} J_{ij} &= c^\dagger_{i\sigma} c_{j\sigma}\, ; \quad \mathbf{J}_{ij} = \frac{1}{2} c^\dagger_{i\sigma} \sigma_{\sigma\sigma'} c_{j\sigma'}\, ; \\ I_{ij} &= c^\dagger_{i\sigma} \epsilon_{\sigma\sigma'} c_{j\sigma'}\, ; \quad \mathbf{I}_{ij} = \frac{1}{2} c^\dagger_{i\sigma} (\epsilon\sigma)_{\sigma\sigma'} c_{j\sigma'}\, . \end{aligned} \tag{6.11}$$

Here σ are the Pauli matrices and $\epsilon_{\sigma\sigma'}$ is the ϵ-tensor. The crystal-momentum conserving interactions divide themselves into forward and backward scattering terms,

$$\begin{aligned} H_B &= \sum_{i,j=1,2} b^\rho_{ij} J^R_{ij} J^L_{ij} - b^\sigma_{ij} \mathbf{J}^R_{ij} \cdot \mathbf{J}^L_{ij}\, , \\ H_F &= \sum_{i\neq j=1,2} f^\rho_{ij} J^R_{ii} J^L_{jj} - f^\sigma_{ij} \mathbf{J}^R_{ii} \cdot \mathbf{J}^L_{ij}\, . \end{aligned} \tag{6.12}$$

Here f and b are the forward and backward scattering amplitudes. From hermiticity and parity, we have $b_{12} = b_{21}$ and $f_{12} = f_{21}$. Furthermore at half-filling, $b_{11} = b_{22}$. Thus we obtain six independent amplitudes. The

Umklapp interactions take the form

$$H_U = \sum_{i,j=1,2} u^{\rho}_{ij} I^R_{ij} I^{L\dagger}_{\hat{i}\hat{j}} - \sum_{i\neq j=1,2} u^{\sigma}_{ij} \mathbf{I}^{R\dagger}_{ij} \cdot \mathbf{I}^{L}_{\hat{i}\hat{j}} + \text{h.c.}\,, \tag{6.13}$$

where $\hat{1} = 2, \hat{2} = 1$. As $\mathbf{I_{ij}}, I_{ij}$ are anti-symmetric, one may choose $u_{12} = u_{21}$ leading to three additional independent couplings. For this set of generic interactions, the one-loop RG equations were derived in Ref. [188]. They show that $H_0 + H_{\text{int}}$ flow onto the SO(8) Gross–Neveu model.

To express this remarkable result compactly we must invoke a change to variables. We begin by bosonizing the $c's$,

$$c_{Pj\alpha} = \kappa_{j\alpha} e^{i\phi_{Pj\alpha}}, \qquad \mathrm{P} = +, - = \mathrm{R}, \mathrm{L}\,. \tag{6.14}$$

Here $\kappa_{j\alpha}$ are Klein factors satisfying

$$\{\kappa_{j\alpha}, \kappa_{i\beta}\} = 2\delta_{ij}\delta_{\alpha\beta}\,. \tag{6.15}$$

In terms of these four Bose fields, four new Bose fields are defined (effectively separating charge and spin):

$$\begin{aligned}
\phi_{P1} &= \frac{1}{2}(\phi_{P1\uparrow} + \phi_{P1\downarrow} + \phi_{P2\uparrow} + \phi_{P2\downarrow})\,;\\
\phi_{P2} &= \frac{1}{2}(\phi_{P1\uparrow} - \phi_{P1\downarrow} + \phi_{P2\uparrow} - \phi_{P2\downarrow})\,;\\
\phi_{P3} &= \frac{1}{2}(\phi_{P1\uparrow} - \phi_{P1\downarrow} - \phi_{P2\uparrow} + \phi_{P2\downarrow})\,;\\
\phi_{P4} &= \frac{P}{2}(\phi_{P1\uparrow} + \phi_{P1\downarrow} - \phi_{P2\uparrow} - \phi_{P2\downarrow}).
\end{aligned} \tag{6.16}$$

Note that ϕ_{P4} has a relative sign between the right and left movers. This sign effectively masks the $SO(8)$ symmetry in the original Hamiltonian. From these chiral bosons, one can define pairs of conjugate bosons in the standard fashion,

$$\begin{aligned}
\varphi_i &= \phi_{Ri} + \phi_{Li}\,,\\
\theta_i &= \phi_{Ri} - \phi_{Li}\,,
\end{aligned} \tag{6.17}$$

which obey the commutation relations,

$$[\varphi(x), \theta(x')] = -i4\pi\Theta(x - x')\,. \tag{6.18}$$

where $\Theta(x - x')$ is the Heaviside step function.

In terms of these variables the free part of the Hamiltonian can be written

$$H_0 = \frac{v_F}{8\pi}\sum_a \left\{(\partial_x\theta_a)^2 + (\partial_x\varphi_a)^2\right\}. \tag{6.19}$$

The interacting momentum conserving interacting term can be written as

$$\begin{aligned}H_B + H_F = &\frac{1}{16\pi^2}\sum_{a=1}^{4} A_a\big\{(\partial_x\theta_a)^2 - (\partial_x\varphi_a)^2\big\}\\ &-2b^\sigma_{12}\cos(\theta_4)\cos(\theta_2) + \cos(\theta_2)(2b^\sigma_{11}\cos(\theta_3) + 2f^\sigma_{12}\cos(\varphi_3))\\ &-\cos(\theta_4)((b^\sigma_{12} + 4b^\rho_{12})\cos(\theta_3) + (b^\sigma_{12} - 4b^\rho_{12})\cos(\varphi_3))\,, \quad (6.20)\end{aligned}$$

where the coefficients A_a are equal to $A_{1/4} = 2(c^\rho_{11} \pm f^\rho_{12})$ and $A_{2/3} = -(c^\sigma_{11} \pm f^\sigma_{12})/2$. The Umklapp interactions in these variables takes the form

$$\begin{aligned}H_U = &-16u^\rho_{11}\cos(\theta_1)\cos(\theta_4) - 4u^\sigma_{12}\cos(\theta_1)\cos(\theta_2)\\ &-\cos(\theta_1)(2(u^\sigma_{12} + 4u^\rho_{12})\cos(\theta_3) + 2(u^\sigma_{12} - 4u^\rho_{12})\cos(\varphi_3))\,. \quad (6.21)\end{aligned}$$

As demonstrated in Ref. [188], the Klein factors combine in such a fashion so as to be equal to 1.

For generically repulsive scattering amplitudes, the various couplings f, b, and u flow to fixed ratios under the RG [188],

$$b^\rho_{12} = \frac{1}{4}b^\sigma_{12} = f^\rho_{12} = -\frac{1}{4}b^\sigma_{11} = 2u^\rho_{11} = 2u^\rho_{12} = \frac{1}{2}u^\sigma_{12} = g > 0\,. \quad (6.22)$$

With these values, the interaction Hamiltonian dramatically simplifies to

$$\begin{aligned}H_{\rm int} &= H_B + H_F + H_U\\ &= -\frac{g}{2\pi^2}\sum_{a=1}^{4}\partial_x\phi_{Ra}\partial_x\phi_{La} - 4g\sum_{a\neq b=1}^{4}\cos(\theta_a)\cos(\theta_b)\,. \quad (6.23)\end{aligned}$$

It will sometimes be useful to write this Hamiltonian in fermionic form. We thus refermionize the bosons ϕ_{Pa}, $a = 1, \cdots, 4$, i.e.,

$$\begin{aligned}\Psi_{Pa} &= \kappa_a e^{i\phi_a}\,, \qquad \mathrm{a} = 1, \cdots, 4\,;\\ \Psi_{P4} &= P\kappa_4 e^{i\phi_4}\,, \quad (6.24)\end{aligned}$$

where the Klein factors are given by

$$\kappa_1 = \kappa_{2\uparrow}, \quad \kappa_2 = \kappa_{1\uparrow}, \quad \kappa_3 = \kappa_{1\downarrow}, \quad \kappa_4 = \kappa_{2\downarrow}\,. \quad (6.25)$$

We then find the free Hamiltonian can be written as

$$H_0 = \int dx \sum_a \big[\Psi^\dagger_{aL} i\partial_x\Psi_{aL} - \Psi^\dagger_{aR} i\partial_x\Psi_{aR}\big]\,, \quad (6.26)$$

where the Fermi velocity, v_F, has been set to 1, while the interaction Hamiltonian can be written as

$$H_{int} = g\big[\sum_{a=1}^{4}(i\Psi^\dagger_{aL}\Psi_{aR} - i\Psi^\dagger_{aR}\Psi_{aL})\big]^2. \tag{6.27}$$

This is, of course, H_{int} for the $SO(8)$ Gross–Neveu model.

It will sometimes prove convenient to recast the theory in terms of Majorana fermions, ψ_{aP}. In terms of the Dirac fermions, Ψ_{aP}, they are given by

$$\Psi_{aP} = \frac{1}{\sqrt{2}}(\psi_{2a,P} + i\psi_{2a-1,P})\,, \qquad (a = 1, ..., 4)\,. \tag{6.28}$$

In this basis, H_{int} can be recast as

$$H_{int} = gG^{ab}_R G^{ab}_L\,, \qquad (a > b = 1, ..., 8)\,, \tag{6.29}$$

where $G^{ab}_P = i\psi_{aP}\psi_{bP}$ is one of the 28 $SO(8)$ Gross–Neveu currents.

6.3. *Limitations of the RG Analysis*

In the previous section we have sketched the argument by which Ref. [188] demonstrated that generically interacting Hubbard ladders/armchair carbon nanotubes behave at low energies according to the SO(8) Gross–Neveu. In this section we want to consider how precise a statement this is.

The analysis in [188] is based on an 1-loop RG. As such the initial microscopic (bare) interactions must be small enough so that the integrable $SO(8)$ invariant RG trajectory is approached sufficiently closely after a number of RG steps, before leaving the range of validity of the 1-loop RG equations. Whenever this is the case, it can be argued that the integrable model is approached independently of the (sufficiently weak) values of the bare interactions. The situation for the 2-leg ladder is thus similar in spirit to that of the point contact device encountered in [101–103], where only a single operator was relevant, and this relevant operator was integrable. In the latter case all other interactions were irrelevant in the RG sense, and could in principle be treated perturbatively.

The requirement of the RG that the interactions be short-ranged is natural in the case of the Hubbard ladders. However it may not seem so in the case of the carbon nanotubes. Both theory [85, 86, 148] and experiment [42,58] have discussed the case where long-ranged Coulomb forces drive Luttinger liquid behavior in single-walled carbon nanotubes. However we do not have such situations in mind for the paper at hand. Rather we want to consider situations such as those found in the experiments [297] where the long range forces are screened.

Although the restriction to such experiments in the case of the carbon nanotubes places us upon safe ground, it is not inconceivable that experiments where the long-ranged forces are present would nevertheless see behavior indicative of the SO(8) symmetry. An unscreened force translates into an unusually large bare coupling (in comparison with other bare couplings) in the forward scattering direction. However this does not mean the RG is inapplicable. The RG still indicates a potential enhancement in the symmetry. Because of the large bare coupling, the RG must be run a longer time before any enhancement would be seen but nevertheless an enhancement may well occur at some low energy scale. In terms of the experiments in [42, 58], this would mean that at medium energy scales, Luttinger liquid behavior would predominate, while at much lower energy scales, SO(8) behavior would be expected. However at current standing, the material science is not advanced to the point where it is possible to accurately probe the very low energy behavior. But the potential for advancement in this area is ever present.

The RG analysis further requires the bare couplings to be weak. With Hubbard ladder compounds, this condition will not be generically met, although it certainly will not be universally violated. However with (N,N)-armchair carbon nanotubes, the bare couplings are naturally weak. It is one of the hallmarks of the physics of the (N,N) armchair carbon nanotubes that the electrons are delocalized around the circumference of the tube. This in turn leads to a scaling of the effective short-ranged interaction by 1/N, making it naturally small [27].

It can, however, be questioned on a more fundamental level whether an 1-loop RG adequately describes the system's behavior. Difficulties with the analysis in [188] take two forms. As a first objection, the authors of Ref. [21] point out that an RG flow can imply a symmetry restoration which in fact does not occur. As an example they consider a U(1) symmetric Thirring model,

$$\mathcal{L} = \bar{\Psi}_\alpha \gamma^\mu \partial_\mu \Psi_\alpha + \frac{1}{4} g_\parallel (j_z)^2 + \frac{1}{4} g_\perp [(j_x)^2 + (j_y)^2] \,, \tag{6.30}$$

where $j^\mu_a = \bar{\Psi}\gamma^\mu \sigma_a \Psi$. Although the 1-loop RG equations for this model seems to indicate a generic symmetry restoration to a more symmetric SU(2) case (i.e. $g_\perp = g_\parallel$), this in fact only occurs in a certain region of coupling space. For $\pi - |g_\perp| > -g_\parallel > |g_\perp| > 0$, the U(1) model maps onto the sine-Gordon model with interaction $\cos(\beta\phi)$ [151], where β is given by

$$8\pi\beta^2 = 8\pi - 8\mu; \qquad \mu = \cos^{-1}[\cos(g_{\|})/\cos(g_{\perp})]. \tag{6.31}$$

The value of β completely characterizes the model. While $g_{\perp}$ and $g_{\|}$ flow under the RG, the particular combination of these parameters forming β does not. Thus for this particular region of parameter space the model moves no closer to the SU(2) symmetric point under an RG flow. In other regions however (for example $|g_{\perp}| > |g_{\|}|$), the situation is better; the effect of the anisotropy in the couplings is exponentially suppressed.

However it is reasonably clear that such pessimism is not warranted in the analysis of the RG of Ref. [188]. A salient criticism of Ref. [21] is that in considering the action of the renormalization group, they fail to consider the consequences of working in the scaling limit. The scaling limit is exactly the limit in which a field theory becomes available. In turn, the scaling limit places constraints upon the possible range of bare couplings consistent with a field theory. In the case of sine-Gordon, the underlying integrability/solvability of the theory allows explicit investigation of this question. It is found that the allowed range is such that even moderate anisotropic deviations are forbidden [171]. The scaling limit, in other words, enforces isotropy. In cases where there are RG flows indicating an enhancement in symmetry (including the case at hand), this enforcement turns out to be a general phenomena and it leads to an expanded notion of symmetry restoration [171].

We can see however that this conclusion is a double edged sword. Strongly anisotropic models will not have sensible continuum limits and so will not be able to be described by a field theory. If the Hubbard ladder/carbon nanotube is strongly anisotropic, the continuum theory is not a good starting point rendering the RG analysis irrelevant. However if interactions are only weakly anisotropic, the continuum theory can be used and the weakly anisotropic Hamiltonian is better able to flow under the RG to the SO(8) symmetric theory.

On a more concrete level, the breaking of the SU(2) symmetry considered in Ref. [21] is a rather special case. Ultimately, the parameter, β, in the sine-Gordon model is protected under an RG flow by the presence of a quantum group symmetry arrived at by deforming a Yangian symmetry present at the SU(2) point. There is, however, no such known way to deform the Yangian in $SO(8)$ Gross–Neveu. Indeed the natural generalization of the sine-Gordon model to $SO(8)$ is not to $SO(8)$ Gross–Neveu but to an affine toda $SO(8)$ theory where such a deformation of the Yangian symmetry is possible [35].

Another question that one must ask in looking at the analysis in Ref. [21] is how the choice of the symmetry breaking terms affects the symmetry restoration. The sine-Gordon model still possesses a U(1) symmetry. However it is certainly possible to consider perturbations that break this U(1). Such perturbations would destroy the quantum group symmetry of sine-Gordon and thus might lead to symmetry restoration. This would be perhaps closer to the RG analysis of Ref. [188] where a large number (nine) of marginal perturbations were included. We in fact consider exactly such a situation in Ref. [171] and find that indeed there is symmetry restoration. We also note in passing that the authors of Ref. [21] consider an anisotropic Gross–Neveu model, a model of direct relevance to the situation at hand. They conclude through a mean-field/large N limit computation that the model is intrinsically anisotropic thus throwing doubts upon the analysis in Lin et al. [188]. However we would point to how the bare couplings are scaled in the large N limit. The anisotropic model they consider has three bare couplings. One is chosen to not scale at all, one scales as $1/N$, and the last scales as $1/N^{d/2}$, $d < 1$. With this scaling [21] the model is intrinsically anisotropic. However this model possesses a diverging bare anisotropy in the large N limit while the RG is not allowed to act. As such, we believe this example is not so directly telling.

The second objection to the analysis of Ref. [188] is its omission of chiral interactions that alter the Fermi velocities [84]. Such interactions, although they are absent from the 1-loop RG, likely play a role at higher order. However their effect is less drastic than envisioned in Ref. [84]. There a scenario was considered where the invariant RG trajectory of higher symmetry was inherently unstable to perturbations. However the $SO(8)$ RG ray in Ref. [188] has a basin of attraction of finite measure. The effect of chiral interactions is to then slightly alter the direction of the ray. In turn the ratio of masses of the various excitations will be slightly perturbed away from one.

In taking account of these objections, prudence suggests a modification in the understanding of the RG analysis of Ref. [188]. This analysis tells us that while the RG flow does not restore an exact symmetry, it leaves us close to the symmetrical situation. In particular, it indicates that while the masses in the actual system may differ from their $SO(8)$ values, they do not wildly diverge. One then understands the $SO(8)$ Gross–Neveu theory, not as precisely representative of the actual system, but in near perturbative vicinity of it, that is, as an excellent starting point about which to perform perturbation theory in the non-integrable interactions breaking $SO(8)$ in much the same spirit as done for a non-critical Ising model in the presence of a magnetic field [68].

6.4. *Excitations and Physical Fields in SO(8) Gross–Neveu*

We now consider the basic excitations of SO(8) Gross–Neveu together with identifying the fields in the theory that correspond to operators of physical interest.

6.4.1. *Excitation Spectrum*

The Gross–Neveu $SO(8)$ model has an exceedingly rich spectrum. There are 24 fermionic particles of mass m organized into one eight dimensional vector representation and two eight dimensional spinor representations. We denote the particles of the vector representation by A_a, $a = 1, \ldots, 8$. The A_a's are the Majorana fermions of Eq. (6.28). We will often refer to these particles as Gross–Neveu fermions. The kink particles, in turn, will be denoted by A_α. Here α is of the form $\alpha = (\pm 1/2, \pm 1/2, \pm 1/2, \pm 1/2)$ and so takes on 16 values. These 16 particles decompose into the two eight-dimensional spinor representations. The division is affected by the chirality (either even or odd) of the kinks. An even chirality kink has an even number of $+1/2$'s in its corresponding α while an odd chirality kink has a correspondingly odd number.

Beyond the eight dimensional representations, there are 29 bosonic particle states of mass $\sqrt{3}m$, transforming as a rank-two tensor of dimension 28 and a singlet. Together they form a representation of the $SO(8)$ Yangian symmetry. These particles can be thought of as bound states of either two kinks or two fundamental fermions.

As $SO(8)$ is a rank 4 algebra, the $SO(8)$ Gross–Neveu model has four Cartan bosons (i.e. the ϕ_{Pa} , $a = 1, \ldots 4$) and so its excitations are characterized by four quantum numbers, N_i, $i = 1, \ldots, 4$. With the Majorana fermions, the combination

$$A_{2a} \pm iA_{2a-1}\,, \tag{6.32}$$

carries quantum number $N_a = \pm 1$, $N_b = 0, b \neq a$. The quantum numbers carried by the kinks A_α are directly encoded in α. If $\alpha = (a_1, a_2, a_3, a_4)$, $a_i = \pm 1/2$, the A_α carries the quantum numbers, $N_i = a_i$. The quantum numbers carried by the rank two tensor states can be directly deduced from the particles forming the bound state. As we will always think of the bound states in this way, we will not list their quantum numbers directly.

The last thing needed in the section is to identify the relationship between the quantum numbers, N_i, and the physical quantum numbers of the system:

the z-component of spin, S_z, the charge, Q, the difference in z-component of spin between the two bands, S_{12}, and the "relative band chirality", P_{12}, defined as $P_{12} = N_{R1} - N_{L1} - N_{R2} + N_{L2}$, where N_{Pj} is the number electrons in band j with chirality P. We have

$$\begin{aligned}
(N_1 = 1, 0, 0, 0) &\leftrightarrow (Q = 2, S_z = 0, S_{12} = 0, P_{12} = 0)\,;\\
(0, N_2 = 1, 0, 0) &\leftrightarrow (Q = 0, S_z = 1, S_{12} = 0, P_{12} = 0)\,;\\
(0, 0, N_3 = 1, 0) &\leftrightarrow (Q = 0, S_z = 0, S_{12} = 1, P_{12} = 0)\,;\\
(0, 0, 0, N_4 = 1) &\leftrightarrow (Q = 0, S_z = 0, S_{12} = 0, P_{12} = 2)\,.
\end{aligned} \tag{6.33}$$

With this assignment, we can see that the vector representation of fundamental fermions corresponds to states of two electrons in the original formulation. For example, the fermion $A_2 \pm iA_1$ carries charge ± 2 and no spin (the cooperons), and the fermion $A_4 \pm iA_3$ carries spin, $S_z = 1$, and no charge (the magnons). The spinor representations, the kinks, in turn correspond to single particle excitations as their quantum numbers are combinations of $N_i/2$.

6.4.2. *Relationship between Lattice Operators and Gross–Neveu Fields*

In this section we make contact between the fields of the $SO(8)$ Gross–Neveu model and the original fields of the Hubbard ladders. This identification is crucial if we are to compute physically relevant correlation functions.

As we have already discussed, the fundamental (Dirac) fermions of the vector representation are given by

$$\begin{aligned}
\Psi_{aP} &= \kappa_a e^{i\phi_{aP}}\,,\\
\Psi_{aP} &= P\kappa_a e^{i\phi_{aP}}\,,
\end{aligned} \tag{6.34}$$

and carry quantum numbers corresponding to two electronic excitations. However the Ψ_{aP} are fermionic, whereas such excitations are bosonic. As such, Ψ_{aP} are not simply related to a fermionic bilinear of the original electrons but must be a fermion bilinear multiplying some non-local field (a Jordan–Wigner string). As we will not compute correlators involving such fields in this review, we will not elaborate upon this.

As discussed previously, the kinks correspond to single particle excitations. Thus we expect to find that the kink fields are related to the original electron operators. This is true in part. There are 32 kinks in total (counting both left and right movers), but only sixteen electron operators, the c's and $c^\dagger$'s (four for each of the four Fermi points). So we expect only 1/2 of the kinks to correspond to actual electron operators.

We represented the fundamental fermions in terms of the four Cartan bosons. There is a corresponding representation for the kink fields

$$\psi_{\alpha P} \sim e^{i\alpha\cdot\bar{\phi}_P}, \tag{6.35}$$

where $\bar{\phi} = (\phi_1, \phi_2, \phi_3, \phi_4)$. The kink fields that then correspond to the electron operators c's are as follows:

$$\begin{aligned}
c_{R1\uparrow} &\sim e^{i(\phi_{1R}+\phi_{2R}+\phi_{3R}+\phi_{4R})/2};\\
c_{R2\uparrow} &\sim e^{i(\phi_{1R}+\phi_{2R}-\phi_{3R}-\phi_{4R})/2};\\
c_{R2\downarrow} &\sim e^{i(\phi_{1R}-\phi_{2R}+\phi_{3R}-\phi_{4R})/2};\\
c_{R1\downarrow} &\sim e^{i(\phi_{1R}-\phi_{2R}-\phi_{3R}+\phi_{4R})/2};\\
&\text{(even chirality)}\\
c_{L1\uparrow} &\sim e^{i(\phi_{1L}+\phi_{2L}+\phi_{3L}-\phi_{4L})/2};\\
c_{L2\uparrow} &\sim e^{i(\phi_{1L}+\phi_{2L}-\phi_{3L}+\phi_{4L})/2};\\
c_{L2\downarrow} &\sim e^{i(\phi_{1L}-\phi_{2L}+\phi_{3L}+\phi_{4L})/2};\\
c_{L1\downarrow} &\sim e^{i(\phi_{1L}-\phi_{2L}-\phi_{3L}-\phi_{4L})/2};\\
&\text{(odd chirality).}
\end{aligned} \tag{6.36}$$

With hermitian conjugates, this totals to sixteen fields. The $\sim$ sign is meant to indicate that these equivalences hold up to Klein factors. The $c_{Pj\alpha}$'s, of course, are fermionic. However the kink fields as defined are not.

The last set of fields that are of concern to us are the currents. The electric current of the ladder has the lattice representation

$$J \sim -i\sum_{l\alpha}\Big[a^\dagger_{l\alpha}(x)a_{l\alpha}(x+1) - a^\dagger_{l\alpha}(x+1)a_{l\alpha}(x)\Big], \tag{6.37}$$

where we have summed over the contribution coming from each spin (α) and each leg (l) of the ladder. Taking the continuum limit, J equals, in Gross–Neveu language,

$$J \sim i\sin k_{F1}\,\partial_t\phi_1 \sim G_{12}, \tag{6.38}$$

where G_{12} is one of the $SO(8)$ currents discussed in Eq. (6.29).

6.5. *Form Factors in SO(8) Gross–Neveu*

Having identified the fields that we need to compute physical correlators, we now turn to the corresponding form factors of these fields. Here we only state the needed form factors. Their derivation may be found in [170] and [156].

6.5.1. *One and Two Particle Current Form-Factors*

At the two particle level, two kinks of the same chirality or two GN fermions can couple to one of the Gross–Neveu current operators (see Eq. (6.29)). The corresponding form-factors are

$$
\begin{aligned}
{}_\mu f^{ab}_{cd}(\theta_1,\theta_2) &\equiv \langle G^{ab}_\mu(0)A_b(\theta_2)A_a(\theta_1)\rangle = iA_G(\delta_{ac}\delta_{bd}-\delta_{ad}\delta_{bc})f_\mu(\theta_1,\theta_2)\,,\\
{}_\mu f^{ab}_{\alpha\beta}(\theta_1,\theta_2) &\equiv \langle G^{ab}_\mu(0)A_\beta(\theta_2)A_\alpha(\theta_1)\rangle = i\,\frac{A_G}{2}\,(C\sigma^{ab})_{\alpha\beta}f_\mu(\theta_1,\theta_2)\,, \qquad (6.39)
\end{aligned}
$$

where

$$
\begin{aligned}
f_\mu(\theta_1,\theta_2) &= (e^{(\theta_1+\theta_2)/2}-(-1)^\mu e^{-(\theta_1+\theta_2)/2})\,\frac{s(\theta_{12}/2)}{c(\theta_{12})-1/2}\\
&\qquad\times\exp\left[\int_0^\infty\frac{dx}{x}\frac{G_c(x)}{s(x)}\sin^2(\frac{x}{2\pi}(i\pi+\theta_{12}))\right],\\
G_c(x) &= 2\,\frac{c(x/6)-s(x/6)e^{-2x/3}}{c(x/2)}\,. \qquad (6.40)
\end{aligned}
$$

Here the current G^{ab}_μ is a particular combination, $G^{ab}_R-(-1)^\mu G^{ab}_L$, of the chiral currents of Eq. (6.29). A_G is some arbitrary (real) normalization constant.

The current operators also possess one particle form factors. The currents are able to couple to one of the 29 bound state excitations. The corresponding form factor can be computed following the discussion in Section 2.6 of this review. We thus have

$$
\begin{aligned}
{}_\mu f^{ab}_{\{cd\}}(\theta) &\equiv \langle G^{ab}(0)A_{\{cd\}}(\theta)\rangle\\
&= iA_G(\delta_{ac}\delta_{bd}-\delta_{ad}\delta_{bc})(e^\theta-(-1)^\mu e^{-\theta})\,\frac{1}{\sqrt{3}}\left(2\sqrt{3\pi}\,\frac{\Gamma(2/3)}{\Gamma(1/6)}\right)^{-1/2}\\
&\times\exp\left[-\int_0^\infty\frac{dx}{x}\,\frac{G_c(x)}{s(x)}\,s^2(x/3)\right]. \qquad (6.41)
\end{aligned}
$$

Notice that the normalization constant A_G is the same as that which appears in the two-particle current form factor.

6.5.2. *One and Two Particle Kink Form-Factors*

We recall that the single electron excitations of the theory are represented by kink fields. A kink field, $\psi^\alpha_\pm$, of a given chirality couples to a combination of excitations consisting of a kink particle of opposite chirality and a Gross–Neveu fermion. The corresponding form factor is given by

$$\begin{aligned} {}_\pm f^\alpha_{a\beta}(\theta_1,\theta_2) = {}_\pm f^\alpha_{\beta a}(\theta_1,\theta_2) &\equiv \langle \psi^\alpha_\pm(0) A_\beta(\theta_2) A_a(\theta_1)\rangle \\ &= -A_F e^{\pm i\pi/4}(C\gamma^a)_{\alpha\beta} f_\pm(\theta_1,\theta_2)\,, \end{aligned} \tag{6.42}$$

where

$$\begin{aligned} f_\pm(\theta_1,\theta_2) &= \frac{e^{\pm(\theta_1+\theta_2)/4}}{c(\theta_{12})+1/2}\exp\left[\int_0^\infty \frac{dx}{x}\,\frac{G_f(x)}{s(x)}\sin^2\left(\frac{x}{2\pi}(i\pi+\theta_{12})\right)\right], \\ G_f(x) &= \frac{2c(x/6)+e^{-7x/6}}{c(x/2)}\ . \end{aligned} \tag{6.43}$$

Here A_F is an arbitrary (real) normalization parameter.

The kink field of course also couples to a single kink. The associated form factor can be computed again using the bound state relations of Section 2.5 (a kink of a given chirality is a bound state of a kink of opposite chirality together with a Gross–Neveu fermion). The result of the calculation is

$${}_\pm f^\alpha_\beta \equiv \langle \psi^\alpha_\pm(0) A_\alpha(\theta)\rangle = c_\pm e^{\pm\theta/2} C_{\alpha\beta}\,, \tag{6.44}$$

where the constant $c_\pm$ is

$$c_\pm = \frac{4}{\sqrt{3}}\,e^{\pm i\pi/4} A_F\left(\sqrt{3\pi}\,\frac{\Gamma(5/3)}{\Gamma(7/6)}\right)^{-1/2}\exp\left[-\int_0^\infty \frac{dx}{x}\,\frac{G_f(x)}{s(x)}\,s^2(x/6)\right]. \tag{6.45}$$

Again A_F is the same normalization constant appearing in the above two-particle form factor.

6.6. *Exact Low Energy Correlation Functions in SO(8) Gross–Neveu*

In this section we study various aspects of carbon nanotubes and Hubbard ladders using the previously stated form factors. In particular we study the optical conductivity of a ladder system, the single particle spectral function of a ladder/nanotube, and finally the associated differential conductance arising from tunneling into a ladder/nanotube via a scanning tunneling microscope (STM). We again emphasize that although we calculate these quantities with a small, finite number of form factors, the results are exact up to some energy scale.

6.6.1. *Behavior of Optical Conductivity in a Hubbard Ladder*

We first consider the response of the ladder system to an electric field polarized along the legs. Apart from the meanfield treatment in Ref. [188], this problem has been examined previously, both theoretically [129] and experimentally [134]. However these two latter papers did not consider undoped ladders at zero temperature.

In linear response, the optical conductivity is given by

$$\mathrm{Re}\big[\sigma(\omega,k)\big] = \mathrm{Im}\Big[\frac{\Delta(\omega,k)}{\omega}\Big]\,, \tag{6.46}$$

where Δ is the current-current correlator

$$\Delta(\omega,k) = \int dx d\tau e^{i\omega\tau} e^{ixk} \langle T(J(x,\tau)J(0,0))\rangle|_{\omega\to -i\omega+\delta}\,. \tag{6.47}$$

J is given by Eq. (6.38)

$$J \sim G_1^{12}. \tag{6.48}$$

As explained in Section 2, to compute the correlator, $\langle T(G_1^{12}(x,\tau)G_1^{12}(0,0))\rangle$, we insert a resolution of the identity between the two $J's$, turning the correlator into a form factor sum. We then have

$$\begin{aligned}
&-\langle T(G_1^{12}(x,\tau)G_1^{12}(0,0))\rangle \\
&=\sum_{n=0}^{\infty}\sum_{a_1,\cdots,a_n}\int\frac{d\theta_1}{2\pi}\cdots\frac{d\theta_n}{2\pi}\,\langle G_1^{12}(0)|A^\dagger_{a_1}(\theta_1)\cdots A^\dagger_{a_n}(\theta_n)\rangle \\
&\times\langle A_{a_n}(\theta_n)\cdots A_{a_1}(\theta_1)|G_1^{12}(0)\rangle \\
&\times\exp\big(-|\tau|\sum_{i=1}^{n} m_{a_i}\cosh(\theta_i) + i\mathrm{sign}(\tau)x\sum_{i=1}^{n} m_{a_i}\sinh(\theta_i)\big)\,,
\end{aligned} \tag{6.49}$$

where the first sum $\sum_n$ runs over the number of particles in the form factor expansion and the second sum $\sum_{a_i}$ runs over the different particle types. We have also extracted the spacetime dependence of each term.

We do not compute this sum in its entirety but truncate at the two particle level,

$$\begin{aligned}
-\langle T(G_1^{12}(x,\tau)G_1^{12}(0,0))\rangle &= \int\frac{d\theta_1}{2\pi}\,\langle G_1^{12}(0)|A^\dagger_{12}(\theta_1)\rangle\langle A_{12}(\theta_1)|G_1^{12}(0)\rangle \\
&\times\exp\big(-|\tau|\sqrt{3}m\cosh(\theta_1)\big) + i\mathrm{sign}(\tau)x\sqrt{3}m\sinh(\theta_1)) \\
&+\frac{1}{2}\int\frac{d\theta_1}{2\pi}\frac{d\theta_2}{2\pi}\exp\big(\sum_{i=1,2}\big(-|\tau|m\cosh(\theta_i)+i\mathrm{sign}(\tau)xm\sinh(\theta_i)\big)\big)
\end{aligned}$$

$$
\begin{aligned}
&\times\Big(\sum_{ab}\langle G_1^{12}(0)|A_a^\dagger(\theta_1)A_b^\dagger(\theta_2)\rangle\langle A_b(\theta_2)A_a(\theta_1)|G_1^{12}(0)\rangle\\
&+\sum_{\alpha\beta}\langle G_1^{12}(0)|A_\alpha^\dagger(\theta_1)A_\beta^\dagger(\theta_2)\rangle\langle A_\beta(\theta_2)A_\alpha(\theta_1)|G_1^{12}(0)\rangle\Big)\,. \qquad (6.50)
\end{aligned}
$$

The first term gives the single particle contribution to the correlation function. The only particle that contributes here is A_{12}, denoting one of the particles belonging to the rank 2 tensor multiplet. At the two particle level a variety of contributions are non-zero. The second term in 6.50 gives the contribution of two Majorana fermions while the third term gives the contribution of kinks with the same chirality.

As discussed in Section 2, this truncation of the form factor sum is better than it may at first seem. Because the correlator is evaluated at zero temperature in a massive system, the higher order terms make contributions only at higher energies, ω. That is, the massiveness of the system leads to particle thresholds. The next contribution comes from a three particle combination of even kink/fermion/odd kink that carries mass $3m$. Thus for $\omega < 3m$, this term gives no contribution to $\mathrm{Re}[\sigma(\omega,k)]$ for arbitrary k. Hence our result for $\mathrm{Re}[\sigma(\omega,k)]$ is exact for $\omega < 3m$.

In the case when ω does exceed $3m$, we expect the higher particle form factors to make only a small contribution to $\sigma(\omega)$. As we saw both in Section 2.5 and Section 4.3.2, terms in the form factor sum involving higher numbers of particles make only negligible contributions to the spectral function at any given energy.

Using the results for the form factors of Section 6.5, we can put everything together and write down an expression for $\mathrm{Re}[\sigma(\omega)]$,

$$
\begin{aligned}
\mathrm{Re}[\sigma(\omega)] &= \delta(w-\sqrt{3m^2+k^2})\,\Big(\frac{A_G}{m}\Big)^2\frac{2}{9}\sqrt{\frac{\pi}{3}}\,\frac{\Gamma(1/6)}{\Gamma(2/3)}\\
&\qquad\times\exp\Big[-2\int_0^\infty\frac{dx}{x}\,\frac{G_c(x)}{s(x)}\,s^2(x/3)\Big]\\
&+\theta(w^2-k^2-4m^2)\,\frac{24m^2A_G^2}{(\omega^2-k^2-3m^2)^2}\,\frac{\omega\sqrt{\omega^2-k^2-4m^2}}{(\omega^2-k^2)^{3/2}}\\
&\qquad\times\exp\Big[\int_0^\infty\frac{dx}{x}\frac{G_c(x)}{s(x)}(1-c(x)\cos(\frac{x\theta_{12}}{\pi}))\Big]\,, \qquad (6.51)
\end{aligned}
$$

where $s(x)=\sinh(x)$, $c(x)=\cosh(x)$, and

$$
\theta_{12}=\cosh^{-1}\Big[\frac{\omega^2-k^2-2m^2}{2m^2}\Big]\,. \qquad (6.52)
$$

As indicated in Section 6.5, A_G is an arbitrary constant normalizing all current form-factors while $G_c(x)$ can be found in Eq. (6.40).

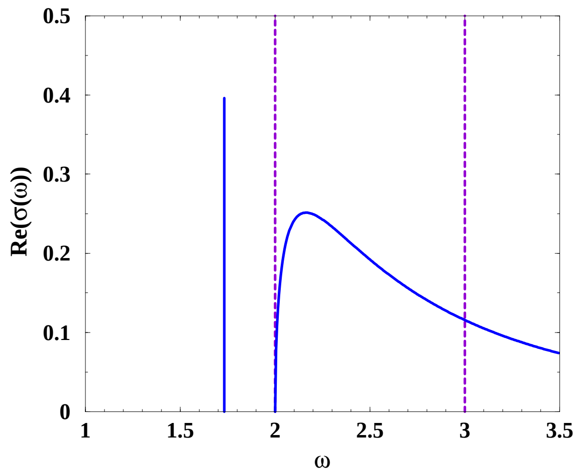

Figure 32. Plot of the optical conductivity at wavevector $k = 0$.

In Fig. 32 we plot the regular real part of the optical conductivity for wavevector $k = 0$.[r] We see there is an exciton type peak at $\omega = \sqrt{3}m$ corresponding to the single particle form factor contribution. The first vertical dashed line marks out the beginning of the two particle form factor contribution to the conductivity. The onset of the two particle contribution behaves as $\sqrt{\omega - 2m}$ and not as $1/\sqrt{\omega - 2m}$ as would be expected in a free theory due to the divergence in the density of states, the van-Hove singularity, that occurs in one dimensional systems. This singularity is removed by the corresponding current matrix element which behaves as $(\omega - 2m)$ with $\omega \to 2m^+$ as the low energy behavior becomes strongly renormalized in the presence of even weak interactions.

The optical conductivity was computed in Ref. [188] using the large N limit of $SO(2N)$, or in an alternate language, an RPA approximation. In such an approximation, the model becomes equivalent to a theory of four massive, non-interacting Dirac fermions. Hence Ref. [188] finds that the van-Hove singularity is present.

The second vertical dashed line in Fig. 32 at $3m$ marks the point where the three particle form factors would begin to make a contribution. Up to this point, the result is exact. We note that the three particle contribution

[r] We will not comment here whether a finite Drude weight exists beyond saying that it is a possibility as the model is integrable.

is strictly a consequence of interactions. In $SO(8)$ language, two kinks of opposite chirality together with a fermion will couple to the current operator. In a free theory these different particles would not all exist and there would be no three particle contribution.

If we were to compute the three particle contribution, three possibilities present themselves. The three particle density of states approaches a constant as $\omega \to 3m^+$. If the corresponding matrix element vanishes as $\omega \to 3m^+$, the contribution will open up gradually, leaving $\sigma(\omega)$ continuous at $\omega = 3m$. If the three particle matrix element also approaches a constant value as $\omega \to 3m^+$, the conductivity will be marked by a jump at $\omega = 3m$. But if the matrix element diverges in this limit, we expect to find a corresponding divergence in the conductivity at $\omega = 3m$. Of these scenarios, it is our belief that the first is most likely. Moreover we expect that the total spectral weight in such a contribution in comparison to the two-particle contribution will be extremely small.

6.6.2. *Single Particle Spectral Function*

In this section we compute the single-particle spectral function of the electrons of the ladder/nanotube. To do so we first consider the correlator,

$$G(k_x, k_y, \tau) = \sum_{l=1,2} \int_{-\infty}^{\infty} dx\ e^{-ik_y l - ik_x x} \langle T(a_{l\alpha}(x,\tau) a^\dagger_{l\alpha}(0,0))\rangle\ . \quad (6.53)$$

Here k_y takes on the values $0, \pi$. We then define the particle/hole spectral functions, $A_{p/h}$, by

$$A_p(\mathbf{k}, \omega) + A_h(-\mathbf{k}, -\omega) = \mathrm{Im} \int_{-\infty}^{\infty} d\tau\ e^{-i\omega\tau} G(k_x, k_y, \tau)\big|_{\omega \to -i\omega+\delta}\ . \quad (6.54)$$

We note that we have not explicitly summed over spin, α.

As described in Section 6.4.2, electronic excitations around the Fermi point correspond in the Gross–Neveu language to low energy excitations of kinks. We thus expect to recast the Greens function, G, above in terms of kink correlators. This in fact can be done with the result,

$$G(Pk_{Fi} + k, k_{yi}, \tau) = \int_{-\infty}^{\infty} dx e^{ikx} \langle T(c_{Pi\alpha}(x,\tau) c^\dagger_{Pi\alpha}(0,0))\rangle\ , \quad (6.55)$$

where $i = 1, 2$ and $k_{yi} = (2-i)\pi$. The c's, the bonding-anti-bonding electrons are in turn related to the various kinks via Eq. (6.36). The Greens function on the r.h.s. of Eq. (6.55) is thus equal to

$$\langle T(c_{Pi\alpha}(x,\tau) c^\dagger_{Pi\alpha}(0,0))\rangle = \langle T(\kappa_\alpha \psi^\alpha_\pm(x,\tau) \kappa_{\bar\alpha} \psi^{\bar\alpha}_\pm(0,0))\rangle\ , \quad (6.56)$$

where α ($\bar{\alpha}$ being its charge conjugate) is the particular kink corresponding to the Fermi point (k_{Fi}, k_{yi}). The κ_α are Klein factors included to ensure the ψ^α are anti-commuting. Because of the $SO(8)$ symmetry together with its associated triality symmetry, $\langle T(\kappa_\alpha\psi^\alpha_\pm(x,\tau)\kappa_{\bar{\alpha}}\psi^{\bar{\alpha}}_\pm(0,0))\rangle$ turns out to be independent of the type α of kink. It is only sensitive to whether the kink field is right $(+)$ or left $(-)$ moving.

To compute this correlator, we again expand to the two lowest contributions,

$$\langle T(\kappa_\alpha\psi^\alpha_\pm(x,\tau>0)\kappa_{\bar{\alpha}}\psi^{\bar{\alpha}}_\pm(0,0))\rangle = \int_{-\infty}^{\infty}\frac{d\theta_1}{2\pi}\langle\psi^\alpha_+(x,\tau)A^\dagger_{\bar{\alpha}}(\theta_1)\rangle\langle A_{\bar{\alpha}}(\theta_1)\psi^{\bar{\alpha}}_+(0)\rangle$$
$$+\frac{1}{2}\sum_{a\beta}\int_{-\infty}^{\infty}\frac{d\theta_1}{2\pi}\frac{d\theta_2}{2\pi}\langle\psi^\alpha_+(x,\tau)A^\dagger_\beta(\theta_2)A^\dagger_a(\theta_1)\rangle\langle A_a(\theta_1)A_\beta(\theta_2)\psi^{\bar{\alpha}}_+(0)\rangle\,. \quad (6.57)$$

The first contribution, the one particle contribution, comes from the kink excitation, $A_{\bar{\alpha}}$, destroyed by the field, ψ_α. The second contribution, a two particle contribution, arises from kinks, A_β, of opposite chirality to A_α, and Majorana fermions, A_a. (This reflects the group theoretical fact that the tensor product of an $SO(8)$ spinor representation with an $SO(8)$ vector representation gives the other $SO(8)$ spinor representation [261].) The first contribution not included is a bound state-kink pair. It begins to contribute at $\omega = (1+\sqrt{3})m$.

From the form factor expressions from Section 6.5, we can then write down the expression for the spectral functions, $A_{p/h}(\omega,k)$,

$$\begin{aligned}A_p(\omega, Pk_{Fi}+k, k_{yi}) &= A_h(\omega, -Pk_{Fi}+k, k_{yi})\\ &= \frac{\pi|c_P|^2}{m}\,\frac{\omega+Pk}{\sqrt{k^2+m^2}}\,\delta(\omega-\sqrt{k^2+m^2})\\ +\theta(\omega-\sqrt{k^2+4m^2})&\,\frac{32m^4A_F^2}{\omega-Pk}\,\frac{1}{(\omega^2-k^2-m^2)^2}\,\frac{1}{\sqrt{\omega^2-k^2-4m^2}}\\ &\times\exp\Big[\int_0^\infty\frac{dx}{x}\,\frac{G_f(x)}{s(x)}\Big(1-c(x)\cos\Big(\frac{x\theta_{12}}{\pi}\Big)\Big)\Big]\,, \qquad (6.58)\end{aligned}$$

where A_F is the (unspecified) normalization of the two particle kink form-factor, $G_f(x)$ is given in Eq.(6.43), and $c_\pm$ is found in Eq.(6.45). For $P = R = +$ (i.e. right-moving electrons/kinks), this function is plotted in Fig. 33.

The parabolic line in Fig. 33 arises from the single particle form factor contribution, and represents the standard dispersion relation of a particle of mass, m. Above this curve comes the two particle form factor contribution to the spectral function. This contribution is bounded by the curve, $\omega =$

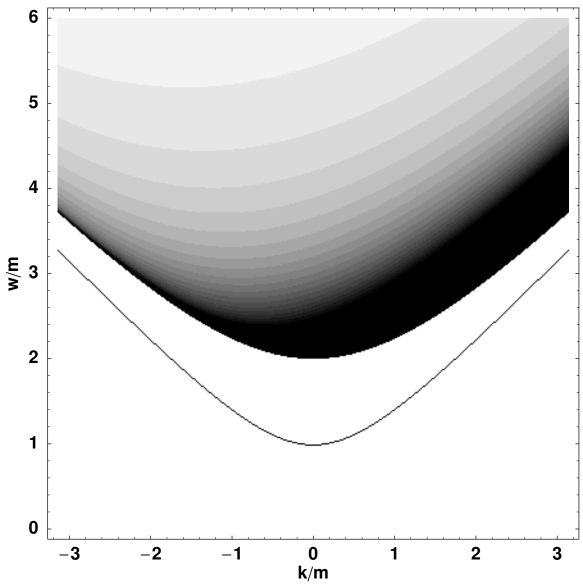

Figure 33. Plot of the single particle spectral function for right moving kinks. The more darkly shaded region corresponds to greater spectral weight.

$\sqrt{k^2+4m^2}$, and so the single particle states do not cross into the two particle region. As can be seen from Eq. (6.58), the two particle contribution opens up at threshold with a square-root singularity, indicative of the van-Hove singularity in the density of states.

The plot is manifestly chiral with weighting greater for $k > 0$ than for $k < 0$. This is to be expected as we are plotting the excitations linearized about the Fermi momentum, $+k_{Fi}$. The heavier weighting for $k > 0$ indicates that is easier to create excitations above the Fermi sea than below it. It is interesting indeed that excitations below the Fermi surface can be created at all and is a mark that interactions are at play.

6.6.3. *STM Tunneling Current*

In this section we study the tunneling between a metallic lead and the carbon nanotube/Hubbard ladder through a point contact. Our starting point is a Lagrangian describing the nanotube/ladder, the metallic lead, and the tunneling interaction

$$\mathcal{L} = \mathcal{L}_{SO(8)} + \mathcal{L}_{lead} + \mathcal{L}_{tun}\,. \tag{6.59}$$

$\mathcal{L}_{SO(8)}$ is the Lagrangian of the $SO(8)$ Gross–Neveu model.

The electron gas in the lead is, in general, three dimensional. However, in the context of tunneling through a point contact, the electron gas can be mapped onto an one dimensional chiral fermion (see for example [8, 12, 56]). The general idea is well illustrated by its application to the Kondo problem. There an electron scatters off a spin impurity at $x = 0$. The scattering is determined by the electron operator, $\psi(x = 0)$. As $\psi(0)$ only depends on its spherically symmetric, $L = 0$, mode, one can consider the scattering electron in terms of an ingoing and outgoing radial model defined on the half-line, $r \in [0, \infty]$. Unfolding the system onto the full line leaves one with a chiral fermion. We emphasize however that the map requires no special symmetry; the result is exact regardless of particular anisotropies [12]. As a consequence, we write $\mathcal{L}_{lead}$ as

$$\mathcal{L}_{lead} = \frac{1}{8\pi}\,\Psi^\dagger\partial_{\bar{z}}\Psi\,, \tag{6.60}$$

where Ψ is a massless, left moving fermion, and $z = (\tau + ix)/2$.

It remains to specify $\mathcal{L}_{tun}$. In order to preserve charge, the electrons must couple to the kinks of the $SO(8)$ Gross–Neveu model, the excitations with the quantum numbers of the electron. Thus

$$\begin{aligned}\mathcal{L}_{tun} = \;& g_L\big[\Psi^\dagger(\tau)\psi^\alpha_-(\tau) + \psi^{\bar\alpha}_-(\tau)\Psi(\tau)\big]\delta(x)\\ &+g_R\big[\Psi^\dagger(\tau)\psi^\alpha_+(\tau) + \psi^{\bar\alpha}_+(\tau)\Psi(\tau)\big]\delta(x)\,.\end{aligned} \tag{6.61}$$

Here we have coupled the lead electrons to both the right and left moving fields creating the kink, α, and have allowed the two couplings, g_L and g_R, to be unequal. However as we will work to lowest non-vanishing order in the tunneling matrix elements $g_{L/R}$, the tunneling current will depend upon the sum, $g_L^2 + g_R^2$, that is, the contribution of the left and right channels to tunneling will add linearly. Similarly, permitting other kinks to couple to the lead electrons will give lowest order contributions which simply add.

The calculation of the current to lowest non-vanishing order in $g_{L/R}$ follows the standard route. The tunneling current operator is given by

$$\begin{aligned}I(\tau) = \;& ig_R(\psi^{\bar\alpha}_+(\tau)\Psi(\tau) - \Psi^\dagger(\tau)\psi^\alpha_+(\tau))\\ &+ig_L(\psi^{\bar\alpha}_-(\tau)\Psi(\tau) - \Psi^\dagger(\tau)\psi^\alpha_-(\tau))\,.\end{aligned} \tag{6.62}$$

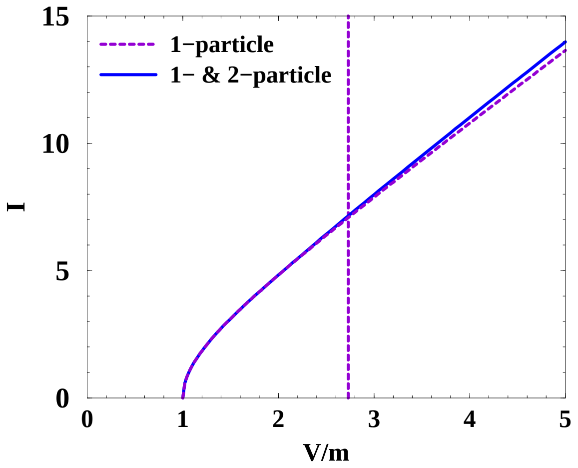

Figure 34. Plot of the tunneling current as a function of applied voltage. The dashed curve describes tunneling into a non-interacting fermionic system of mass, m. The vertical dashed line marks where a second set of two particle states begins to make a contribution.

In order to induce current flow, $\langle I(\tau)\rangle$, through the point contact, one biases the lead with a voltage, V. This bias can be taken into account via a gauge transformation,

$$\Psi(\tau) \rightarrow e^{iV\tau}\Psi(\tau)\,. \tag{6.63}$$

In effect we have shifted the energy levels of the electrons. Treating the couplings, g_L/g_R, with linear response theory, we find

$$\begin{aligned}\langle I(\omega)\rangle = g_L^2\mathrm{Re}\Big\{ \int d\tau\, ie^{i\omega\tau}\big[e^{-iV\tau}\langle\psi_-^\alpha(\tau)\psi_-^{\bar\alpha}(0)\rangle\langle\Psi^\dagger(\tau)\Psi(0)\rangle \\ - e^{iV\tau}\langle\psi_-^{\bar\alpha}(\tau)\psi_-^\alpha(0)\rangle\langle\Psi(\tau)\Psi^\dagger(0)\rangle\big]\big|_{\substack{\omega\to -i\omega+\delta\\ V\to -iV}}\Big\} \\ + (L\rightarrow R, \psi_-^\alpha/\psi_-^{\bar\alpha}\rightarrow\psi_+^\alpha/\psi_+^{\bar\alpha})\,.\end{aligned} \tag{6.64}$$

The lead electron correlator $\langle\Psi^\dagger(\tau)\Psi(0)\rangle$ is well known to be

$$\langle\Psi^\dagger(\tau,x)\Psi(0)\rangle = \langle\Psi(\tau,x)\Psi^\dagger(0)\rangle = \frac{1}{\tau+ix}\,. \tag{6.65}$$

With this it is straightforward to express the dc current, $\langle I(\omega=0)\rangle$, in terms of the single particle kink spectral function,

$$\langle I(\omega=0)\rangle = \frac{1}{2\pi}\int_{-V}^{V} d\omega\int_{-\infty}^{\infty} dk\big[g_L^2 A_-(\omega,k) + g_R^2 A_+(\omega,k)\big], \tag{6.66}$$

where $A_\pm(\omega,k) = A_p(\omega, \pm k_{Fi}+k, k_{yi}) + A_h(-\omega, \mp k_{Fi}-k, k_{yi})$, and $A_{p/h}$ are the spectral functions given in Eq. (6.48). We note that as a technical point, in deriving the above equation we have displaced, Ψ, the lead electron operator, slightly from $x = 0$. In this way we cure the UV divergence attendant as $\tau \to 0$. At the end of the calculation we then take x to 0.

In the previous section we have computed $A_\pm(\omega,k)$ exactly for energies $\omega < (\sqrt{3}+1)m$. Inserting Eq. (6.58) into Eq. (6.66), we find $\langle I(0)\rangle$ takes the form

$$\begin{aligned}\langle I(0)\rangle = &\frac{|c_\pm|^2}{m}(g_R^2+g_L^2)(V^2-m^2)^{1/2}\theta(|V|-m)\mathrm{sgn}(V)\\ &+\theta(|V|-2m)\mathrm{sgn}(V)\times \text{two particle contribution}\,. \qquad (6.67)\end{aligned}$$

We see that for $|V| < 2m$, the system behaves as a gapped free fermion. The first sign that there is any interaction comes for $|V| > 2m$ where the voltage begins to probe the two particle states, a signature of interacting fermions.

We explicitly plot $\langle I(0)\rangle$ in Fig. 34. The square root behavior near $V/m = 1$ and subsequent linear form is typical of a gapped fermion. At $V/m = 2$, the two particle states begin to contribute leading to a small change in the slope of the $I - V$ curve. At $V/m = \sqrt{3}+1$ (marked by the the vertical dashed line), a second set of two particle states (a mass $\sqrt{3}m$ bound state together with a kink) begin to contribute and at this point the result ceases to be exact. However as with the current correlators, we expect this higher energy contribution to be small.

The change in slope in the $I - V$ curve at $V/m = 2$ can be explicitly computed. To do so we consider $\partial_V\langle I(0)\rangle$. This quantity is given by

$$\partial_V\langle I(0)\rangle = \frac{1}{\pi}\,(g_R^2+g_L^2)\int_{-\infty}^{\infty} dk\; A_\pm(V,k)\,. \qquad (6.68)$$

We can thus see $\partial_V\langle I(0)\rangle$ directly measures the local density of states at $x = 0$ of the nanotube/ladder system.

We plot $\partial_V\langle I(0)\rangle$ in Fig. 35. The square root singularity at $V = m$ signals the singularity of the density of states in an one dimensional system. At $V = 2m$ we see a sudden jump, indicative of the onset of the two particle contribution. The height of the jump can be determined exactly,

$$\begin{aligned}&\partial_V\langle I(0)\rangle(V/m=2^+) - \partial_V\langle I(0)\rangle(V/m=2^-)\\ &\quad = \frac{16A_F^2}{9m}\,(g_R^2+g_L^2)\exp\Big[\int_0^\infty \frac{dx}{x}\,\frac{G_f(x)}{s(x)}\,(1-c(x))\Big]\,. \qquad (6.69)\end{aligned}$$

The region $m < V < 2m$ of $\partial_V\langle I(0)\rangle$ completely determines m (by the location of the jump), as well as an overall scale (the product of $(g_L^2+g_R^2)$ and the constant A_F, normalizing the spectral function). Dividing out these non-universal quantities leaves a universal number, characterizing the magnitude of the jump,

$$\frac{16}{9}\exp\left[\int_0^\infty \frac{dx}{x}\,\frac{G_f(x)}{s(x)}\,(1-c(x))\right]. \tag{6.70}$$

This number represents a definite prediction based upon the integrability of the model.

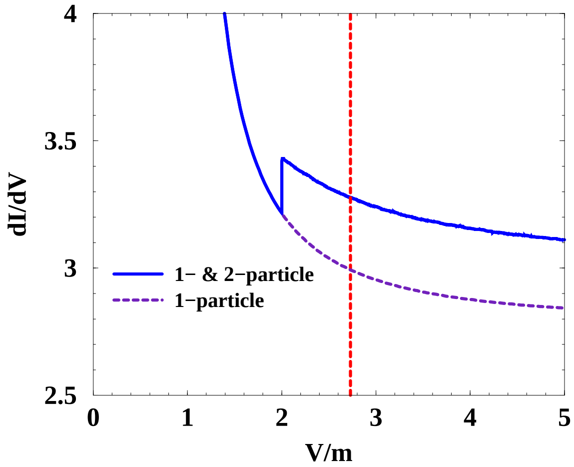

Figure 35. Plot of the differential conductance as a function of applied voltage. The dashed curve marks the single particle contribution to this quantity while the solid curves give both the single and two particle contribution. The latter plot is exact up to $V/m = \sqrt{3}+1$ (indicated by the dashed vertical line) where a bound state-kink pair begins to make a contribution.

6.7. *Effect of Integrable Breaking Perturbations*

It can now be asked how perturbations to $SO(8)$ Gross–Neveu will affect the various computations discussed in the previous section. We consider this in the broadest terms by focusing upon how the spectrum of $SO(8)$ Gross–Neveu is changed under a perturbing term. We do so through straightforward stationary perturbation theory, in the same spirit that Ref. [68] treated the off-critical Ising model in a magnetic field. The most general possible perturbation takes the form

$$H_{\rm pert} = \lambda G_{ab} G_{cd}\,, \tag{6.71}$$

where G_{ab}, G_{cd} are $SO(8)$ currents (of unspecified chirality). For such a perturbation it is necessary to consider degenerate perturbation theory. Thus in a given particle multiplet (for example, the fundamental fermions in the vector representation), the perturbed energies arise through diagonalizing the matrix

$$M_{ij} = \langle A_i^\dagger(\theta) H_{\rm pert} A_j(\theta)\rangle, \tag{6.72}$$

where here the index i,j indicates the particles A_i,A_j belong to the multiplet of concern. In the case that $G_{ab} = G_{cd}$, M_{ij} is necessarily diagonal, i.e. nondegenerate perturbation theory is sufficient.

It is important to emphasize that this procedure can be handled in the context of integrability. The expression in Eq. (6.72) is no more than a form-factor which can readily be computed. Moreover as the theory is massive, perturbation theory is well controlled. We expect the unperturbed theory to describe all qualitative features of the model while the perturbations to only introduce small quantitative changes.

We first consider the consequences of such a perturbation on the optical conductivity. They are two-fold. We expect the exciton peak (found, for example, in Fig. 32 at $k = 0$ and $\omega = \sqrt{3}$) to split. In the unperturbed model the peak results from a single rank-two bosonic bound state coupling to the current operator. When the matrix M_{ab} above is diagonalized, this particular state should be mixed into many others resulting in several states that couple to the current operator. However we do not expect the functional forms of the exciton peaks to change: they should remain delta functions. They must do so provided the perturbation is not so large as to push the exciton peak past the threshold of two particle states where it then conceivably could decay. As there is a gap between the excitonic peak and the two particle threshold, this will not happen for small perturbations. Experimentally changes to the exciton peak may not be detectable. Given that any experiment will be conducted at finite temperature, the excitonic peak will be thermally broadened, perhaps washing out any splitting of the original zero temperature peak.

We also expect the perturbation to affect the onset of the two particle threshold, although in a less dramatic fashion. Like the unperturbed case, there will be several two particle contributions to the optical conductivity. However unlike the unperturbed case, the thresholds of the two particle contributions will not all occur at $\omega = 2m$ but be distributed about this energy. Thus the two particle contribution is arrived at (approximately) by superimposing several slightly shifted two-particle contributions similar to that found in Fig. 32. But given the optical conductivity vanishes at threshold, the qualitative picture remains effectively unchanged (i.e. the superimposed contributions will appear nearly identical to the original picture). That the optical conductivity vanishes at the two particle threshold is a result of the vanishing of the relevant matrix element at threshold. This should be robust under perturbation as it is ultimately a consequence of the mere presence of interactions and not some particular type of interactions.

We can also consider in a similar spirit the approximate effect of perturbations breaking integrability on the tunneling conductance. As the tunneling conductance is determined directly from the single particle spectral function, we can deduce how the former is affected from how the latter is changed. At a given momentum, the single particle contribution to the single particle spectral function under perturbation comes at a discrete set of energies. In terms of the tunneling conductance, we expect a series of closely spaced square root divergences (a sawtooth behavior) about $V = m$ indicative of a series of van-Hove singularities. As the perturbation is removed these singularities would collapse on top of one another leaving the original picture in Fig. 35.

In the unperturbed case the two-particle threshold is characterized by a jump in the differential conductance. Under a perturbation, this jump would become a staircase or a series of smaller, closely spaced jumps. This is a reflection of the series of van-Hove singularities found about $\omega = \sqrt{k^2 + 4m^2}$ in the two particle contribution to the single particle spectral function.

Acknowledgments

We thank L. Balents, P. Fendley, M.P.A. Fisher, A. LeClair, H H. Lin, A.W.W. Ludwig, G. Mussardo, A.A. Nersesyan, E. Orignac, H. Saleur, A.M. Tsvelik, I. Zaliznyak, and A. Zheludev for enlightening discussions over the course of the work appearing in this review.

References

1. A. Abada, A.H. Bougourzi and B. Si-Lakhal, Nucl. Phys. B **497**, 733 (1997).
2. A.A. Abrikosov, L.P. Gorkov and I.E. Dzyaloshinski, *Methods of Quantum Field Theory in Statistical Physics*, (Dover, New York, 1975), page 168.
3. I. Affleck, Nucl. Phys. B **265**, 409 (1986).
4. I. Affleck, T. Kennedy, E. Lieb and H. Tasaki, Comm. Math. Phys. **115**, 477 (1988).
5. I. Affleck, in *Fields, Strings and Critical Phenomena*, eds E. Brézin and J. Zinn-Justin, (Elsevier, Amsterdam, 1989).
6. I. Affleck, D. Gepner, H. J. Schulz and T. Ziman, J. Phys. A **22**, 511 (1989).
7. I. Affleck, Phys. Rev. B **41**, 6697 (1990).
8. I. Affleck and A.W.W. Ludwig, Nucl. Phys. B **330**, 641 (1991).
9. I. Affleck, Phys. Rev. B **41**, 6697 (1990).
10. I. Affleck, Phys. Rev. B **43**, 3215 (1991).
11. I. Affleck and R. Weston, Phys. Rev. B **45**, 4667 (1992).
12. I. Affleck, A.W.W. Ludwig and B. Jones, Phys. Rev. B **52**, 9528 (1995).
13. I. Affleck and B.I. Halperin, J. Phys. A **29**, 2627 (1996).
14. I. Affleck, J. Phys A **31**, 4573 (1998).
15. I. Affleck and M. Oshikawa, Phys. Rev. B **60**, 1038 (1999).
16. Y. Ajiro, T. Asano, Y. Inagaki, J.P. Boucher, H. Nojiri, S. Luther, T. Sakon and M. Motokawa, J. Phys. Soc. Jpn **69**, 297 (2000).
17. F. Alcaraz and W.F. Wreszinski, J. Stat. Phys. **58**, 45 (1989).
18. E. Arrigoni, Phys. Rev. B **61**, 7909 (2000).
19. T. Asano, H. Nojiri, Y. Inagaki, J.P. Boucher, T. Sakon, Y. Ajiro and M. Motokawa, Phys. Rev. Lett **84**, 5880 (2000).
20. T. Asano, H. Nojiri, W. Higemoto, A. Koda, R. Kadono and Y. Ajiro, J. Phys. Soc. Jpn **69**, 594 (2002).
21. P. Azaria, P. Lecheminant and A.M. Tsvelik, cond-mat/9806099 (unpublished).
22. H. M. Babujian, Phys. Lett. A **90**, 479 (1982); ibid. Nucl. Phys. B **215**, 317 (1983).
23. H. Babujian, A. Fring, M. Karowski and A. Zapletal, Nucl. Phys. B **538**, 535 (1999).
24. H. M. Babujian and M. Karowski, Nucl. Phys. B **620**, 407 (2002).
25. H. M. Babujian and M. Karowski, J. Phys. A **35**, 9081 (2002).
26. L. Balents and M.P.A. Fisher, Phys. Rev. B **53**, 12133 (1996);
27. L. Balents and M.P.A. Fisher, Phys. Rev. B **55**, R11973 (1997).
28. L. Balents and R. Egger, Phys. Rev. B **64**, 035310 (2001).
29. J. Balog, Nucl. Phys. B **419**, 480 (1994).
30. J. Balog and M. Niedermaier, Nucl. Phys. B **500**, 421 (1997).
31. R.N. Bannister and N. d'Ambrumenil, Phys. Rev. B **61**, 4651 (2000).
32. T. Barnes and J. Riera, Phys. Rev. B **50**, 6817 (1994).
33. V. Barzykin and I. Affleck, J. Phys. A **32**, 867 (1999).
34. V. Barzykin, J. Phys. Cond. Mat. **12**, 2053 (2000).
35. D. Bernard and A. LeClair, Commun. Math. Phys. **142**, 99 (1991).
36. D. Bernard and A. LeClair, Nucl. Phys. B **399**, 709 (1993).
37. H. Bethe, Z. Phys. **71**, 205 (1931).
38. H. Bergknoff and H. Thacker, Phys. Rev. D **19**, 3666 (1979).
39. B. Berg, M. Karowski and P. Weisz, Phys. Rev. D **19**, 2477 (1979).
40. M.J. Bhaseen, F.H.L. Essler and A. Grage, *Itineracy Effects on Spin Correlations in 1D Mott Insulators*, cond-mat/0312055.
41. M. Bockrath, D. Cobden, P. McEuen, N. Chopra, A. Zettl, A. Thess and R. Smalley, Science **275**, 1922 (1997);

42. M. Bockrath, D. H. Cobden, J. Lu, A. G. Rinzler, R. Smalley, L. Balents and P. McEuen, Nature **417**, 725 (2002).
43. M. Bocquet, Phys. Rev. B **65**, 184415 (2002).
44. D. Boies, C. Bourbonnais and A.-M. S. Tremblay, Phys. Rev. Lett. **74**, 968 (1995).
45. A.H. Bougourzi, M. Couture and M. Kacir, Phys. Rev. B **54**, 12669 (1996).
46. A. H. Bougourzi, M. Karbach and G. Müller, Phys. Rev. B **57**, 11429-11438 (1998).
47. C. Bourbonnais and D. Jerome, in *Advances in Synthetic Metals, Twenty years of Progress in Science and Technology*, ed. by P. Bernier, S. Lefrant and G. Bidan (Elsevier, New York, 1999), pp. 206-301 and references therein. See also cond-mat/903101.
48. W.J.L. Buyers, R.M. Morra, R.L. Armstrong, M.J. Hogan, P. Gerlach and K. Hirakawa, Phys. Rev. Lett. **56**, 371 (1986).
49. L. Campos Venuti, E. Ercolessi, G. Morandi, P. Pieri and M. Roncaglia, *Spin Chains in an External Magnetic Field. Closure of the Haldane Gap and Effective Field Theories*, cond-mat/9908044.
50. F. Capraro and C. Gros, Eur. Phys. J. **B29**, 35 (2002).
51. O. A. Castro-Alvaredo and A. Fring, Nucl. Phys. B **636**, 611 (2002).
52. J. Cardy and G. Mussardo, Nucl. Phys. B **340**, 387 (1990).
53. J. Cardy and G. Mussardo, Nucl. Phys. B **410**, 451 (1993).
54. J.-S. Caux, F.H.L. Essler and U. Löw, Phys. Rev. B **68**, 134431 (2003).
55. H. Castella, X. Zotos and P. Prelovsek, Phys. Rev. Lett. **74**, 972 (1995).
56. C. Chamon and E. Fradkin, Phys. Rev. B **56**, 2012 (1997).
57. Y. Chen, Z. Honda, A. Zheludev, C. Broholm, K. Katsumata and S. M. Shapiro, Phys. Rev. Lett. **86**, 1618 (2001).
58. D. H. Cobden, J. Nygard, M. Bockrath and P. McEuen, *One-dimensional transport in bundles of single-walled carbon nanotubes*, Proceedings of IWEPNM 99 (Kirchberg), cond-mat/9904179.
59. D. Controzzi, F.H.L. Essler and A.M. Tsvelik, Phys. Rev. Lett. **86**, 680 (2001).
60. D. Controzzi, F.H.L. Essler and A.M. Tsvelik, in *New Theoretical Approaches to Strongly Correlated Systems*, ed. A.M. Tsvelik, NATO Science Series II Vol. 23 [cond-mat/0011439].
61. D. Controzzi and F.H.L. Essler, Phys. Rev. B **66**, 165112 (2002).
62. R. Dashen and Y. Frishman, Phys. Rev. D **11**, 2781 (1975).
63. R.F. Dashen, B. Hasslacher and A. Neveu, Phys. Rev. D **11**, 3424 (1975).
64. E. Dagotto and T. Rice, Science **271**, 618 (1996).
65. E. Dagotto, J. Riera and D. Scalapino, Phys. Rev. B **45**, 5744 (1992).
66. K. Damle and S. Sachdev, Phys. Rev. B **57**, 8307 (1998).
67. J. Deisz, M. Jarrell and D. Cox, Phys. Rev. B **48**, 10227 (1993).
68. G. Delfino, G. Mussardo and P. Simonetti, Nucl. Phys. B **473**, 469 (1996).
69. G. Delfino and G. Mussardo, Nucl. Phys B **455** 724 (1995).
70. G. Delfino and J. Cardy, Nucl.Phys. B **519**, 551 (1998).
71. D.C. Dender, D. Davidović, D.H. Reich, C. Broholm, K. Lefmann and G. Aeppli, Phys. Rev. B **53**, 2583 (1996).
72. D.C. Dender, P.R. Hammar, D.H. Reich, C. Broholm and G. Aeppli, Phys. Rev. Lett. **79**, 1750 (1997).
73. C. Destri and H.J. de Vega, Phys. Rev. Lett. **69**, 2313 (1992).
74. C. Destri and H.J. de Vega, Nucl. Phys. B **438**, 413 (1995).
75. D.V. Dmitriev, V.Y. Krivnov and A.A. Ovchinnikov, Phys. Rev. B **65**, 172409 (2002).
76. D.V.Dmitriev, V.Ya.Krivnov, A.A.Ovchinnikov, A.Langari, JETP **95**, 538 (2002).
77. B. Doyon and S. Lukyanov, Nucl. Phys. B **644**, 451 (2002).
78. M. S. Dresselhaus, Nature **391**, 19 (1998).

79. D. Duffy, S. Haas and E. Kim, Phys. Rev. B **58**, R5932 (1998).
80. G. I. Dzhaparidze and A. A. Nersesyan, JETP Lett. **27**, 224 (1978).
81. I.E. Dzyaloshinski, J. Phys. Chem. Solids **4**, 241 (1958).
82. I.E. Dzyaloshinski, Phys. Rev. B **68**, 085113 (2003).
83. T. Ebbesen, Phys. Today **49**, 26 (1996).
84. V. Emery, S. Kivelson and O. Zachar, Phys. Rev. B **59**, 15641 (1999).
85. R. Egger and A.O. Gogolin, Phys. Rev. Lett. **79**, 5082 (1998).
86. R. Egger and A.O. Gogolin, Eur. Phys. J. B **3**, 281 (1998).
87. F.H.L. Essler, A.M. Tsvelik and G. Delfino, Phys. Rev. B **56**, 11001 (1997).
88. F.H.L. Essler and A.M. Tsvelik, Phys. Rev. B **57**, 10592 (1998).
89. F.H.L. Essler, Phys. Rev. B **59**, 14376 (1999).
90. F.H.L. Essler, Phys. Rev. B **62**, 3264 (2000).
91. F.H.L. Essler, F. Gebhard and E. Jeckelmann, Phys. Rev. B **64**, 5119 (2001).
92. F.H.L. Essler and A.M. Tsvelik, Phys. Rev. B **65**, 115117 (2002).
93. F.H.L. Essler and A.M. Tsvelik, Phys. Rev. Lett. **88**, 096403 (2002).
94. F.H.L. Essler and A.M. Tsvelik, Phys. Rev. Lett. **90**, 126401 (2003).
95. F.H.L. Essler, A. Furusaki and T. Hikihara, Phys. Rev. B **68**, 064410 (2003).
96. M. Fabrizio, Phys. Rev. B **48**, 15838 (1993).
97. L.D. Faddeev and V.E. Korepin, Phys. Rept. C **42**, 1 (1978).
98. L.D. Faddeev and L. Takhtajan, Phys. Lett. A **85**, 375 (1981).
99. L.D. Faddeev and L. Takhtajan, Jour. Sov. Math. **24**, 241 (1984).
100. G. Fáth and P. Littlewood, Phys. Rev. B **58**, R14709 (1998).
101. P. Fendley, A.W.W. Ludwig and H. Saleur, Phys. Rev. Lett. **74**, 3005 (1995).
102. P. Fendley, A.W.W. Ludwig and H. Saleur, **75**, 2196 (1995).
103. P. Fendley, A.W.W. Ludwig and H. Saleur, Phys. Rev. B **52**, 8934 (1995).
104. R. Feyerherm *et al.*, J. Phys.: Condens. Matter **12**, 8495 (2000).
105. M. Fowler and X. Zotos, Phys. Rev. B **24**, 2634 (1981),
106. M. Fowler and X. Zotos, Phys. Rev. B **25**, 5806 (1982).
107. F. Lesage and H. Saleur, Nucl. Phys. B **490**, 543 (1997).
108. F. Lesage and H. Saleur, Nucl. Phys. B **493**, 613 (1997).
109. A. Fring, G. Mussardo and P. Simonetti, Nucl.Phys. B **393**, 413 (1993).
110. S. Fujimoto and N. Kawakami, J. Phys. A **31**, 465 (1998).
111. S. Fujimoto, J. Phys. Soc. Jpn. **68**, 2810 (1999).
112. H. Fujisawa et al, Phys. Rev. B **59**, 7358 (1999).
113. A. Furusaki and S.C. Zhang, Phys. Rev. B **60**, 1175 (1999).
114. M. Garst and A. Rosch, Europhys. Lett. **55**, 66 (2001) [cond-mat/0102109].
115. F. Gebhard, *The Mott Metal-Insulator Transition*, (Springer, Berlin, 1997).
116. T. Giamarchi, Physica B **230-232**, 975 (1997).
117. T. Giamarchi and A.M. Tsvelik, Phys. Rev. B **59**, 11398 (1999).
118. Y.Y. Goldschmidt and E. Witten, Phys. Lett. B **91**, 392 (1980).
119. A.O. Gogolin, A.A. Nersesyan and A.M. Tsvelik, *Bosonization in Strongly Correlated Systems* (Cambridge University Press, 1999).
120. O. Golinelli, Th. Jolicoeur and R. Lacaze, Phys. Rev. B **46**, 10854 (1992).
121. S. Haas, J. Riera and E. Dagotto, Phys. Rev. B **48**, 3281 (1993).
122. M. Hagiwara, Z. Honda, K. Katsumata, A. K. Kolezhuk and H.-J. Mikeska, Phys. Rev. Lett. **91** 177601 (2003).
123. N. Hamada, S. Sawada and A. Oshiyama, Phys. Rev. Lett. **68**, 1579 (1992).
124. F.D.M. Haldane, Phys. Rev. Lett. **47**, 1840 (1981).
125. F.D.M. Haldane, J. Phys. C **14**, 2585 (1981).
126. F.D.M. Haldane, Phys. Rev. B **25**, 4925 (1982).

127. F.D.M. Haldane, J. Phys. A **15**, 507 (1982).
128. F.D.M. Haldane, Phys. Lett. A **93**, 464 (1983).
129. C. Hayward, D. Poilblanc and D. Scalapino, Phys. Rev. B **53**, 11721 (1996).
130. W. Henderson, V. Vescoli, P. Tran, L. Degiorgi and G. Grüner, Eur. Phys. J. B **11**, 365 (1999).
131. T. Hikihara and A. Furusaki, Phys. Rev. B **63**, 134438 (2001).
132. T. Hikihara and A. Furusaki, Phys. Rev. B **69**, 064427 (2004).
133. Z. Hiroi, M. Azuma, M. Takano, Y. Bando, J. Solid State Chem. **95**, 230 (1991).
134. Z. Hiroi and M. Takano, Nature **377**, 41 (1995).
135. Z. Hiroi, J. Solid State Chem. **123**, 223 (1996).
136. Z. Honda, K. Katsumata, H. Aruga Katori, K. Yamada, T. Ohishi, T. Manabe and M. Yamashita, J. Phys.: Condensed Matter **9**, L83 (1997).
137. Z. Honda, K. Katsumata, H. Aruga Katori, K. Yamada, T. Ohishi, T. Manabe and M. Yamashita, J. Phys.: Condensed Matter **9**, 3487 (1997).
138. Z. Honda, H. Asakawa and K. Katsumata, Phys. Rev. Lett. **81**, 2566 (1998).
139. Z. Honda, K. Katsumata, M. Hagiwara and M. Tokunaga, Phys. Rev. B **60**, 9272 (1999).
140. M. Horton and I. Affleck, Phys. Rev. B **60**, 11891 (1999).
141. L. Hulthén, Arkiv Mat. Astron. Fysik **26A**, No. 11 (1938).
142. V. Y. Irkhin and A.A. Katanin, Phys. Rev. B **61**, 6757 (2000).
143. E. Jeckelmann, F. Gebhard and F. H. L. Essler, Phys. Rev. Lett. **85**, 3910 (2000).
144. E. Jeckelmann, Phys. Rev. B **66**, 045114 (2002).
145. E. Jeckelmann, Phys. Rev. B **67**, 075106 (2003).
146. D.C. Johnston, Phys. Rev. B **54**, 13009 (1996).
147. D.C. Johnston, M. Troyer, S. Miyahara, D. Lidsky, K. Ueda, M. Azuma, Z. Hiroi, M. Takano, M. Isobe, Y. Ueda, M.A. Korotin, V.I. Anisimov, A.V. Mahajan and L.L. Miller, *Magnetic Susceptibilities of Spin-1/2 Antiferromagnetic Heisenberg Ladders and Applications to Ladder Oxide Compounds*, cond-mat/0001147. See extensive references therein.
148. C. Kane, L. Balents and M. P. A. Fisher, Phys. Rev. Lett. **79**, 5086 (1997).
149. J.W. Janssen, S.G. Lemay, M. van den Hout, M. Mooij, L.P. Kouwenhoven and C. Dekker, *Scanning Tunneling Spectroscopy on a Carbon Nanotube Buckle*, Conference Proceedings AIP 519, p. 293-297 (Kirchberg, March 2001).
150. J.W. Janssen, S.G. Lemay, L.P. Kouwenhoven and C. Dekker, Phys. Rev. B **65**, 115423 (2002).
151. G. E. Japaridze, A. A. Nersesyan and P. Wiegmann, Nucl. Phys. B **230**, 511 (1984).
152. M. Jimbo and T. Miwa, *Algebraic Analysis of Solvable Lattice Models*, American Mathematical Society (1994).
153. J.D. Johnson and B.M. McCoy, Phys. Rev. A **6**, 1613 (1972).
154. M. Karbach, G. Müller, A.H. Bougourzi, A. Fledderjohann and K.H. Mütter, Phys. Rev. B **55**, 12510 (1997).
155. M. Karbach, D. Biegel and G. Müller, Phys. Rev. B **66**, 054405 (2002).
156. M. Karowski and P. Weisz, Nucl. Phys. B **139**, 455 (1978).
157. M. Kenzelmann, R.A. Cowley, W.J.L. Buyers, R. Coldea, J.S. Gardner, M. Enderle, D.F. McMorrow, S.M. Bennington, Phys. Rev. Lett. **87**, 017201 (2001).
158. M. Kenzelmann, A. Zheludev, S. Raymond, E. Ressouche, T. Masuda, P. Böni, K. Kakurai, I. Tsukada, K. Uchinokura, and R. Coldea Phys. Rev. B **64**, 054422 (2001).
159. M. Kenzelmann, R. A. Cowley, W. J. L. Buyers, Z. Tun, R. Coldea, M. Enderle, Phys. Rev. B **66**, 024407 (2002).

160. M. Kenzelmann, R. Coldea, D.A. Tennant, D. Visser, M. Hofmann, P. Smeibidl and Z. Tylczynski, Phys. Rev. B **65**, 144432 (2002).
161. M. Kenzelmann, Y. Chen, C. Broholm, D.H. Reich and Y. Qiu, Phys. Rev. Lett. **93**, 017204 (2004).
162. C. Kim, A.Y. Matsuura, Z.X. Shen, N. Montoyama, H. Eisaki, S. Uchida, T. Tohyama and S. Maekawa, Phys. Rev. Lett. **77**, 4054(1996).
163. K. Kuroki and H. Aoki, Phys. Rev. Lett. **72**, 2947 (1994);
164. A. Klümper, Z. Phys. **91**, 507 (1993).
165. K. Kobayashi *et. al.*, Phys. Rev. Lett. **82**, 803 (1999).
166. M. Kohgi, K. Iwasa, J.M. Mignot, B. Fak, P. Gegenwart, M. Lang, A. Ochiai, H. Aoki and T. Suzuki, Phys. Rev. Lett. **86**, 2439 (2001).
167. T. Koma, Prog. Theor. Phys. **78**, 1213 (1987).
168. R. M. Konik, A. LeClair and G. Mussardo, Int. J. of Mod. Phys. A **11**, 2765 (1996).
169. R. M. Konik, F. Lesage, A.W.W. Ludwig and H. Saleur, Phys. Rev. B **64**, 155112 (2001).
170. R. M. Konik and A. W. W. Ludwig, Phys. Rev. B **64**, 155112 (2001).
171. R. M. Konik, H. Saleur and A. W. W. Ludwig, Phys. Rev. B **66**, 075105 (2002).
172. R. M. Konik and P. Fendley, Phys. Rev. B **66**, 144416 (2002).
173. R. M. Konik, Phys. Rev. B **68**, 104435 (2003).
174. Y. Krotov, D. Lee and S. Louie, Phys. Rev. Lett. **78**, 4245 (1997) [cond-mat/9611073].
175. V.E. Korepin, Theor. Math. Phys. **41**, 169 (1979).
176. V.E. Korepin, A.G. Izergin and N.M. Bogoliubov, *Quantum Inverse Scattering Method, Correlation Functions and Algebraic Bethe Ansatz* (Cambridge University Press, 1993).
177. B. Lake, D.A. Tennant and S.E. Nagler, Phys. Rev. Lett. **85**, 832 (2000).
178. P.P. Kulish, Theor. Math. Phys. **26**, 132 (1976);
179. P. Kulish, N. Reshetikhin, and E. Sklyanin, Lett. Math. Phys. **5**, 393 (1981).
180. S.J. La Placa, J.F. Bringley, B.A. Scott and D.E. Cox, Acta Crystallogr. C **49**, 1415 (1993).
181. A. LeClair, F. Lesage, S. Lukyanov and H. Saleur, Phys. Lett. A **235**, 203 (1997).
182. A. LeClair, F. Lesage, S. Sachdev and H. Saleur, Nucl. Phys. B **482**, 579 (1996).
183. A. LeClair and G. Mussardo, Nucl. Phys. B **552**, 624 (1999).
184. L.S. Levitov and A.M. Tsvelik, Phys. Rev. Lett. **90**, 016401 (2003).
185. F. Lesage, H. Saleur and S. Skorik, Nucl. Phys. B **474**, 602 (1996).
186. E.H. Lieb and F.Y. Wu, Phys.Rev. Lett. **20**, 1445 (1968).
187. H.H. Lin, L. Balents and M. Fisher, Phys. Rev. B **56**, 6569 (1997).
188. H. L. Lin, L. Balents and M. Fisher, Phys. Rev. B **58**, 1794 (1998).
189. H. L. Lin, Phys. Rev. B **58**, 4963 (1998).
190. D. Loss and B. Normand, *Quantum Antiferromagnets in a Magnetic Field*, cond-mat/9804151.
191. J.Z. Lou, S.J. Qin, C.F. Chen, Z.B. Su and L. Yu, Phys. Rev. B **65**, 064420 (2002).
192. M. Lüscher, Nucl. Phys. B **135**, 1 (1978). The conserved charge here is non-local. For a discussion of local conserved charges in the model see [118, 238].
193. S. Lukyanov, Comm. Math. Phys. **167**, 183 (1995);
194. S. Lukyanov, Mod. Phys. Lett. A **12**, 2911 (1997).
195. S. Lukyanov and A. Zamolodchikov, Nucl. Phys. B **493**, 571 (1997).
196. S. Lukyanov, Nucl. Phys. B **522**, 533 (1998).
197. S. Lukyanov and A. B. Zamolodchikov, Nucl. Phys. B **607**, 437 (2001).
198. S. Lukyanov and V. Terras, Nucl. Phys. B **654**, 323 (2003).

199. A. Luther and I. Peschel, Phys. Rev. B **12**, 3908 (1975).
200. B.M. McCoy and T.T. Wu, Il Nuovo Cimento **LVI**, 311 (1968).
201. S. Ma, C. Broholm, D. H. Reich, B. J. Sternlieb and R. W. Erwin, Phys. Rev. Lett. **69**, 3571 (1992).
202. S. Ma, D. H. Reich, C. Broholm, B. J. Sternlieb and R. W. Erwin, Phys. Rev. B **51**, 3289 (1995).
203. E. M. McCarron, M. A. Subramanian, J. C. Calabrese and R. L. Harlow, Mater. Res. Bull. **23**, 1429 (1988).
204. F. Mila, Eur. Phys. J. B **6**, 201 (1998).
205. J. Mintmire, B. Dunlap and C. White, Phys. Rev. Lett. **68**, 631 (1992).
206. T. Mizokawa et. al., Phys. Rev. Lett. **85**, 4779 (2000).
207. S. Meshkov, Phys. Rev. B **48**, 6167 (1993).
208. A. Moreo, Phys. Rev. B **35**, (1987) 8562.
209. R. Morra, W. Buyers, R. Armstrong and K. Hirakawa, Phys. Rev. B **38**, 543 (1988).
210. T. Moriya, Phys. Rev. **120**, 91 (1960).
211. N. F. Mott, Proc. Roy. Soc. A **62**, 416 (1949); Canad. J. Phys. **34**, 1356 (1964); Phil. Mag. **6**, 287 (1961).
212. N. F. Mott, *Metal-Insulator Transitions*, 2^{nd} ed. (Taylor and Francis, London, 1990).
213. G. Müller, H. Thomas, H. Beck and J.C. Bonner, Phys. Rev. B **24**, 1429 (1981).
214. G. Mussardo, *Spectral representation of correlation functions in two-dimensional quantum field theories*, hep-th/9405128.
215. H. Mutka, C. Payen, P. Molinié, J. L. Soubeyroux, P. Colombet and A.D. Taylor, Phys. Rev. Lett. **67**, 497 (1991).
216. M. Nakamura, Phys. Rev. B **61**, 16377 (2000).
217. T. Nakano and H. Fukuyama, J. Phys. Soc. Jpn **50**, 2489 (1981).
218. A.A. Nersesyan and A.M. Tsvelik, Phys. Rev. Lett. **78**, 3939 (1997).
219. A.A. Nersesyan and A.M. Tsvelik, Phys. Rev. B **68**, 235419 (2003).
220. R. Noack, D. J. Scalapino and S. White, Europhys. Lett. **30**, 163 (1995).
221. R. Noack, D. J. Scalapino and S. White, Physica C **270**, 281 (1996).
222. R. Noack, D. J. Scalapino and S. White, Phil. Mag. B **74**, 485 (1996).
223. B. Normand, J. Kyriakidis and D. Loss, Ann. Phys.(Leipzig) **9**, 133 (2000) [cond-mat/9902104].
224. B. Normand, Acta Phys. Polonica B **31**, 3005 (2000).
225. E. Orignac, *Quantitative expression of the spin gap via bosonization for a dimerized spin-1/2 chain*, cond-mat/0403175.
226. M. Oshikawa and I. Affleck, Phys. Rev. Lett. **78**, 1984 (1997).
227. M. Oshikawa, K. Ueda, H. Aoki, A. Ochiai and M. Kohgi, J. Phys. Soc. Jpn. **68**, 3181 (1999).
228. M. Oshikawa and I. Affleck, Phys. Rev. B **65**, 134410 (2002).
229. K. Oshima, K. Okuda and M. Date, J. Phys. Soc. Jpn. **41**, 475 (1976), J. Phys. Soc. Jpn. **44**, 757 (1978).
230. K. Oshima, K. Okuda and M. Date, J. Phys. Soc. Jpn. **44**, 757 (1978).
231. A. Parola and S. Sorella, Phys. Rev. Lett. **76**, 4604 (1996).
232. A. Parola and S. Sorella, Phys. Rev. B **57**, 6444 (1998).
233. J.B. Parkinson, J.C. Bonner, Phys. Rev. B **32**, (1985) 4703.
234. K. Penc and F. Mila, Phys. Rev. B **49**, 9670 (1994).
235. K. Penc, K. Hallberg, F. Mila and H. Shiba, Phys. Rev. Lett. **77**, 1390 (1996).
236. S. Peysson and K. Schoutens, J. Phys. A **35**, 6471 (2002).
237. V. L. Pokrovsky and A. L. Talapov, Phys. Rev. Lett. **42**, 65 (1979).
238. A. M. Polyakov, Phys. Lett. B **72**, 224 (1977).

239. A. Rao, E. Richter, S. Bandow, B. Chase, P. Eklund, K. Williams, S. Fang, K. Subbaswamy, M. Menon, A. Thess, R. Smalley, G. Dresselhaus and M. Dresselhaus, Science **275**, 187 (1997);
240. L.-P. Regnault, I. Zaliznyak, J. P. Renard and C. Vettier; Phys. Rev. B **50**, 9174 (1994).
241. J.P. Renard, M. Verdaguer, L.P. Regnault, W.A.C. Erkelens, J. Rossat-Mignod and W.G. Stirling, Europhys. Lett. **3**, 945 (1987).
242. T. M. Rice, S. Gopalan and M. Sigrist, Europhys. Lett. **23**, 445 (1993).
243. S. Sachdev and K. Damle, Phys. Rev. Lett. **78**, 943 (1997).
244. S. Sachdev and K. Damle, J. Phys. Soc. Jpn. **69**, 2712 (2000).
245. J. Sagi and I. Affleck, Phys. Rev. B. **53**, 9188 (1996).
246. T. Sakai and M. Takahashi, Phys. Rev. B **43**, 13383 (1991).
247. A.W. Sandvik, Phys. Rev. Lett. **83**, 3069 (1999).
248. R. Saito, M. Fujita, G. Dresselhaus and M. Dresselhaus, Appl. Phys. Lett. **60**, 2204 (1992).
249. H. Saleur, Nucl. Phys. B **567**, 602 (2000).
250. S.K. Satija, J.D. Axe, G. Shirane, H. Yoshizawa and K. Hirakawa, Phys. Rev. B **21**, 2001 (1980).
251. T. Siegrist, L.F. Schneemeyer, S.A. Sunshine and J.V. Waszczak, Mater. Res. Bull. **23**, 1429 (1988).
252. D.J. Scalapino, Y. Imry and P. Pincus, Phys. Rev. B **11**, 2042 (1975).
253. H.J. Schulz, Phys. Rev. B **22**, 5274 (1980).
254. H.J. Schulz, Phys. Rev. B **34**, 6372 (1986).
255. H. J. Schulz, Phys. Rev. Lett. **77**, 2790 (1996).
256. H.J. Schulz, Phys. Rev. B **53**, R 2959 (1996);
257. H.J. Schulz, *SO(N) symmetries in the two-chain model of correlated fermions*, cond-mat/9808167.
258. A. Schwartz, M. Dressel, G. Grüner, V. Vescoli, L. Degiorgi, T. Giamarchi, Phys. Rev. B **58**, 1261 (1998).
259. D. Senechal, D. Perez and M. Pioro-Ladiere, Phys. Rev. Lett. **84**, 522 (2000).
260. D. Shelton, A.A. Nersesyan and A.M. Tsvelik, Phys. Rev. B **53**, 8521 (1996).
261. R. Slansky, Phys. Rept. **79**, 1 (1981).
262. F.A. Smirnov, J. Phys. A **19**, L575 (1986).
263. F. A. Smirnov, Commum. Math. Phys. **132**, 415 (1990).
264. F.A. Smirnov, *Form Factors in Completely Integrable Models of Quantum Field Theory* (World Scientific, Singapore, 1992).
265. E. Sorensen and I. Affleck, Phys. Rev. B **49**, 13235 (1994).
266. O.A. Starykh, D.L. Maslov, W. Häusler and L.I. Glazman, in *Low-Dimensional Systems*, ed. T. Brandes, Lecture Notes in Physics (Springer, 2000)
267. M. Steiner, K. Kakurai, J. K. Kjems, D. Petitgrand and R. Pynn, J. Appl. Phys. **61** 3953 (1987).
268. M. Suzuki, Phys. Rev. B **31**, 2957 (1985).
269. M. Takigawa, T. Asano, Y. Ajiro, M. Mekata and Y. Uemura, Phys. Rev. Lett. **76**, 2173 (1996).
270. M. Takahashi, Prog. Theor. Phys. **46**, 401 (1971).
271. M. Takahashi and M. Suzuki, Prog. Theor. Phys. **48**, 2187 (1972).
272. M. Takahashi, Prog. Theor. Phys. **50**, 1519 (1974).
273. M. Takahashi, Phys. Rev. B **43**, 5788 (1990).
274. M. Takahashi, Phys. Rev. Lett. **62**, 2313 (1989).
275. M. Takahashi and T. Sakai, J. Phys. Soc. of Japan, **60**, 760 (1991).

276. M. Takahashi, Phys. Rev. B **48**, 311 (1993).
277. J.C. Talstra and F.D.M. Haldane, Phys. Rev. B **54**, 12594 (1996).
278. L. Takhtajan, Phys. Lett. A **87**, 479 (1982).
279. S. Tans, M. Devoret, H. Dai, A. Thess, R. Smalley, L. Geerligs and C. Dekker, Nature **386**, 474 (1997).
280. D.A. Tennant, R. Cowley, S.E. Nagler and A.M. Tsvelik, Phys. Rev. B **52**, 13368 (1995).
281. D.A. Tennant, S.E. Nagler, S. Welz, G. Shirane and K. Yamada, Phys. Rev. B **52**, 13381 (1995).
282. H.-J. Thun, T.T. Truong and P.H. Weisz, Phys. Lett. B **67**, 321 (1977).
283. K. Totsuka, Phys. Rev. B **57**, 3454 (1998).
284. A.M. Tsvelik, Sov. Phys. JETP **66**, 221 (1987).
285. A.M. Tsvelik, Phys. Rev. B **42**, 10499 (1990).
286. Z. Tun, W. Buyers, R. Armstrong, K. Hirakawa and B. Briat, Phys. Rev. B **42**, 4677 (1990).
287. L.C. Venema, J.W. Janssen, M.R. Buitelaar, J.W.G. Wildöer, S.G. Lemay, L.P. Kouwenhoven and C. Dekker, Phys. Rev. B **62**, 5238 (2000).
288. V. Vescoli, L. Degiorgi, W. Henderson, G. Grüner, K. P. Starkey and L. K. Montgomery, *Science* **281**, 1181 (1998).
289. J. Voit, Eur. Phys. J. B **5**, 505 (1998).
290. Y.-J. Wang and A.A. Nersesyan, Nucl. Phys. B **583**, 671 (2000).
291. X.G. Wen, Phys. Rev. B **42**, 6623 (1990).
292. S. White, Phys. Rev. Lett. **69**, 2863 (1992).
293. S. White and D. Huse, Phys. Rev. B **48**, 3844 (1993).
294. S. White, R. Noack and D. Scalapino, Phys. Rev. Lett. **73**, 886 (1994).
295. P. B. Wiegmann, Sov. Sci. Rev. Ser. A **2**, 43 (1980).
296. P. Wiegmann, JETP Lett. **41**, 95 (1985).
297. J. Wildöer, L. Venema, A. Rinzler, R. Smalley and C. Dekker, Nature **391**, 59 (1998).
298. A.U.B. Wolter, P. Wzietek, F.J. Litterst, S. Sullow, D. Jerome, R. Feyerherm and H.H. Klauss, Polyhedron **22**, 2273 (2003).
299. A.U.B. Wolter, H. Rakoto, M. Costes, A. Honecker, W. Brenig, A. Klümper, H.H. Klauss, F.J. Litterst, R. Feyerherm, D. Jerome and S. Sullow, Phys. Rev. B **68**, 220406 (2003).
300. S. Yamamoto, Phys. Rev. Lett. **75**, 3348 (1995).
301. C.N. Yang and C.P. Yang, Phys. Rev. **150**, 321 (1966).
302. C.N. Yang and C.P. Yang, Phys. Rev. **150**, 327 (1966).
303. C.N. Yang and C.P. Yang, Phys. Rev. **151**, 258 (1966).
304. V. P. Yurov and Al. B. Zamolodchikov, Int. J. Mod. Phys. A **6**, 3419 (1991).
305. H. Yoshioka, M. Tsuchizu and Y. Suzumura, J. Phys. Soc. Jpn **70**, 762 (2001).
306. M.G. Zacher, E. Arrigoni, W. Hanke and J.R. Schrieffer, Phys. Rev. B **57**, 6370 (1998).
307. I. A. Zaliznyak, L.-P. Regnault, and D. Petitgrand, Phys. Rev. B **50**, 15824 (1994).
308. I. A. Zaliznyak, D. C. Dender, C. Broholm and D. H. Reich, Phys. Rev. B **57**, 5200 (1998).
309. I. A. Zaliznyak, C. Broholm, M. Kibune, M. Nohara and H. Takagi, Phys. Rev. Lett. **83**, 5370 (1999).
310. I. A. Zaliznyak, S.-H. Lee and S. V. Petrov, Phys. Rev. Lett. **87**, 017202 (2001); ibid. Phys. Rev. Lett. **91**, 039902 (2003).

311. I. A. Zaliznyak, H. Woo, T. G. Perring, C. L. Broholm, C. D. Frost and H. Takagi, Phys. Rev. Lett **93**, 087202 (2004).
312. A. B. Zamolodchikov, Comm. Math. Phys. **55**, 183 (1977).
313. A. B. Zamolodchikov, JETP Lett. **25**, 468 (1977).
314. A. B. Zamolodchikov and Al. B. Zamolodchikov, Nucl. Phys. B **133**, 525 (1978).
315. A. B. Zamolodchikov and Al. B. Zamolodchikov, Ann. of Phys. **120**, 253 (1979).
316. A. B. Zamolodchikov and Al. B. Zamolodchikov, Nucl. Phys. B **379**, 602 (1992).
317. Al.B. Zamolodchikov, Int. J. Mod. Phys. A **10**, 1125 (1995).
318. S.C. Zhang, Science **275**, 1089 (1997).
319. A. Zheludev, M. Kenzelmann, S. Raymond, E. Ressouche, T. Masuda, K. Kakurai, S. Maslov, I. Tsukada, K. Uchinokura and A. Wildes, Phys. Rev. Lett. **85**, 4799 (2000).
320. A. Zheludev, M. Kenzelmann, S. Raymond, T. Masuda, K. Uchinokura and S.-H. Lee, Phys. Rev. B **65**, 014402 (2002).
321. A. Zheludev, Y. Chen, C. L. Broholm, Z. Honda and K. Katsumata, Phys. Rev. B **63**, 104410 (2001).
322. A. Zheludev, Z. Honda, K. Katsumata, R. Feyerherm and K. Prokes, Europhys. Lett. **55**, 868 (2001).
323. A. Zheludev, K. Kakurai, T. Masuda, K. Uchinokura and K. Nakajima, Phys. Rev. Lett. **89**, 197205 (2002).
324. A. Zheludev, Z. Honda, Y. Chen, C. L. Broholm, K. Katsumata and S. M. Shapiro, Phys. Rev. Lett. **88**, 077206 (2002).
325. A. Zheludev, S. Raymond, L.-P. Regnault, F. H. L. Essler, K. Kakurai, T. Masuda and K. Uchinokura, Phys. Rev. B **67**, 134406 (2003).
326. A. Zheludev, S. M. Shapiro, Z. Honda, K. Katsumata, B. Grenier, E. Ressouche, L.-P. Regnault, Y. Chen, P. Vorderwisch, H.-J. Mikeska and A. K. Kolezhuk, Phys. Rev. B **69**, 054414 (2004).
327. A. Zheludev, Z. Honda, C. L. Broholm, K. Katsumata, S. M. Shapiro, A. Kolezhuk, S. Park and Y. Qiu, Phys. Rev. B **68**, 134438 (2003).
328. X. Zotos and P. Prelovsek, Phys. Rev. B **53**, 983 (1996).
329. X. Zotos, F. Naef and P. Prelovsek, Phys. Rev. B **55**, 11029 (1997).